

PEOPLE'S DEMOCRATIC REPUBLIC OF ALGERIA
MINISTRY OF HIGHER EDUCATION AND SCIENTIFIC RESEARCH



IBN KHALDOUN UNIVERSITY OF TIARET
FACULTY OF APPLIED SCIENCES



THESIS

Presented by:

Mr. BENGHARBI Abdelkader Azzeddine

Thesis Submitted in Fulfillment of the Requirements for:

Degree of Ph.D (Doctorat L.M.D)

Renewable Energies in Electrotechnics

THEME

**Contribution to Diagnostic and Tolerant Control of
Photovoltaic Pumping System**

Presented on 05/02/ 2024

Under Board of Examiners composed of:

President	BELFEDAL Cheikh	Pr	Ibn Khaldoun University, Tiaret
Examiner	BERKANI Abderrahmane	M.C.A	Ibn Khaldoun University, Tiaret
Examiner	BOUDIAF Mohamed	M.C.A	Zian Achour University, Djelfa
Examiner	TALEB Rachid	Pr	Hassiba Benbouali University, Chelf
Supervisor	Laribi Souad	M.C.A	Ibn Khaldoun University, Tiaret
Co-Supervisor	Allaoui Tayeb	Pr	Ibn Khaldoun University, Tiaret

ملخص

في مواجهة تصاعد الطلب العالمي على الطاقة والمخاوف البيئية الناجمة عن الاعتماد على الوقود الأحفوري ، توفر الطاقات المتجددة حلا واعداء. لقد برز إنتاج الطاقة الكهروضوئية، ولا سيما من خلال أنظمة ضخ الطاقة الشمسية الكهروضوئية، كبديل نظيف وفعال. توفر هذه الأنظمة، التي تستخدم الألواح الشمسية لتشغيل مضخات المياه، حلاً موثوقاً لإمدادات المياه، خاصة في المناطق النائية وخارج الشبكة.

ومع ذلك، فإن التحديات التقنية، بما في ذلك الأخطاء والفشل، يمكن أن تعطل أداء أنظمة الضخ الكهروضوئية الشمسية. ولمواجهة هذه التحديات، تعد تقنيات اكتشاف الأخطاء والتحكم المتسامحة أمراً بالغ الأهمية. تهدف هذه التقنيات إلى تصنيف الأخطاء وتشخيصها بشكل منهجي، مما يسمح بإجراء الصيانة والإصلاح في الوقت المناسب. كما أنها تمكن النظام من التكيف ومواصلة العمل بكفاءة على الرغم من وجود أخطاء، مما يقلل من وقت التوقف عن العمل ويقلل التكاليف.

تتمثل الأهداف الأساسية لهذا البحث في تطوير مجال أنظمة الضخ بالطاقة الشمسية الكهروضوئية من خلال تطوير تقنيات شاملة للكشف عن الأخطاء وتنفيذ استراتيجيات التحكم المتسامحة مع الأخطاء. تتضمن هذه الأهداف نمذجة النظام، وبناء الأخطاء، وتحليل الأخطاء، واكتشاف الأخطاء باستخدام تحويل المويجات المنفصلة (DWT) والشبكات العصبية الاصطناعية (ANN) ، والتحكم في تحمل الأخطاء باستخدام التحكم الشعاعي (FOC) مع التحكم التكيفي Fuzzy-PID .

من خلال معالجة هذه الأهداف، تسعى هذه الأطروحة إلى تعزيز موثوقية وكفاءة واستدامة أنظمة ضخ المياه بالطاقة الشمسية الكهروضوئية، مع آثارها على خدمات إمدادات المياه دون انقطاع. تتمتع هذه التطورات في تشخيص الأخطاء والتحكم المتسامح بالقدرة على تحسين تشغيل وصيانة أنظمة ضخ الطاقة الشمسية الكهروضوئية بشكل كبير في كل من البيئات النائية والتقليدية، مما يؤدي في النهاية إلى تقليل التكاليف وضمان خدمات موثوقة لإمدادات المياه.

Abstract

In the face of escalating global energy demands and environmental concerns stemming from fossil fuel reliance, renewable energies offer a promising solution. Photovoltaic (PV) energy production, notably through solar PV pumping systems, has emerged as a clean and efficient alternative. These systems, using solar panels to power water pumps, provide reliable water supply solutions, particularly in remote and off-grid areas.

However, technical challenges, including faults and failures, can disrupt the performance of solar PV pumping systems. To address these challenges, fault detection and tolerant control techniques are crucial. These techniques aim to classify and diagnose faults systematically, allowing for timely maintenance and repair. They also enable the system to adapt and continue operating efficiently despite the presence of faults, minimizing downtime and reducing costs.

The primary objectives of this research are to advance the field of solar PV pumping systems by developing comprehensive fault detection techniques and implementing fault-tolerant control strategies. These objectives include system modeling, fault construction, fault analysis, fault detection using Discrete Wavelet Transform (DWT) and Artificial Neural Networks (ANN), and fault-tolerant control using Field-Oriented Control (FOC) with adaptive Fuzzy-PID control.

By addressing these objectives, this thesis seeks to enhance the reliability, efficiency, and sustainability of solar PV pumping systems, with implications for uninterrupted water supply services. These advancements in fault diagnosis and tolerant control have the potential to significantly improve the operation and maintenance of solar PV pumping systems in both remote and conventional settings, ultimately reducing costs and ensuring reliable water supply services.

Resume

Face à l'augmentation de la demande énergétique mondiale et aux préoccupations environnementales liées à la dépendance aux combustibles fossiles, les énergies renouvelables offrent une solution prometteuse. La production d'énergie photovoltaïque (PV), notamment via des systèmes de pompage solaire photovoltaïque, est apparue comme une alternative propre et efficace. Ces systèmes, utilisant des panneaux solaires pour alimenter les pompes à eau, fournissent des solutions d'approvisionnement en eau fiables, en particulier dans les zones reculées et hors réseau.

Cependant, des problèmes techniques, notamment des pannes et des défaillances, peuvent perturber les performances des systèmes de pompage solaire photovoltaïque. Pour relever ces défis, les techniques de détection des pannes et de contrôle tolérant sont cruciales. Ces techniques visent à classer et à diagnostiquer systématiquement les défauts, permettant ainsi une maintenance et une réparation en temps opportun. Ils permettent également au système de s'adapter et de continuer à fonctionner efficacement malgré la présence de défauts, minimisant ainsi les temps d'arrêt et les coûts.

Les principaux objectifs de cette recherche sont de faire progresser le domaine des systèmes de pompage solaire photovoltaïque en développant des techniques complètes de détection des pannes et en mettant en œuvre des stratégies de contrôle tolérantes aux pannes. Ces objectifs incluent la modélisation du système, la construction des défauts, l'analyse des défauts, la détection des défauts à l'aide de la transformation en ondelettes discrètes (DWT) et des réseaux de neurones artificiels (ANN), ainsi que le contrôle tolérant aux pannes à l'aide du contrôle orienté champ (FOC) avec contrôle adaptatif Fuzzy-PID.

En abordant ces objectifs, cette thèse cherche à améliorer la fiabilité, l'efficacité et la durabilité des systèmes de pompage solaire photovoltaïque, avec des implications pour les services d'approvisionnement en eau ininterrompus. Ces progrès en matière de diagnostic des pannes et de contrôle tolérant ont le potentiel d'améliorer considérablement le fonctionnement et la maintenance des systèmes de pompage solaire photovoltaïque dans des contextes éloignés et conventionnels, réduisant ainsi les coûts et garantissant des services d'approvisionnement en eau fiables.

Dedication

I dedicate this work:

To my lovely parents

To my brothers and sisters, to my entire family.

To all those dear to me.

Acknowledgments

"I extend my heartfelt gratitude to the Almighty ALLAH, whose blessings have been a constant source of strength throughout this journey.

I am deeply thankful to the dedicated teams at the Energy Engineering and Computer Engineering Laboratory of Ibn Khaldoun University of Tiaret. Their unwavering cooperation and technical expertise were invaluable in the successful completion of this work.

I would like to express my sincere appreciation to my thesis advisor, Ms. Laribi Souad, a respected lecturer at the University of Tiaret, for her guidance, support, and insightful advice that significantly enriched this research.

My gratitude extends to my thesis co-supervisor, Mr. ALLAoui Tayeb, a distinguished professor at the University of Tiaret, for his patient guidance, continuous encouragement, and expertise that played a pivotal role in the success of this endeavor.

I extend my thanks to Mr. BELFEDAL Cheikh, a professor at the University of Tiaret, for accepting the honor of chairing the thesis jury, to Mr. BERKANI Abderrahmane, a respected lecturer at the University of Tiaret, to Mr. BOUDIAF Mohamed, a respected lecturer at the University of Djelfa, and to Mr. TALEB Rachid, a professor at the University of Chlef, for their valuable evaluation of this work.

Lastly, I would like to acknowledge and thank all individuals who, in various ways, contributed to the completion of this thesis. Your support has been deeply appreciated.

With immense gratitude,

[*BENGHARBI Abdelkader Azzeddine*]"

Publications

Articles:

- ❖ - M. Boukhalfa, A. Benaissa, **A. A. Bengharbi**, M. R. Bengourina, A. Khoudiri; "Fuzzy-PI Based Sliding Mode Control to Management of Hybrid Energy System Grid Connected"; *INTERNATIONAL JOURNAL OF ADVANCED STUDIES; IN COMPUTER SCIENCE & ENGINEERING; IJASCSE VOLUME 11 ISSUE 9 2022.*
- ❖ - **Bengharbi, A. A.**, Laribi, S., Allaoui, T., & Mimouni, A. (2022). Photovoltaic system faults diagnosis using discrete wavelet transform based artificial neural networks. *Electrical Engineering & Electromechanics*, (6), 42–47. <https://doi.org/10.20998/2074-272X.2022.6.07>
- ❖ - Mimouni, A., Laribi, S., Sebaa, M., Allaoui, T., & **Bengharbi, A. A.** (2023). Fault diagnosis of power converters in a grid connected photovoltaic system using artificial neural networks. *Electrical Engineering & Electromechanics*, (1), 25–30. <https://doi.org/10.20998/2074-272X.2023.1.04>
- ❖ - **A. A. Bengharbi**, S. Laribi, T. Allaoui and A. Mimouni, "Open-circuit fault diagnosis for three-phase inverter in photovoltaic solar pumping system using neural network and neuro-fuzzy techniques," *Electrica*, 23(3), 505-515, 2023.
- ❖ - Karboua, Djaloul and Toulal, Belgacem and **Bengharbi, A. A.** and Youcef, Chouiha, A Hybrid Control between the Nonlinear Backstepping and a Novel Optimal Design to the Linear Quadratic Regulator Technique Based on a Steady-State Error for the PMSM. Available at SSRN: <https://ssrn.com/abstract=4594191> or <http://dx.doi.org/10.2139/ssrn.4594191>
- ❖ - Mimouni, A., Laribi, S., Sebaa, M., Allaoui, T., & **Bengharbi, A. A.**(2023). «Identification of Open-Circuit Faults in T-Type Inverters Using Fuzzy Logic Approach». *Power Engineering And Electrical Engineering.VOLUME: 21 | NUMBER: 4/2023/DECEMBER .DOI: 10.15598/aeec.v21i4.5218*

CONFERENCES AND SEMINARS:

- ❖ **A. Bengharbi**, S. Laribi, and T. Allaoui, "Single And Double Open Switch Fault Diagnosis Based On Artificial Neural Network In Three Phase Inverter Of Solar Pumping System". International Hazar scientific researches conference – II; April 10 - 12, 2021; Baku, Azerbaijan, Khazar university; ISBN:978-605-74616-2-9
- ❖ **A. Bengharbi**, S. Laribi, T. Allaoui, and A. Mimouni. "A Fuzzy Logic Approach For The Diagnosis Of Single And Double Open Switch Fault In Three Phase Inverter Of Solar Pumping System". The first international conference on renewable energy advanced technologies and applications; 25-27 October 2021, Research unit for renewable energies in Saharan region, Adrar. ISBN:978-9931-9819-0-9

- ✧ **A. Bengharbi**, S. Laribi, T. Allaoui, and A. Mimouni. «REDUNDANT EMERGENCY INVERTER LEG FOR SOLAR PUMPING SYSTEM INVERTER FAULT»;6th INTERNATIONAL CONGRESS ON INNOVATIVE SCIENTIFIC APPROACHES ;December 19-20, 2021. SAMSUN, TURKEY. ISBN:978-625-8423-61-7
- ✧ **A. Bengharbi**, S. Laribi, T. Allaoui, and A. Mimouni. “Partial Shading Impact on The Characteristic Curves and Generated Power of Photovoltaic Modules”. 2nd International Architectural Sciences and Applications Symposium held on September 09-11, 2022 /Baku Engineering University, Baku, Azerbaijan
- ✧ A. Mimouni, S. Laribi, M. SEBAA, T. Allaoui and **A. Bengharbi**. «COMPARISON OF DIFFERENT DC-DC CONVERTERS IN PHOTOVOLTAIC SYSTEM»; 6th INTERNATIONAL CONGRESS ON INNOVATIVE SCIENTIFIC APPROACHES ;December 19-20, 2021. SAMSUN, TURKEY. ISBN: 978-625-8423-61-7
- ✧ A. Mimouni, S. Laribi, M. SEBAA, T. Allaoui and **A. Bengharbi**. «Open circuit fault diagnosis of power converters in photovoltaic system », The 1 st international conference on modern electrical engineering and technology (CIETM’22) held at the University of Soukahras, Algeria, During February 18-19, 2022.
- ✧ A. Mimouni, S. Laribi, M. SEBAA, T. Allaoui and **A. Bengharbi**. « Open circuit fault diagnosis of NPC inverter in grid connected photovoltaic system », 19th IEEE International Multi- Conference on Systems, Signals & Devices SSD 2022 held in SETIF, Algeria, During May 06 th-10 th , 2022.
- ✧ A. Mimouni, S. Laribi, M. SEBAA, T. Allaoui and **A. Bengharbi**. «Diagnosis Method of an Open circuit fault for a T-Type inverter in PV System»; 2nd International Architectural Sciences and Applications Symposium held on September 09-11, 2022 /Baku Engineering University, Baku, Azerbaijan
- ✧ **A. A. Bengharbi**, S. Laribi, T. Allaoui, A. Mimouni,“ Open-Switch Fault Detection And Isolation For DC-DC Converter Of Photo-Voltaic System”, The first national conference in Materials Science and Engineering (NCMSE’1_2022), November 27–28, 2022, Djilali Bounaâma Khemis Milliana University, Algeria.
- ✧ A. Mimouni, S. Laribi, T. Allaoui, **A. A. Bengharbi**,“Open Switch Fault Diagnosis Method of inverter in Photovoltaic system using Phase Currents”, The first national conference in Materials Science and Engineering (NCMSE’1_2022), November 27–28, 2022, Djilali Bounaâma Khemis Milliana University, Algeria.
- ✧ **A. A. Bengharbi**, S. Laribi, T. Allaoui, A. Mimouni, H. Chibani.«ENHANCING ENERGY EFFICIENCY IN PHOTOVOLTAIC SYSTEMS USING (AI) FUZZY-BASED MPPT METHOD». « CNI-2023 »,05-06 décembre 2023, Université Ibn Khaldoun de Tiaret, Algeria.
- ✧ M. R. Morakchi, A. Chibani, B. Larbi, **A. A. Bengharbi**. « OPTIMIZING ENERGY FOR ENHANCED CAPACITIVE ACCELEROMETER VIA MULTI-OBJECTIVE PARTICLE SWARM OPTIMIZATION-BASED DESIGN ». « CNI-2023 »,05-06 décembre 2023, Université Ibn Khaldoun de Tiaret, Algeria.
- ✧ H. Chibani, S. Laribi, T. Allaoui, S. Heroual , **A. A. Bengharbi**,«*NEURAL NETWORK DIAGNOSIS OF THREE-PHASE INVERTER OPEN-CIRCUIT FAULTS IN A PHOTOVOLTAIC SOLAR PUMPING SYSTEM*».2nd International Paris Applied Science Congress December 21-24 / Paris, France.

Contents

Abstract

Dedication

Acknowledgments

Contents

List of Figures

List of Tables

General Introduction	1
1. Background	1
2. Motivation	2
3. Objectives of the thesis	4
4. Thesis Structure	5
I Chapter 01: State of Art on Photo-Voltaic and Pumping Systems	7
I.1. Introduction	8
I.2. Photovoltaic Solar Energy	9
I.2.1. Solar radiation	9
I.2.2. Photovoltaic Energy Technologies	11
I.2.3. Different Types of Photovoltaic Systems	20
I.2.4. Advantages and Disadvantages of PV Solar Energy	22
I.3. Solar Photovoltaic Pumping System	24
I.3.1. Composition of a PV Pumping System	25
I.3.2. Configurations of a PV Pumping System	28
I.4. PV pumping system Sizing Method	29
I.4.1. Water Needs Assessment	29
I.4.2. Calculation of Required Hydraulic Energy	30
I.4.3. Determination of Available Solar Energy	31
I.5. Conclusion	33
II Chapter 02 : Overview On Fault Diagnosis And Fault Tolerant Control	34
II.1. Introduction	35
II.2. Basic Concepts of Fault Diagnosis (FD):	36
II.3. Fault classification and Types	37
II.3.1. Based on the Occurrence's Location:	38
II.3.2. Based on the Behavior of Fault:	39
II.3.3. Based on the Way Faults are Modeled:	40
II.3.4. Unknown Inputs:	40

II.4. Classification of fault detection and diagnosis methods	40
II.4.1. Model-based approaches:	40
II.4.2. Signal-based approaches:	42
II.4.3. Knowledge-based approaches:	43
II.4.4. Hardware-based:	45
II.4.5. History-based:	46
II.4.6. Hybrid approaches:	47
II.5. Fault Tolerant Control (FTC)	49
II.5.1. The Need for FTC	49
II.5.2. Classification of FTC	49
II.5.3. Fundamental Mechanisms in FTC	51
II.5.4. Challenges and Considerations	51
II.6. Conclusion	51
III Chapter 03 : PV Pumping System Modeling and Control	53
III.1. Introduction	54
III.2. Proposed system description	54
III.3. System Modeling	55
III.3.1. Photovoltaic (PV) Modeling	55
III.3.2. Converters Modeling	58
III.3.3. Induction Machine Modeling	66
III.3.4. Centrifugal pump modeling	75
III.3.5. Storage modeling	76
III.4. System Control	78
III.4.1. Maximum Power Point	78
III.4.2. DC-Bus Control (Vdc)	82
III.4.3. Battrey management & control	83
III.4.4. Inverter Control	83
III.4.5. Induction machine control	84
III.5. Conclasion	85
IV Chapter 04 : PV Pumping System Fault Modeling and Simulation	86
IV.1. Introduction	87
IV.2. Fault Modeling and Faults Generation in Simulation	87
IV.2.1. Converters Fault	87
IV.2.2. Induction Motor Fault	89
IV.3. System Simulation & Results (Healfy & Faulty Modes)	92

IV.3.1. Healthy Mode	93
IV.3.2. Converters Fault effects	94
IV.3.3. Induction Motor Fault effects	104
IV.4. Conclusion	107
V Chapter 05: Fault Detection Using DWT-ANN	108
V.1. Introduction	109
V.2. DWT-ANN Fault Detection Framework	110
V.2.1. Data Collection and Preprocessing	110
V.2.2. Feature Extraction Using DWT	113
V.2.3. ANN Model Development	119
V.2.4. Training Process	121
V.2.5. Training Results	122
V.3. ANN Results	126
V.4. Limitations and Challenges	128
V.5. Conclusion	129
VI Chapter 06 : Tolerant Control For PV Pumping System	131
VI.1. Introduction	132
VI.2. Classic vector control	132
VI.2.1. Principle of vector control by flux orientation	132
VI.2.2. Asynchronous machine Model for control purpose	132
VI.2.3. Indirect vector control	134
VI.3. Adaptive-Fuzzy-PID based Field-Oriented Control	137
VI.3.1. PID Controller:	137
VI.3.2. Fuzzy Logic Controller (FLC)	138
VI.4. Stator Fault Results	144
VI.5. Rotor Fault Results	146
VI.6. Conclusion	148
General Conclusion	149
Referances	151
Appendices	158

List of Figures

Figure I.1 : Spectral response of solar radiation.	10
Figure I.2 : The components of global solar radiation.	11
Figure I.3 : Photovoltaic Effect.	11
Figure I.4 : Monocrystalline Cells & Polycrystalline Cells.	13
Figure I.5 : Amorphous Cells.	13
Figure I.6 : Organic cells.	14
Figure I.7 : $I=f(V)$ characteristic of a photovoltaic panel.	15
Figure I.8 : Constitution of a Photovoltaic Array.	17
Figure I.9 : Series Association of Cells.	18
Figure I.10 : Parallel Association of Cells.	19
Figure I.11 : Mixed Association.	19
Figure I.12 : Solar panels.	20
Figure I.13 : Photovoltaic Systems classification.	20
Figure I.14 : Systems Connected to the Grid.	21
Figure I.15 : Standalone Systems.	21
Figure I.16 : Hybrid Systems.	22
Figure I.17 : Solar Photovoltaic Pumping System.	24
Figure I.18 : Volumetric Pump.	27
Figure I.19 : Centrifugal Pump.	28
Figure II.1 : Fault type a effects in system.	37
Figure II.2 : Common types of actuator faults: (a) floationg trim, (b) lock-in-place, (c) hard-over failure, and (d) loss of effectiveness.	38
Figure II.3 : Common types of sensor faults: (a) bias, (b) drift, (c) performance degradation (or loss of accuracy), (d) sensor freezing, and (e) calibration.	39
Figure II.4 : Types of faults based on behavior: (a) Abrupt fault, (b) Incipient fault, and (c) Intermittent fault.	40
Figure II.5 : Model-based approaches.	41
Figure II.6 : Signal-based approaches.	42
Figure II.7 : Knowledge-based approaches.	44
Figure II.8 : Classification of FTC.	49
Figure II.9 : Architecture of the passive FTC.	50
Figure II.10 : Architecture of the active FTC.	51
Figure III.1 : Proposed system description.	55
Figure III.2 : Ideal photovoltaic cell model.	56

Figure III.3 : Real photovoltaic cell model.	57
Figure III.4 : Asymptotic electrical diagram of a photovoltaic module.	58
Figure III.5 : Boost Converter.	59
Figure III.6 : Boost Converter (ON state).....	59
Figure III.7 : Boost Converter (OFF state).....	60
Figure III.8 : Buck Converter.....	61
Figure III.9 : Buck Converter (ON state).....	61
Figure III.10 : Buck Converter (OFF state).....	62
Figure III.11 : Buck-boost Converter.....	63
Figure III.12 : Buck-boost Converter (ON state).....	63
Figure III.13 : Buck-boost Converter (OFF state).....	64
Figure III.14 : Three-Phase Inverter.	65
Figure III.15 : Three-phase model of the asynchronous machine [].	68
Figure III.16 : Angular registration of axis systems in space.	70
Figure III.17 : Battery electrical diagram.	77
Figure III.18 : Maximum Power Point.	79
Figure III.19 : Perturb and Observe.	80
Figure III.20 : Incremental Conductance.	81
Figure III.21 : Scaler Control.	84
Figure IV.1 : Open-Circuit Switch Fault.....	88
Figure IV.2 : Short-Circuit Switch Fault.....	88
Figure IV.3 : Reduction in the number of turns by short-circuit effect.	89
Figure IV.4 : broken bars rotor fault.	91
Figure IV.5 : Proposed system Faults.	92
Figure IV.6 : Healthy Mode simulation results.	94
Figure IV.7 : Boost Converter Fault effects (Open switch Fault).	95
Figure IV.8 : Boost Converter Fault effects (short switch Fault).	96
Figure IV.9 : Buck-Boost Converter Fault effects (Open switch Fault).	98
Figure IV.10 : Buck-Boost Converter Fault effects (Short switch Fault).	100
Figure IV.11 : Three-Phase Inverter Fault effects (Open switch Fault).....	102
Figure IV.12 : Three-Phase Inverter Fault effects (Short switch Fault).....	104
Figure IV.13 : Induction motor stator fault effects.	105
Figure IV.14 : Induction motor rotor fault effects.	106
Figure V.1 : DWT-ANN Fault Detection Framework.	110
Figure V.2 : wavelet functions (db 6).....	114

Figure V.3 : DWT implementation procedure [88].	115
Figure V.4 : Extracted Features.	118
Figure V.5 : Standard Multilayer Perceptron Architecture.	119
Figure V.6 : Sigmoid activation function.	120
Figure V.7 : ANN training progress.	123
Figure V.8 : ANN training state.	123
Figure V.9 : Best Validation Performance.	123
Figure V.10 : Regression plots.	125
Figure VI.1 : Speed regulation by indirect vector control.	135
Figure VI.2 : Field weakening.	137
Figure VI.3 : Structure of Adaptive Fuzzy PID controller.	139
Figure VI.4 : Membership Functions For $e(k)$ and $\Delta e(k)$.	140
Figure VI.5 : Membership Functions For $Kp_normalized$ and $Kd_normalized$.	140
Figure VI.6 : Membership Functions For 'a'.	141
Figure VI.7 : Fuzzy PID controller.	144
Figure VI.8 : Stator Fault Results (Speed).	145
Figure VI.9 : Stator Fault Results (Error).	145
Figure VI.10 : Stator Fault Results (Kp , Ki and Kd).	146
Figure VI.11 : Rotor Fault Results (Speed).	147
Figure VI.12 : Rotor Fault Results (Error).	147
Figure VI.13 : Rotor Fault Results (Kp , Ki and Kd).	147

List of Tables

Table V.1 : Collected data of Phase A current.	111
Table V.2 : Frequency bands obtained by multi-level decomposition.	115
Table V.3 : Dataset Label Table.	121
Table V.4 : ANN Results.	126
Table VI.1 : Fuzzy Tuning Rules For ' $Kp_normalized$ '.	142
Table VI.2 : Fuzzy Tuning Rules For ' $Kd_normalized$ '.	142
Table VI.3 : Fuzzy Tuning Rules For 'a'.	143

List of Principal Symbols

ε	Albedo
I_{sc}	Short Circuit Current
V_{oc}	Open Circuit Voltage
P_{max}	Maximum Power Point
V_{mp} & I_{mp}	Optimal voltage and current
η	Energy Efficiency
G	Solar irradiance (illuminance)
A	Total surface area of the photocells
FF	Form Factor
N_s	Number of cells in series
N_p	Number of cells in parallel
E_h	Hydraulic energy (Wh/day)
V	Water volume (m ³ /day)
H	Total head (m)
ρ	Water density (1000 kg/m ³)
g	Acceleration due to gravity (9.81 m/s ²)
V_d	Voltage across the diode (V)
R_s	Series resistance (Ω)
N_{ss}	Number of modules connected in series.
N_{pp}	Number of modules connected in parallel.
P_h	Hydrolic power to the fluid by the pump (W)
P_{ele}	Electric power of the asynchronous motor (W)
R_{mp}	Pump set efficiency (%)
Q	Flow rate / Volume flow (m ³ /s)
f	Coefficient of friction of the pipe walls

L	Piping length (m)
v	Average fluid speed (m/s)
D	Pipe diameter (m)
PC	Output power under CSM (W)
η_g	Generator efficiency at reference temperature (25°C)
F_m	Coupling factor
γ	Cell temperature coefficient.
T_c	Average daily cell temperature during sunny hours.
I	Output current (A)
I_d	Diode current (A)
I_s	Reverse saturation current of the diode (A)
I_{ph}	Photo-current (A)
k	Boltzmann constant (1,38e-23 J/K)
n	Quality factor of the diode
q	Charge of the electron (1.6 10e-19 C)
T	PN junction temperature in (K)

List of General Abbreviations

PV	PHOTOVOLTAÏQUE
DWT	DISCRETE WAVELET TRANSFORM
ANN	ARTIFICIAL NEURAL NETWORKS
FOC	FIELD-ORIENTED CONTROL
AI	ARTIFICIAL INTELLIGENCE
PVG	PHOTOVOLTAIC GENERATOR
TDH	TOTAL DYNAMIC HEAD
RIE	RELATIVE IRRADIANCE EFFICIENCY
FDD	FAULT DETECTION AND DIAGNOSIS
FTC	FAULT-TOLERANT CONTROL
MPPT	MAXIMUM POWER POINT TRACKING
SPWM	SINUSOIDAL PULSE WIDTH MODULATION
IM	INDUCTION MOTOR
P&O	PERTURB AND OBSERVE
INC	INCREMENTAL CONDUCTANCE
OCF	OPEN CIRCUIT FAULT
SCF	SHORT CIRCUIT FAULT
THD	TOTAL HARMONIC DISTORTION
MLP	MULTILAYER PERCEPTRON
MSE	MEAN SQUARED ERROR
R	CORRELATION COEFFICIENT
SOC	STATE OF CHARGE
DOD	DEPTH OF DISCHARGE

General Introduction

1. Background

As we look ahead to the forthcoming years, the challenge of energy production looms large on the global stage. The energy demands of industrialized societies are on an unrelenting upward trajectory, while developing nations are poised to require even more energy to propel their economies forward.

Yet, the systematic reliance on fossil fuels, including petroleum, coal, and natural gas, though cost-effective, exacts a hefty environmental toll. These fuels are the primary culprits behind the emission of polluting gases, resulting in a staggering 40% of global CO₂ emissions stemming from electricity generation using these combustible resources. These emissions are a major contributor to the alarming global warming trend [1][2].

In stark contrast, renewable energies hold a distinct advantage. They are not only devoid of atmospheric pollution but also refrain from producing greenhouse gases like carbon dioxide and nitrogen oxides, the culprits responsible for Earth's warming [3]. Renewable energies offer a path to clean and resource-efficient electricity production.

Today, photovoltaic energy production stands out as an unrivaled source of clean and non-polluting energy. Its significance is amplified by photovoltaic pumping systems, which have played a pivotal role in projects leveraging photovoltaic energy since their inaugural implementations in the late 1970s. Currently, they constitute one of the most significant applications of photovoltaic energy. Their prominence is primarily rooted in the economic infeasibility of connecting remote areas to the conventional electrical grid [4].

The distinction between solar power pumps lies in their operational dependence on batteries. Some operate with a battery to store electricity generated by solar cells, while others employ a reservoir to store water until needed [5].

These systems harness the power of the sun to drive pumps that extract water from sources such as wells, boreholes, or rivers and transport it to storage tanks or distribution networks. These systems offer several advantages over conventional pumping methods reliant on grid power or diesel engines[6].

This is particularly pronounced in remote and off-grid regions where conventional power sources are not readily accessible. Photovoltaic solar pumping systems have emerged as efficient and environmentally friendly solutions for water pumping applications. They have gained popularity as a reliable and cost-effective means of providing water supply for irrigation, livestock, and domestic use in remote areas[6].

Typically, the components of a solar PV pumping system include:

- Solar panels, which convert sunlight into direct current (DC) electricity.

General Introduction

- A power converter, responsible for adjusting the voltage and current to power the pump.
- A motor-pump, which draws water from a source and delivers it, where it can be either a surface pump or a submersible pump, depending on the depth and location of the water source.
- A battery and/or a water storage tank for storing water or excess electricity for later use.

These systems are versatile and can be designed to operate in various environmental conditions, tailored to meet the specific water pumping needs of a given project.

2. Motivation

Solar PV pumping systems offer a multitude of compelling advantages over traditional water pumping systems. These advantages include reduced operating costs due to the elimination of fuel and grid electricity purchases, lower environmental impact, and the ability to function independently of the grid [7]. Moreover, they often prove to be more reliable and easier to install, especially in remote areas where access to conventional power sources may be limited. However, despite these benefits, there are several technical challenges that can affect the performance of solar PV pumping systems.

One of the primary technical challenges pertains to faults and failures within the system, encompassing both electrical and mechanical issues. These faults can manifest as misoperations, malfunctions, efficiency degradation, and more. The presence of such faults not only jeopardizes the system's performance but also poses a potential service disruption.

To effectively address these technical challenges, it is crucial to classify solar PV pumping system faults into distinct categories. These categories, which may include internal faults, external faults, transient faults, permanent faults, among others, serve as a framework for diagnosing and rectifying issues within the system. This classification makes it easier to pinpoint the root cause of a problem and take appropriate corrective actions, ultimately restoring the power system to normal operation [8].

Additionally, these technical challenges can give rise to service-related issues. Notably, the maintenance and repair of solar PV pumping systems often require the expertise of technical specialists. This necessity introduces both time and cost considerations, and in some instances, technical expertise may not be readily available in remote areas. Consequently, system shutdowns due to faults can lead to interruptions in water supply services.

To mitigate these challenges, diagnosis and tolerant control techniques are employed. Diagnosis involves the continuous monitoring and analysis of the system's

General Introduction

behavior to detect faults or anomalies in its components. This proactive approach enables the early identification of issues before they escalate into major problems.

Tolerant control, on the other hand, refers to the system's ability to adapt and continue operating effectively and efficiently despite the presence of faults or anomalies. It achieves this by adjusting its control strategy and modifying its operating parameters in real-time to accommodate the existing faults. This resilience allows the system to maintain functionality even in the face of technical issues.

These techniques, diagnosis, and tolerant control, are invaluable tools in the maintenance and repair of solar PV pumping systems. They enable swift and accurate fault identification, aiding in the rapid resolution of problems within the system. By leveraging these techniques, system operators can minimize downtime, reduce maintenance costs, and ensure the continuous provision of water services, even in remote and challenging environments.

Where the primary goals of diagnosis and tolerant control of solar PV pumping systems are:

- **Fault detection and diagnosis:** To detect any faults or anomalies in the system's components, including the solar panels, DC-DC converter, pump, and storage tank. This can help identify potential issues before they lead to system failure, allowing for timely maintenance and repair.
- **System optimization:** To optimize the system's performance and efficiency under varying operating conditions, such as changes in solar irradiance and temperature. By adapting the system's control strategy and operating parameters, tolerant control can help maximize the system's output while minimizing energy consumption.
- **Reliability and availability improvement:** To improve the system's reliability and availability by minimizing downtime due to faults or failures. By detecting and mitigating faults early, tolerant control can help prevent catastrophic failure and reduce repair and maintenance costs.
- **Safety enhancement:** To enhance the safety of the system for operators and users. Fault detection and tolerant control can help prevent dangerous situations, such as overloading or overheating of the system's components.

Basically, diagnosis and tolerant control of solar PV pumping systems aim to improve efficiency and accuracy of repair and maintenance work, reducing costs, avoiding the time-consuming, and improving safety by helping to minimize the risk of human error, guarantee the service continuity, and maximizing the system's lifespan.

Besides that, Artificial Intelligence (AI) has a lot of potential applications in the area of fault detection and tolerant control. This is due to the fact that AI algorithms are capable of analyzing vast amounts of data and spotting patterns and anomalies that human operators might not immediately notice [9]. It can be utilized as:

General Introduction

AI algorithms for Fault Detection: it can be used to monitor the operation of machinery and systems in real-time, detecting any deviations from normal operating conditions that may indicate a fault or failure. This can be done using machine learning algorithms that are trained on historical data to identify patterns and trends that may indicate a fault. Once a fault is detected, the system can take corrective action, such as shutting down a machine or triggering an alarm to alert operators.

AI algorithms for Fault Diagnosis: AI algorithms can be used to diagnose the cause of a fault or failure, based on data collected from sensors and other sources. This can be done using machine learning algorithms that are trained on historical data to identify the most likely cause of a fault based on the symptoms observed. Once the cause of the fault is identified, the system can take corrective action, such as adjusting the operation of a machine or replacing a faulty component.

AI algorithms for Fault Tolerant Control: AI algorithms can be used to implement fault-tolerant control strategies, where the system is designed to continue operating even in the presence of faults or failures. This can be done by monitor the system and make adjustments to maintain optimal performance, even in the presence of faults. For instance, an AI algorithm can modulate the speed or torque of a motor to compensate for a malfunctioning sensor, allowing the machinery to operate until the sensor is replaced.

Overall, AI is a valuable tool in the domain of fault detection and tolerant control. Its ability to analyze data, detect anomalies, diagnose faults, and adapt to changing conditions can significantly improve the reliability and resilience of solar PV pumping systems and other complex machinery, ultimately contributing to more efficient and cost-effective operations.

3. Objectives of the thesis

In light of the compelling considerations and challenges outlined, the primary objective of this thesis is to advance the field of solar PV pumping systems by developing a comprehensive fault detection technique and implementing fault-tolerant control strategies. The central tasks and goals of this research endeavor are as follows:

System Modeling: The first task involves the development of a mathematical model for the solar PV pumping system. This model will serve as the foundation for subsequent analyses and control strategies.

Construction of Faults: Building upon the system model, simulated faults will be systematically introduced into the system to replicate real-world scenarios and challenges. These constructed faults will be used for subsequent analyses and validation of the fault detection and tolerant control techniques.

Fault Analyses: Thorough analyses of the constructed faults will be conducted. This involves a comprehensive examination of the effects of faults on the system's performance, behavior, and parameters. Understanding the characteristics and implications of faults is pivotal for their effective detection and management.

General Introduction

Design of Fault Detection Technique: A fault detection technique will be designed and implemented based on the Discrete Wavelet Transform (DWT) and Artificial Neural Networks (ANN). This technique will be tailored to the entire solar PV pumping system and will aim to detect and identify faults. It will leverage the power of data analysis and machine learning to recognize deviations from normal system behavior.

Design of Fault Tolerant Control: A fault-tolerant control strategy for the induction motor will be developed using Field-Oriented Control (FOC) technique based on adaptive Fuzzy PID controller. This control system will be capable of adapting to the presence of faults and maintaining optimal system performance despite the disruptions caused by faults.

By addressing these tasks and objectives, this thesis seeks to make significant contributions to the field of solar PV pumping systems. It aims to enhance the reliability, efficiency, and sustainability of these systems by equipping them with advanced fault detection and tolerant control capabilities. Ultimately, the research endeavors outlined in this dissertation will have implications for the operation and maintenance of solar PV pumping systems in both remote and conventional settings, reducing downtime, improving system longevity, and ensuring uninterrupted water supply services.

4. Thesis Structure

The rest of the thesis is structured as follows:

Chapter 1: State of Art on Photo-Voltaic and Pumping Systems

This chapter offers a general introduction to photovoltaic systems, providing an overview of their key components, operational principles, and diverse applications. In addition, photovoltaic solar pumping systems. It sets the stage for the subsequent exploration of fault diagnosis and tolerant control.

Chapter 2: Overview on Fault Diagnosis and Fault Tolerant Control

In this chapter, an overview of fault diagnosis and fault-tolerant control concepts is presented. It establishes the foundational knowledge necessary to delve deeper into the specific techniques and strategies applied in electrical and mechanical systems.

Chapter 3: PV Pumping System Modeling and Control (Detailed Model of a Photovoltaic Solar Pumping System)

This chapter focuses on the development of a comprehensive model for a photovoltaic solar pumping system. The model provides a detailed representation of the system's components, behavior, and interactions, serving as the basis for subsequent analysis and experimentation.

Chapter 4: PV Pumping System Fault Modeling and Simulation (Case Studies and Fault Analysis)

General Introduction

Chapter 4 presents a series of case studies in which faults are systematically constructed within the photovoltaic solar pumping system. The chapter meticulously analyzes the effects of these faults on the system's performance, behavior, and parameters. This empirical analysis informs the development of fault detection and tolerant control techniques.

Chapter 5: Fault Detection Using DWT-ANN

In this chapter, a dedicated fault detection technique is designed and implemented. The technique leverages the Discrete Wavelet Transform (DWT) and Artificial Neural Networks (ANN) to detect and identify faults within the photovoltaic solar pumping system. This chapter delves into the methodology and implementation of the fault detection approach.

Chapter 6: Fault Tolerant Control For PV Pumping System (FOC-Fuzzy-PID)

Chapter 6 is dedicated to the development of a fault-tolerant control strategy tailored to the photovoltaic solar pumping system; specifically, the induction motor. The control system is based on Field-Oriented Control (FOC) with an adaptive Fuzzy-PID controller. It explores how this control strategy adapts to the presence of faults and sustains optimal system performance.

Conclusion and Future Directions

Finally, a Conclusion summarizes the main findings and contributions of the thesis. It discusses the implications of the fault diagnosis and tolerant control techniques developed for photovoltaic solar pumping systems. Moreover, it explores potential avenues for future research and advancements in this field.

I Chapter 01: State of Art on Photo-Voltaic and Pumping Systems

I.1. Introduction

In the contemporary world, the pursuit of sustainable energy sources has become a paramount endeavor. Conventional fossil fuels, once the cornerstone of global energy production, have engendered remarkable advancements while concurrently exacting a detrimental toll on the environment. The specter of climate change, driven by the release of greenhouse gases such as carbon dioxide and nitrogen oxides, necessitates a decisive shift towards cleaner and renewable energy alternatives. In this context, the focus converges on renewable energy sources, characterized by their minimal environmental impact and perpetual availability on human timescales.

Renewable energy sources encompass an array of natural phenomena that can be harnessed for sustainable power generation, offering a departure from carbon-intensive energy production. These resources, owing to their regenerative nature, present a sustainable pathway to meet our energy needs [5]. Notably, the following sources exemplify the breadth and potential of renewable energy:

Wind Energy: Harvested through wind turbines, this form of energy derives from the kinetic energy of moving air, efficiently converted into electricity.

Solar Energy: Solar power manifests in two primary forms: photovoltaic (PV) and solar thermal. PV systems directly convert sunlight into electricity using semiconductors, while solar thermal systems capture the Sun's heat for electricity generation or thermal applications.

Geothermal Energy: Delving into the Earth's subterranean heat reservoirs, geothermal power plants utilize the natural gradient to produce electricity and provide heating.

Hydroelectric Energy: Exploiting the kinetic energy of flowing water—be it from rivers or tides—hydroelectric installations are a dependable source of electrical power.

Biomass Energy: This energy source revolves around organic materials, such as agricultural residues and forestry byproducts, which can be converted into energy through processes like combustion and fermentation.

Biofuels: Liquid fuels derived from organic feedstocks, like bioethanol and biodiesel, provide sustainable alternatives to traditional petroleum-based fuels.

Within the realm of renewable energy, our focus narrows onto photovoltaic technology, a particularly promising avenue for power generation. Photovoltaic systems leverage the photovoltaic effect to directly convert sunlight into electrical energy, offering an environmentally friendly and inexhaustible source of power [4].

The focus of this work, however, delves deeper into the application of photovoltaic energy in the context of pumping systems. This specialization underscores the versatility and efficiency of photovoltaic technology in providing sustainable solutions to the pressing need for water supply.

Throughout this exploration, we will delve into the intricacies of photovoltaic pumping systems, scrutinizing their constituent components, operational mechanisms, and applications. By the culmination of this journey, we aim to elucidate the profound potential of photovoltaic energy in addressing one of humanity's most fundamental requirements: access to clean, sustainable, and technically advanced water supply solutions and energy.

I.2. Photovoltaic Solar Energy

Photovoltaic solar energy, as the name suggests, draws its essence from the Greek language: "photo," meaning light, and "voltaic," an homage to the Italian physicist Alessandro Volta (1754-1827), a pioneer in the realm of electricity. In its literal translation, "photovoltaic" signifies "electricity of light"[10].

This form of solar energy hinges on the direct conversion of sunlight into electrical energy, facilitated by the use of semiconductor materials, with silicon being the preeminent choice. Silicon's supremacy in the manufacturing of photovoltaic cells stems from its abundance on Earth, primarily in the benign and widely available form of non-toxic silica. The photovoltaic effect, the core principle underlying this technology, emanates from the intrinsic properties of these photosensitive materials. They possess the remarkable capability to liberate electrons when exposed to external energy[10].

In this transformative process, energy is supplied by photons (the fundamental constituents of light) which impinge upon these photosensitive materials, thereby dislodging electrons and inducing the generation of a direct electric current. This resultant micro-power electricity can be channeled into electrical networks for broader distribution or consumed at the local level, serving as a testament to the remarkable potential of photovoltaic solar energy[10].

I.2.1. Solar radiation

Solar radiation, often referred to simply as "sunlight," is the energy emitted by the Sun in the form of electromagnetic waves. This radiant energy is a fundamental driver of Earth's climate, weather patterns, and, importantly, serves as a primary energy source for various applications, including photovoltaic power generation. Solar radiation spans a wide range of wavelengths, and it is a crucial factor in understanding and harnessing solar energy for practical use [7][11][12].

The solar radiation that reaches the Earth's atmosphere consists of a vast quantity of energy, totaling approximately 180,106 Gigawatts (GW). This energy spans a range of wavelengths from 0.22 to 10 micrometers (μm). This broad spectrum of solar radiation can be broken down into three main components based on their wavelength ranges:

Ultraviolet (UV) Radiation: Comprising roughly 9% of the total solar radiation, this is the energy in the wavelength range below 0.4 μm . UV radiation is responsible

for various natural processes and plays a role in phenomena like the ozone layer's formation.

Visible Radiation: The largest portion, about 47% of solar radiation, falls within the visible spectrum, spanning from 0.4 to 0.8 μm . This is the light that is visible to the human eye and is responsible for providing illumination during the day.

Infrared (IR) Radiation: Approximately 44% of solar radiation falls in the infrared range, with wavelengths greater than 0.8 μm . IR radiation carries heat energy and is crucial for maintaining Earth's temperature and climate.

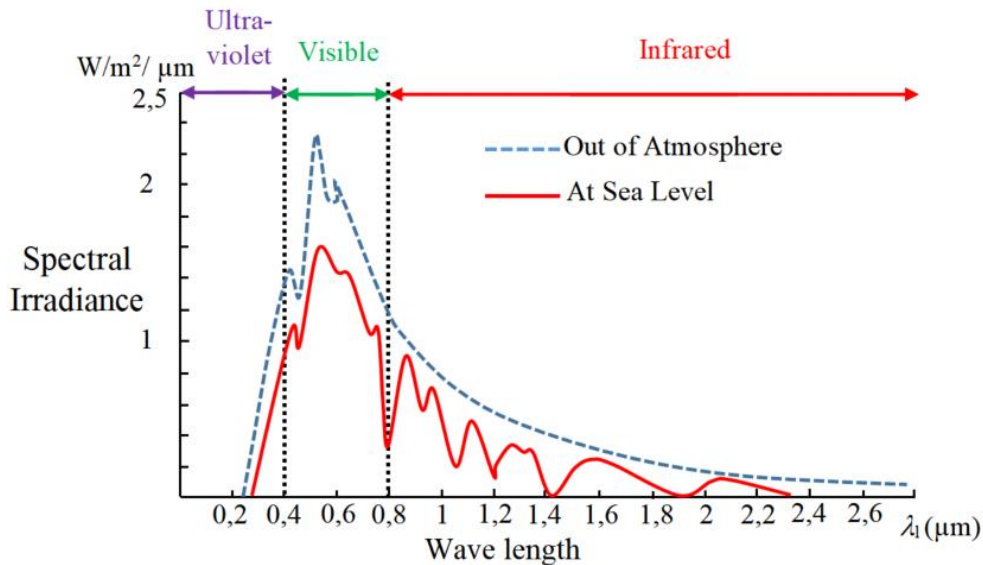


Figure I.1 : Spectral response of solar radiation.

The Earth's atmosphere intercepts this solar radiation, with an average power density of approximately 1.37 kilowatts per square meter (kW/m^2). However, this value is subject to slight variations (plus or minus 3%) due to factors like the Earth's orbit around the Sun, which leads to seasonal changes in solar radiation. Additionally, the amount of solar radiation received at a specific location is influenced by its geographical latitude, meteorological conditions (e.g., humidity and dust in the atmosphere), and time of day [7][11].

At the surface of the Earth, solar radiation can be categorized into three primary components:

Direct Radiation: This component consists of solar flux that arrives at the Earth's surface in parallel rays directly from the Sun's disk without significant scattering by the atmosphere.

Diffuse Radiation: Diffuse radiation is the portion of solar energy that has been scattered and reflected multiple times within the Earth's atmosphere before reaching the surface. It does not follow a direct path from the Sun.

Reflected Radiation: This component is the solar energy that is reflected off the Earth's surface and depends on the nature of the surface material, such as soil, water,

or vegetation. The reflectivity of a surface is quantified by a coefficient called the albedo (ϵ), which ranges from 0 (no reflection) to 1 (complete reflection).

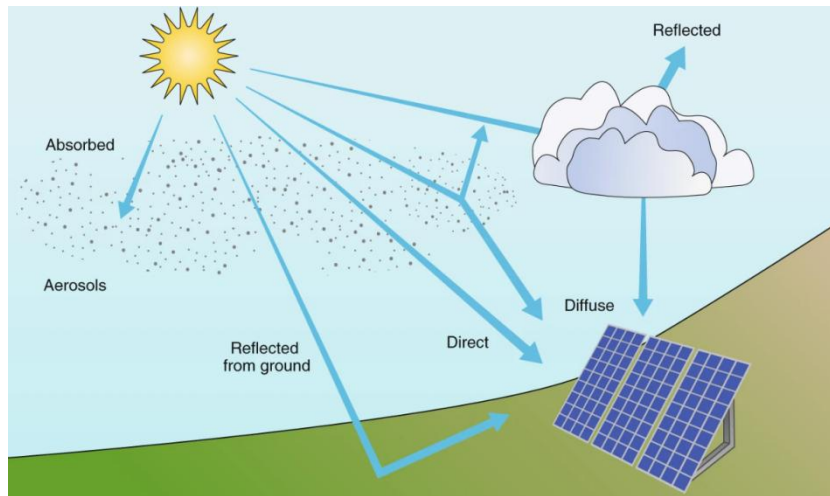


Figure I.2 : The components of global solar radiation.

The total solar radiation received at the Earth's surface is often referred to as "global radiation," which is the summation of the direct, diffuse, and reflected components. Understanding these components and their variations is essential for a range of applications, including solar energy generation, climate modeling, and meteorology [7][11].

I.2.2. Photovoltaic Energy Technologies

I.2.2.1 Photovoltaic Conversion «Photovoltaic Effect»

The photovoltaic effect is the foundation of solar energy technology, enabling the direct conversion of sunlight into electricity without the need for moving parts or heat-based processes.

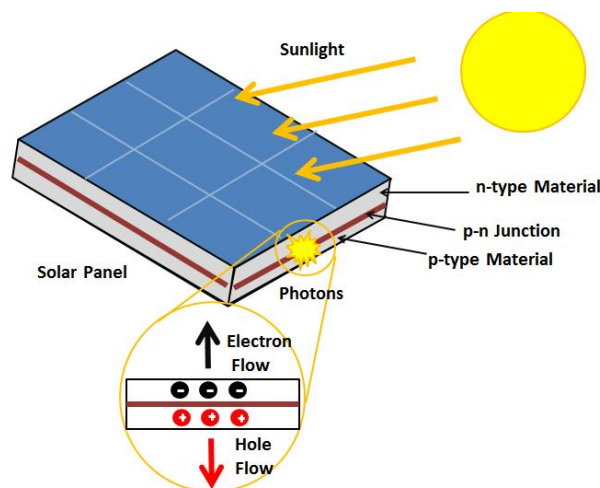


Figure I.3 : Photovoltaic Effect.

The principle of photovoltaic conversion, often referred to as the "photovoltaic effect," is the fundamental physical process underlying the operation of photovoltaic (PV) devices, such as solar cells [13][14][15]. The photovoltaic effect can be summarized as follows:

Absorption of Photons: When sunlight, composed of photons (particles of light), strikes the surface of a semiconductor material, such as silicon (commonly used in solar cells), the photons transfer their energy to the electrons in the material.

Generation of Electron-Hole Pairs: The absorbed energy excites electrons in the semiconductor's valence band to a higher energy state, creating electron-hole pairs. This process generates mobile charge carriers—an electron with a negative charge and a positively charged hole—within the semiconductor material.

Charge Separation: Due to the internal electric field within the semiconductor material, caused by its specific structure (typically a p-n junction in solar cells), the generated electron and hole are separated. The electric field directs the electron towards the n-type (negative) region of the semiconductor and the hole towards the p-type (positive) region.

Electric Current: As the separated charge carriers move through the semiconductor material under the influence of the electric field, an electric current is established. This current consists of electrons flowing from the n-type region to the p-type region and holes flowing in the opposite direction.

Collection of Current: Metal contacts on the surface of the semiconductor allow the collected electrons and holes to be harnessed as an electric current. This current can then be utilized for various electrical applications.

I.2.2.2 Types of Photovoltaic cells

Solar cells come in various types, each with its own set of characteristics, including efficiency and cost. However, across all types, solar cell efficiency generally ranges from 8% to 23%, indicating that a portion of the incoming sunlight can be converted into electricity [5][12].

a) 1st Generation Technology: Crystalline Silicon (c-Si) Solar Cells

These are the most prevalent and widely used PV cells, primarily available in two main forms: monocrystalline and polycrystalline. Monocrystalline cells offer higher efficiency but are costlier to produce, while polycrystalline cells are less efficient but more cost-effective [12][16][17].

● Monocrystalline Cells:

Exhibit excellent efficiency, typically in the range of 12% to 16% (with laboratory results reaching up to 23%).

Production involves a laborious and challenging manufacturing process, making them relatively expensive.

Requires a significant amount of energy to produce pure crystalline material.

- **Polycrystalline Cells:**

Offer lower production costs compared to monocrystalline cells.

Require less energy during the manufacturing process.

Display an average efficiency ranging from 11% to 13% (with laboratory efficiency reaching up to 18%).



Figure I.4 : Monocrystalline Cells & Polycrystalline Cells.

b) 2nd Generation Technology: Thin-Film Solar Cells

Thin-film technologies employ various materials, such as amorphous silicon (a-Si), cadmium telluride (CdTe), and copper indium gallium selenide (CIGS), to create solar cells. These cells are generally less efficient compared to crystalline silicon cells but are known for their lighter weight and flexibility, making them suitable for specific applications [16][17][18].

- **Amorphous Cells:**

Characterized by much lower production costs than crystalline cells.

Have lower efficiency, typically ranging from 8% to 10% (with laboratory efficiency reaching up to 13%).

Tend to have a shorter lifespan compared to crystalline cells.



Figure I.5 : Amorphous Cells.

c) **3rd Generation Technology: Organic Solar Cells (OPV)**

- **Multilayer cells:** superposition of multiple cells with different properties (using different energy bands allowing a wider sweep of the spectrum solar).
- **Concentration cells:** (allows the use of low energy photons which are not usually not absorbed by the cell). The yields obtained under concentration are very promising (around 30%).
- **Organic cells:** are photovoltaic cells with at least the active layer is made up of organic molecules. There are mainly cells organic photovoltaics and organic photovoltaic cells made of polymers molecular.

Organic photovoltaic cells utilize organic materials, typically polymers, to capture sunlight. They are lightweight and flexible, making them suitable for applications like solar-powered clothing and portable chargers.

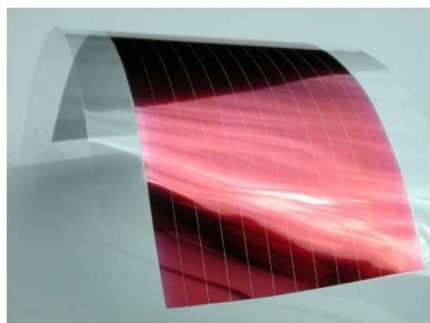


Figure I.6 : Organic cells.

In terms of material selection, silicon remains the predominant choice for industrial-scale PV cell production, owing to its abundance in nature, primarily as quartz sand (silicon dioxide). The main industrialized PV cell technologies to date include mono- and polycrystalline silicon (comprising over 80% of global production) and thin-film silicon-based cells, which can be amorphous or based on materials like Copper Indium Selenium (CIS) [5][12].

Additionally, there are other specialized PV cell types, including tandem cells that stack multiple layers of different materials for enhanced efficiency and cells made of organic materials, although they currently exhibit lower efficiency levels (around 3.6%) compared to their crystalline counterparts [16][17][18].

I.2.2.3 Parameters of a Photovoltaic Cell

Photovoltaic cells, the building blocks of solar panels, are characterized by several important parameters that determine their performance. These parameters are often obtained from current-voltage curves or through the characteristic equation of the cell [5][18][19]. Here are the key parameters of a photovoltaic cell:

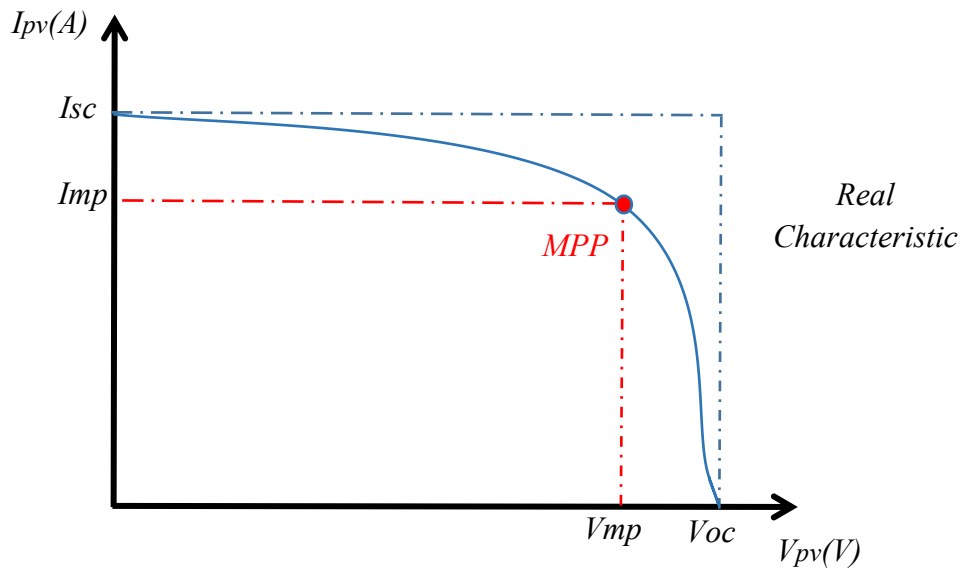


Figure I.7 : $I=f(V)$ characteristic of a photovoltaic panel.

a) Short Circuit Current (I_{sc}):

I_{sc} is the current at which the voltage across the cell is zero. In ideal conditions (zero R_s and infinite R_p), I_{sc} is essentially equal to the photocurrent generated by the cell.

b) Open Circuit Voltage (V_{oc}):

V_{oc} is the voltage at which the current delivered by the photovoltaic generator is zero. It represents the maximum voltage a solar cell or photovoltaic generator can produce.

c) Maximum Power Point (P_{max}):

P_m is the point on the current-voltage curve of a photovoltaic cell where the power output is maximized. Achieving maximum power is the goal for users of photovoltaic generators.

$$P_{max} = V_{mp} * I_{mp} \tag{I.1}$$

This point is associated with an optimal voltage and current (V_{mp} and I_{mp} , respectively) and is crucial for Maximum Power Point Tracking (MPPT) by charge controllers or inverters.

d) Energy Efficiency (η):

Energy efficiency represents the ratio of the maximum electrical power supplied by the cell (P_m) to the incident solar power. It is expressed as:

$$\eta = P_{max} / (G * A) \quad (I.2)$$

where G is the solar irradiance (illuminance) and A is the total surface area of the photocells. This parameter indicates how effectively the cell converts solar energy into electrical energy.

e) Form Factor (FF):

The form factor, also known as curve factor or filling factor, quantifies the quality of a photovoltaic cell. The form factor is defined as:

$$FF = P_{max} / (I_{sc} * V_{oc}) \quad (I.3)$$

It is the ratio of the maximum power supplied by the cell (P_m) to the product of the short-circuit current (I_{sc}) and the open-circuit voltage (V_{oc}) of an ideal cell (I_{max}).

Efficient cells have a form factor close to unity (around 0.7), and it decreases with increasing temperature due to parasitic resistances.

f) The Point of Operation (V_{mp} , I_{mp}):

To evaluate a photovoltaic cell's performance, the point of operation is crucial. It represents the cell's voltage (V_{mp}) and current (I_{mp}) at a specific operating condition.

The maximum power point (P_m) corresponds to the point of operation where the cell generates the highest power output.

g) Peak Power (P_c):

Peak power is the maximum electrical power that a photovoltaic module (or panel) can provide under standard test conditions (typically 25°C and an illumination of 1000 W/m²). It is an important specification for evaluating the performance of solar panels.

I.2.2.4 Constitution of a Photovoltaic Array

A single photovoltaic cell typically generates a very low power output, often just a few watts at a potential difference of less than one volt, which corresponds to the PN junction voltage. To harness more power from solar energy, multiple cells are

combined in series and parallel configurations to create a photovoltaic module or panel [20].

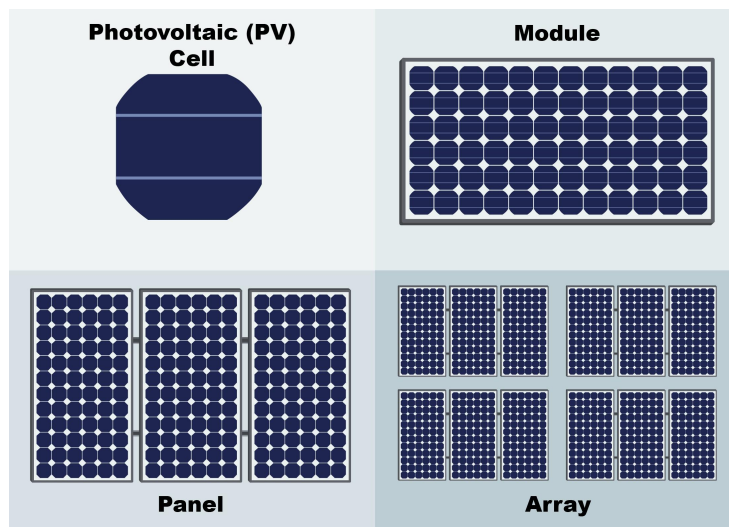


Figure I.8 : Constitution of a Photovoltaic Array.

I.2.2.4.a. Series Association of Cells:

Connecting cells in series increases the voltage of the photovoltaic generator (GPV). In this configuration, the cells are connected end-to-end so that they all carry the same current. The resulting characteristic of the series association is obtained by adding the elementary voltages of each cell. Equation ((I.4) & (I.5)) summarizes the electrical characteristics of cells in series:

$$V_{coNs} = N_s * V_{co} \tag{I.4}$$

$$I_{cc} = I_c \tag{I.5}$$

where:

V_{coNs} : The sum of the open circuit voltages of N_s cells in series.

I_{ccNs} : Short-circuit current of N_s series cell.

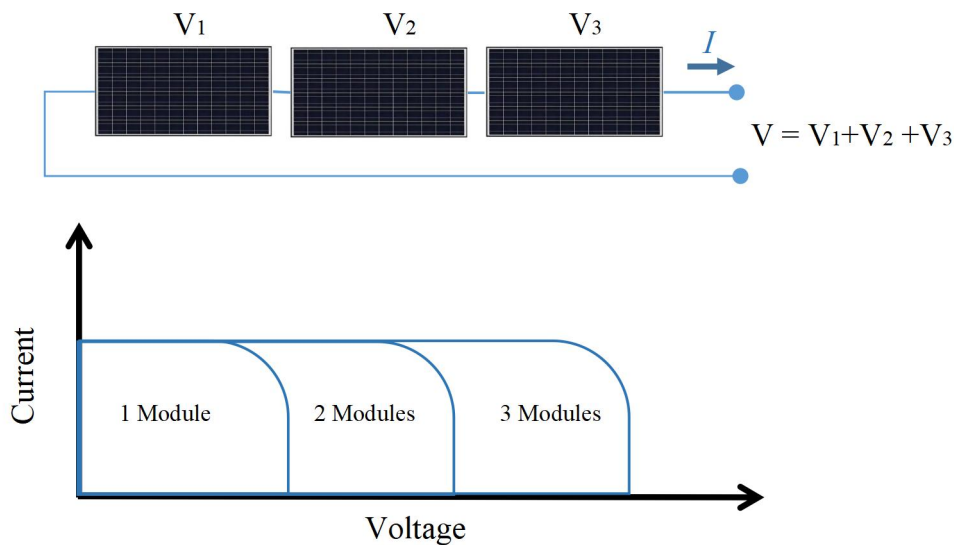


Figure I.9 : Series Association of Cells.

I.2.2.4.b. Parallel Association of Cells:

Connecting cells in parallel increases the output current of the generator. In this arrangement, the cells are connected side by side, and they all experience the same voltage. The resulting characteristic of the parallel association is obtained by adding the currents from each cell. The equations for parallel-connected cells are as follows:

$$I_{ccNP} = N_p * I_{sc} \tag{I.6}$$

$$V_{co} = V_{coNp} \tag{I.7}$$

where:

I_{ccNp} : The sum of the short circuit currents of Np cell in parallel.

V_{coNp} : Open circuit voltage of Np cells in parallel.

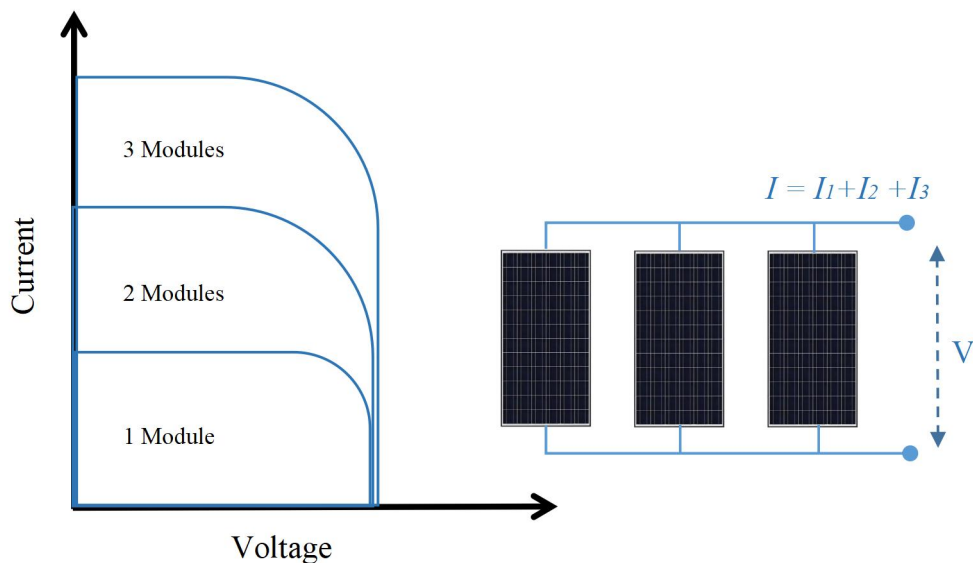


Figure I.10 : Parallel Association of Cells.

I.2.2.4.c. Mixed Association:

To achieve the desired total power output from the photovoltaic generator, a mixed wiring configuration (series/parallel) is often used. When cells are connected in series, their voltages add up, increasing the voltage of the generator. Conversely, when cells are connected in parallel, the current increases. This mixed association allows for flexibility in designing photovoltaic modules and panels that can meet specific power and voltage requirements for different applications.

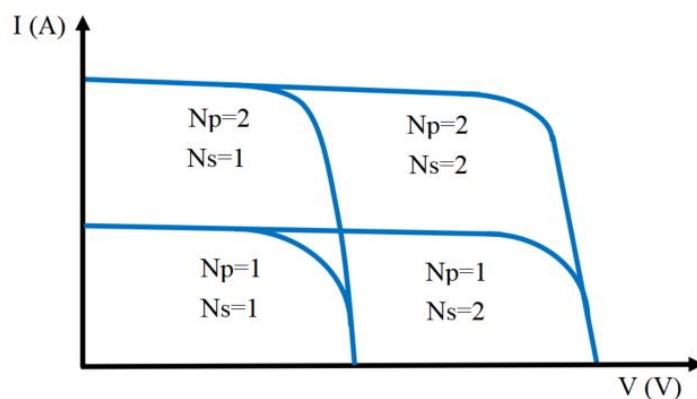


Figure I.11 : Mixed Association.

I.2.2.4.d. The solar panel:

The solar panel or (solar field) consists of photovoltaic modules interconnected in series and/or parallel in order to produce the required power. These modules are mounted on a metal frame which allows the solar field to be supported with a specific tilt angle [21].



Figure I.12 : Solar panels.

I.2.3. Different Types of Photovoltaic Systems

Photovoltaic systems can be categorized into three main types: those connected to the electricity grid, standalone systems, and hybrid systems [22][23].

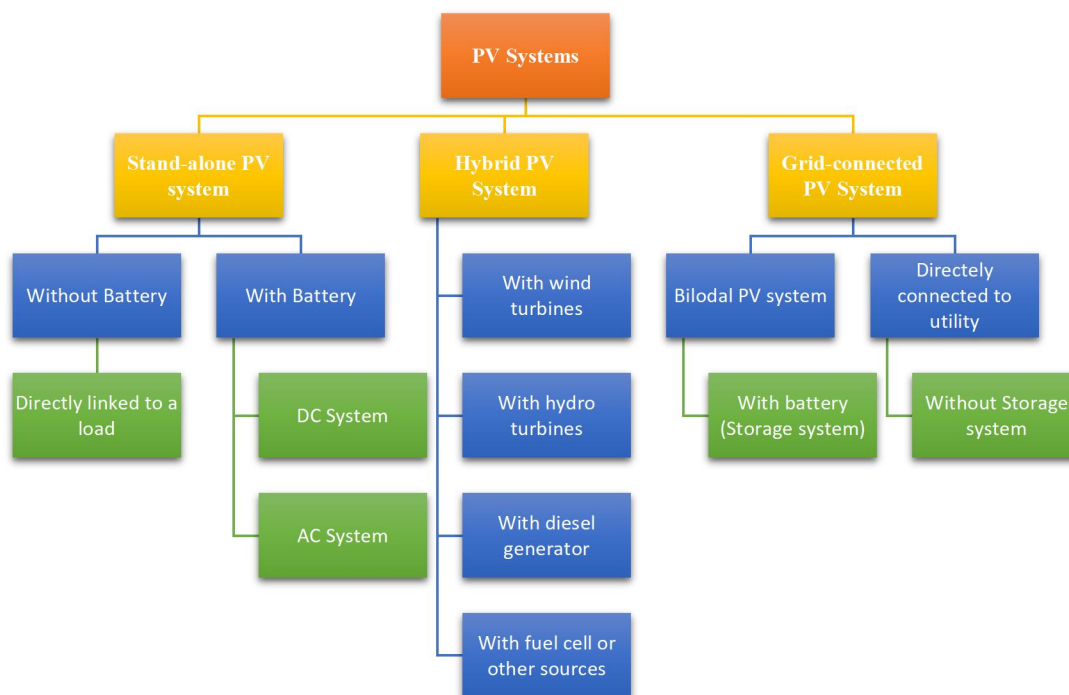


Figure I.13 : Photovoltaic Systems classification.

I.2.3.1 Systems Connected to the Grid:

Photovoltaic energy production systems that are connected to an existing electricity grid represent a shift towards decentralization in the electricity network. In this setup, energy is generated closer to where it will be consumed, reducing the need for significant expansions of transmission and distribution infrastructure. These grid-connected systems generate their own electricity and can feed excess energy back into

the grid. They also have the capability to draw energy from the grid when needed. Additionally, these systems can serve as backup power sources during network outages.

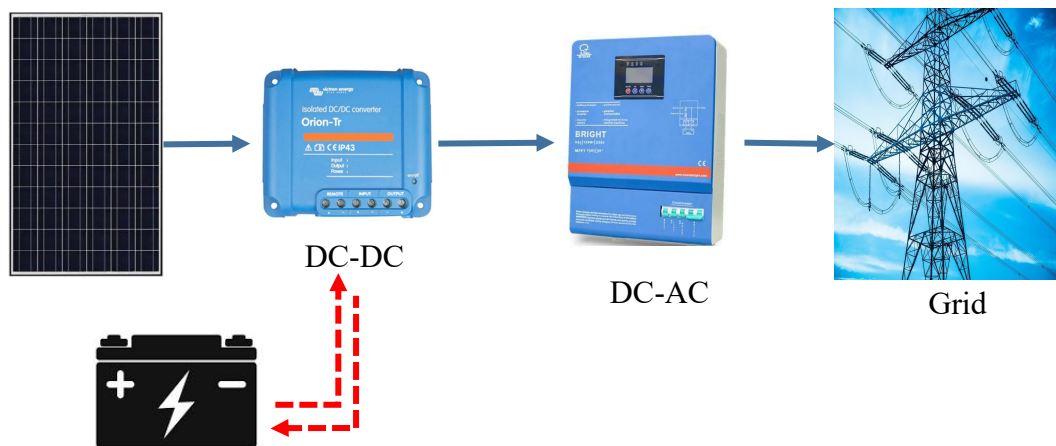


Figure I.14 : Systems Connected to the Grid.

I.2.3.2 Standalone Systems:

Standalone photovoltaic systems are designed to provide power to one or more consumers located in areas that are isolated from the electricity grid. There are two subtypes of standalone systems:

a. Autonomous System Without Battery: In this configuration, the load is directly powered by the photovoltaic panels. The energy production from the panels is sufficient to meet the load's operational requirements without the need for energy storage in batteries.

b. Autonomous System With Battery: These systems incorporate a battery component that stores excess energy generated by the photovoltaic panels. This stored energy can be used at any time, even when there is no solar radiation available. Batteries are essential for providing continuous power in the absence of sunlight.

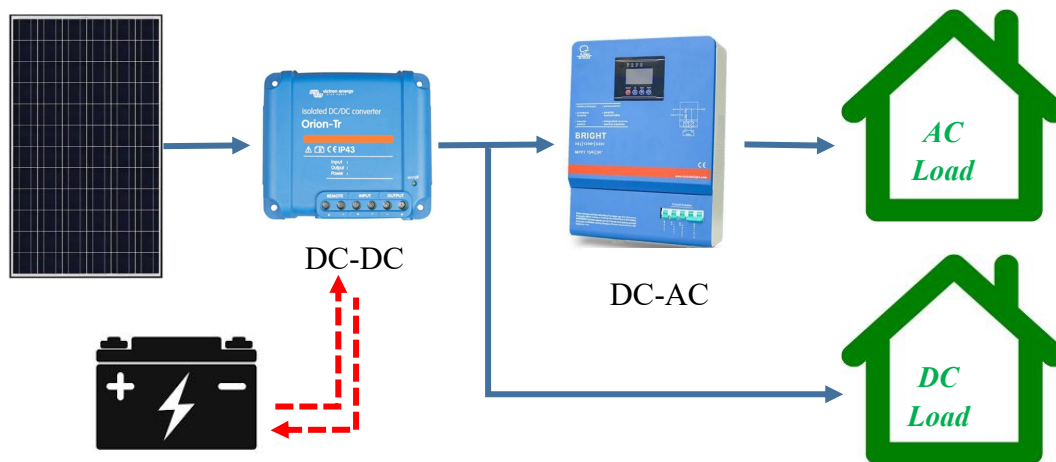


Figure I.15: Standalone Systems.

I.2.3.3 Hybrid Systems:

Hybrid systems with renewable energy sources are electrical systems that combine multiple energy sources, with at least one of them being renewable. This type of system is particularly suitable for remote locations where it's crucial to have a consistent supply of electricity. Hybrid systems are often deployed in areas where transporting conventional fuel for power generation is costly and where it may not yet be economically viable to rely solely on photovoltaic systems with batteries. They find application in sensitive and strategic areas such as telecommunications relays, border crossings, isolated housing, and other scenarios where access to the conventional electricity grid is limited or non-existent.

The choice of system type depends on factors such as energy requirements, grid availability, and the cost-effectiveness of energy storage solutions.

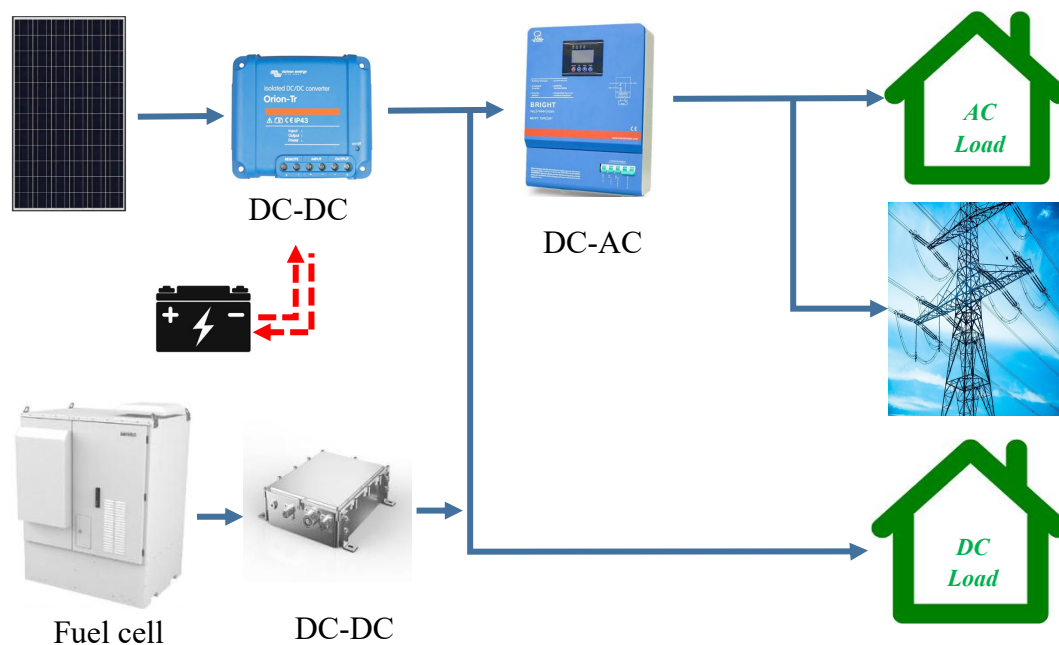


Figure I.16 : Hybrid Systems.

I.2.4. Advantages and Disadvantages of PV Solar Energy

Photovoltaic systems offer both advantages and disadvantages, where it should be considered when planning and implementing solar energy [5][12][19][24], which are outlined as follows:

I.2.4.4 Advantages:

- Non-Polluting: Photovoltaic systems are environmentally friendly and produce no emissions or odors, making them a clean energy source.
- Reliability: They can operate autonomously for extended periods without human intervention, ensuring reliable power generation.

Chapter 01: State of Art on Photo-Voltaic and Pumping Systems

- Independence: Photovoltaic systems don't rely on other energy sources or fuel supplies, making them self-sufficient.
- Compatibility: They can be integrated with other energy sources to enhance system reliability and energy availability.
- Weather Resistance: Photovoltaic systems are durable and can withstand harsh weather conditions, including snow and ice.
- Abundant and Free Fuel: Solar energy is derived from sunlight, which is abundant and freely available.
- High Reliability: Photovoltaic installations have no moving parts, resulting in high reliability. This makes them suitable for remote and isolated areas and even for use in spacecraft.
- Modular Design: The modular nature of photovoltaic panels allows for flexible system configurations tailored to varying energy needs, ranging from small-scale to large-scale applications.
- Environmental Friendliness: Photovoltaic technology is ecologically friendly because it generates electricity without pollution, noise, or environmental disturbance.
- Reduced Transport Costs: Solar energy eliminates the need for transporting fossil fuels, reducing associated costs and risks.

I.2.4.5 Disadvantages:

while photovoltaic systems offer numerous environmental and operational advantages, they also come with some limitations, including:

- High Manufacturing Cost: The production of photovoltaic modules involves high-tech processes, resulting in relatively high manufacturing costs.
- Moderate Efficiency: The efficiency of photovoltaic modules typically ranges from 10% to 15%, which means a portion of the sunlight they capture is converted into electricity.
- Weather Dependency: Photovoltaic systems rely on sunlight, so their energy generation is dependent on weather conditions. They are less effective on cloudy or rainy days and during nighttime.
- Low Voltage Output: Photovoltaic generators produce low-voltage DC (typically less than 30 V), requiring the use of inverters to convert the electricity to the higher-voltage AC used by many devices.
- Compatibility Issues: Many devices in the market operate on 230 V AC, which may necessitate additional equipment, like inverters, to use the power generated by photovoltaic systems.

- Energy Storage: For continuous use, it may be necessary to invest in energy storage systems, such as batteries, which can increase costs.
- Space Requirements: Solar panels require a certain amount of space for significant electricity production, which can be a limitation in densely populated urban areas.
- Environmental Impact of Manufacturing: The manufacturing of solar panels can have an environmental impact due to the use of specific materials, although this impact is typically outweighed by the environmental benefits of emissions-free electricity production.

I.3. Solar Photovoltaic Pumping System

A Solar Photovoltaic Pumping System is an innovative and sustainable solution designed to harness solar energy to power water pumps for various applications, including agriculture, irrigation, livestock watering, and domestic water supply. This technology addresses the need for reliable and environmentally friendly water pumping, particularly in regions with abundant sunlight and limited access to grid electricity.

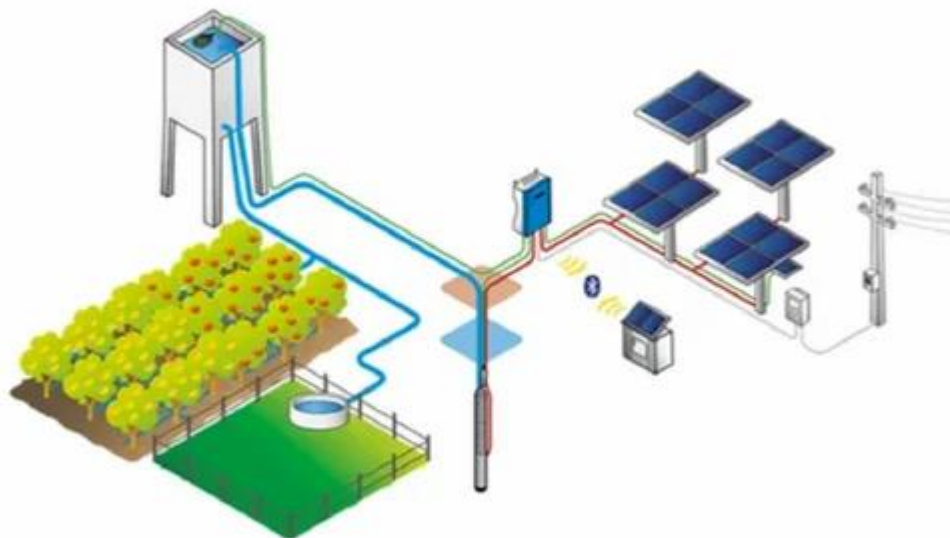


Figure I.17 : Solar Photovoltaic Pumping System.

A pump is a machine engineered to convert mechanical input power into hydraulic power efficiently. It is directly coupled to the motor and is characterized by torque, speed, and flow rate. The success of a pump system depends on the compatibility between the pump and the motor[7][18].

The term "pump" describes any device that draws a fluid from a low-pressure area and delivers it to a higher-pressure area. In essence, a pump's role is to increase fluid pressure. This pressure increase, facilitated by the pump, results from the conversion of mechanical energy supplied by a motor driving the pump into an

enhancement of hydraulic energy within the liquid as it moves from the pump's inlet to its outlet.

The volume of water pumped in a solar photovoltaic pumping system depends on several key factors:

- Solar Radiation Level: This parameter quantifies the available solar energy, which is a critical factor for power generation.
- Photovoltaic Generator: The performance of the photovoltaic generator, including the efficiency and capacity of the solar panels.
- Ambient Temperature: The temperature of the surrounding environment, as temperature can influence the efficiency of the photovoltaic system.

I.3.1. Composition of a PV Pumping System

Water pumping using solar energy is a common application for tasks like irrigation and providing drinking water. The system's performance depends on site-specific factors like sunlight, ambient temperature, and geographical obstacles. It also relies on the efficiency of various components, including photovoltaic (PV) modules, inverters, motors, and pumps. A PV pumping system is a complex setup with interactive elements where each component affects the others. These components include the PV generator, the conversion system, the drive motor, the discharge pump, and the hydraulic circuit [18].

I.3.1.1 Photovoltaic Generator

The Photovoltaic Generator acts as the electrical energy source that drives the pump motor. It comprises multiple modules formed by connecting cells in series. Connecting panels in series and parallel allows us to achieve the required voltage and current.

I.3.1.2 Conversion System (Converters)

An energy converter is typically placed between the PV and the load. When dealing with a direct current (DC) load, it is referred to as a DC/DC converter, whereas for an alternating current (AC) load, it's called an inverter or a DC/AC converter. Besides converting the current, it also serves to protect the PV.

I.3.1.2.a. DC-DC Converters:

To extract the maximum available power from the PV and deliver it to the load, a common technique is to use a DC/DC converter. This process is controlled by adjusting its duty cycle.

I.3.1.2.b. DC/AC Inverters:

Inverters transform the DC produced by the PV into AC. Pumping inverters are usually variable frequency (f) inverters, allowing for pump speed variation. The

voltage-to-frequency ratio (U/f) remains constant. The AC frequency is directly proportional to sunlight intensity.

I.3.1.3 Drive Motors:

To operate a pump, a drive mechanism is necessary to induce rotation. The choice of the pump drive depends on various factors, including efficiency, operational flexibility, system reliability, and low starting power. Two main types of motors are commonly used for PV pumping applications:

I.3.1.3.a. Direct Current (DC) Motors:

These motors are often preferred for PV pumping systems due to their ease of control, natural decoupling between flux and torque, and simplicity. Since PV modules produce DC, no inverter is required. Commutation of current in the rotor of a DC motor is done using brushes made of carbon and graphite or by electronic commutation. Types of DC motors include independently excited motors, parallel excitation motors, series excitation motors, and compound excitation motors. It's important to note that DC motors may require more maintenance, resulting in additional costs, and have limitations related to switch arcing, which can restrict their size and speed in certain areas.

I.3.1.3.b. Alternating Current (AC) Motors:

In recent years, the availability of inverters capable of controlling AC motor speed has allowed for their use in solar pumping applications. There are two main types of AC machines:

- **Synchronous Motors:** These motors have an output shaft speed equal to the speed of the rotating field. There are three types: wound rotor synchronous motors, reluctance synchronous motors, and permanent magnet synchronous motors.
- **Asynchronous Motors (Induction Motors):** These motors, known as induction machines, are increasingly used in industrial settings due to their robustness, availability, efficiency, low cost, and minimal maintenance requirements. PV pumping systems driven by asynchronous motors have attracted significant interest from researchers and manufacturers. However, they require a variable frequency inverter to control speed, which adds to the cost.

I.3.1.4 Pumps

For solar pumping systems, centrifugal and volumetric pumps are the most commonly used types due to their better efficiency. Other pump types that operate on different principles are generally not recommended for solar pumping applications due to their lower efficiency [18][25]. The choice of pump depends on the application and the water source (surface water, river, well, etc.). Centrifugal pumps are designed for constant depth and have flow rates that increase with rotational speed, while

volumetric pumps have nearly independent discharge rates and are directly proportional to rotational speed. Where the pumps fall into two primary categories:

- Centrifugal Pumps
- Volumetric Pumps

The choice between these two types of pumps depends on the fluid flow conditions. In general, if the goal is to increase fluid pressure, positive displacement pumps are preferred, while if the aim is to boost flow rate, centrifugal pumps are more suitable[26][27].

I.3.1.4.a. The Volumetric Pump

A positive displacement pump operates by transmitting the kinetic energy from the motor through reciprocating movements, enabling the fluid to overcome gravitational forces by cyclically altering the volume connected to the suction and discharge ports. In a positive displacement pump, there is always a moving part within a cavity, and this movement varies the volume inside the cavity, propelling the liquid. A notable advantage of positive displacement pumps is their ability to transport fluids at very high pressures.

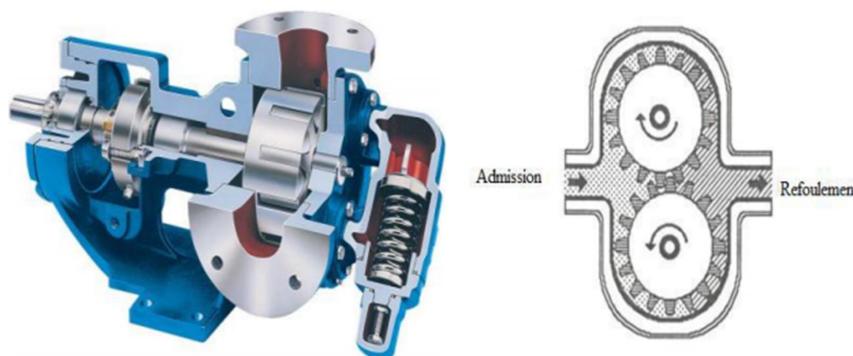


Figure I.18 : Volumetric Pump.

Positive displacement pumps encompass various types, including screw pumps, vane pumps, piston pumps, and diaphragm pumps. The latter two are commonly used in deep wells or boreholes, especially those exceeding 100 meters in depth. Typically, power is transmitted through an extended drive shaft, usually from a surface-mounted electric motor [28].

I.3.1.4.b. The Centrifugal Pump

The centrifugal pump is designed for applications requiring relatively constant total head (THM). The flow rate of this pump is directly proportional to the rotational speed of the motor. As the speed increases, the torque rises rapidly, and the head delivery depends on the square of the motor's speed. Thus, the motor's rotation speed must be quite high to ensure efficient flow. Power consumption, which is proportional to the product of flow rate (Q) and total head (HMT), varies with the cube of the

speed. Centrifugal pumps are typically chosen for situations with high flow rates and medium to shallow depths (10 to 100 meters).

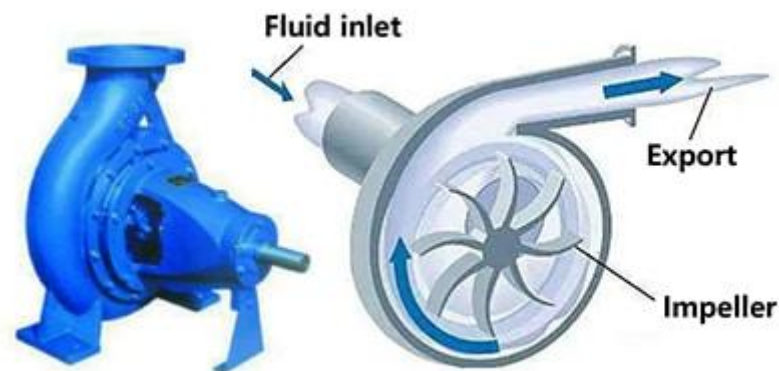


Figure I.19 : Centrifugal Pump.

Centrifugal pumps offer numerous advantages over other pump types, including a compact design, relatively quiet operation, compatibility with various electric motor types available in the market, and adaptability to a wide range of fluid handling challenges. These advantages make the centrifugal pump a preferred choice for many pumping systems[29][30].

I.3.2. Configurations of a PV Pumping System

There are various configurations of a PV (Photovoltaic) pumping system. Selecting the most suitable configuration for a specific application and location is crucial for ensuring the economic viability and long-term performance of the PV system [5][18]. Here, we provide an overview of these configurations:

I.3.2.1 Direct Current (DC) Pumping System:

In this configuration, the pump is driven by an electric motor that operates on direct current. It is a straightforward setup without the need for an inverter to convert the electricity generated by the PV panels. This configuration is efficient for applications where direct current is compatible with the pump's operation.

I.3.2.2 Alternating Current (AC) Pumping System:

In cases where the pump operates on alternating current (AC), an electronic DC/AC converter is necessary. This converter transforms the direct current generated by the PV panels into alternating current, which powers the AC motor driving the pump. AC pumping systems are versatile and can accommodate a wider range of pump types.

I.3.2.3 Battery-Backed System:

Batteries are sometimes essential components in PV pumping systems, especially when the water demand exceeds the supply rate from the water source. Batteries store excess energy generated by the PV panels, ensuring a continuous water supply even when sunlight is insufficient. Additionally, they can provide energy during periods of bad weather. However, it's worth noting that using storage batteries in these systems can present challenges such as relatively short battery life, maintenance requirements, reliability concerns, high costs, and the need for voltage regulators. For these reasons, some systems opt for alternative solutions like hydraulic storage to overcome these limitations.

I.3.2.4 Hydraulic Storage System:

In lieu of storage batteries, hydraulic storage systems can be employed. These systems store water as a form of potential energy. When energy is needed, the stored water is released to drive the pump, providing the required mechanical energy to lift water. This approach eliminates many of the drawbacks associated with battery-based systems, including their relatively short lifespan and maintenance needs. It can be an environmentally friendly and cost-effective alternative.

The choice of configuration depends on various factors, including the type of pump, the water source, the water demand, and the local climate. Each configuration offers its advantages and limitations, making it essential to assess the specific requirements of the application and site to determine the most appropriate setup for a PV pumping system.

I.4. PV pumping system Sizing Method

Sizing a pumping system involves a number of steps [31], including:

- ✓ Evaluation of water needs.
- ✓ Calculation of the hydraulic energy required.
- ✓ Determination of available solar energy.
- ✓ Choice of components.

I.4.1. Water Needs Assessment

Determining the water requirements for a specific population largely depends on their way of life. Estimated water needs for rural areas in impoverished countries are typically around 20 liters per person [31], where water needs for irrigation depend on several factors:

- ◆ Type of crops
- ◆ Meteorological factors (e.g., temperature, humidity, wind speed)

- ◆ Evapotranspiration of the soil
- ◆ Season of the year
- ◆ Irrigation method.
- ◆ It's important to rely on local practices and experience.

The reservoir's capacity is determined based on daily needs and the system's required autonomy.

I.4.2. Calculation of Required Hydraulic Energy

Once water needs for each month of the year and borehole characteristics are defined, the average daily hydraulic energy required is calculated:

$$E_h = g \cdot \rho \cdot V \cdot h / 3600 \quad (\text{I.8})$$

E_h : Hydraulic energy (Wh/day)

V : Water volume (m³/day)

h : Total head (m)

ρ : Water density (1000 kg/m³)

g : Acceleration due to gravity (9.81 m/s²)

The total pumping head (h) is the sum of static head (h_s) and dynamic head (h_d).

$$h = h_s + h_d \quad (\text{I.9})$$

Static head (h_s) is the distance from the static water level in the well to the highest point where water must be pumped.

Dynamic head (h_d) represents water losses in the piping.

Dynamic head (Darcy-Weisbach formula):

$$H_d = f \frac{L}{D} \frac{v^2}{2 \cdot g} \quad (\text{I.10})$$

f : Coefficient of friction of the pipe walls

L : Piping length (m)

v : Average fluid speed (m/s)

D : Pipe diameter (m)

g : Acceleration of gravity (m/s²)

It is Recommended that the dynamic head should not exceed 10% of the total pumping head.

I.4.3. Determination of Available Solar Energy

To size a PV pumping system, we need to understand how much solar energy is available throughout the year. Solar irradiance is the measure of solar energy received per unit area, typically expressed in watts per square meter (W/m²).

The sizing method involves calculating the average daily values of available solar irradiance (G_{jm}) for each month. This calculation takes into account the angle at which the PV modules are positioned (β) [31].

I.4.3.1 Inclination of Photovoltaic Generator (β):

The inclination (β) refers to the tilt or angle at which the PV modules are set relative to the horizontal plane. The goal is to find the optimal β that maximizes the ratio between solar irradiance (G_{jm}) and the required hydraulic energy (E_h) for pumping.

In simpler terms, we want to position the PV modules in a way that captures the most sunlight and generates the most electricity for our water pumping needs.

I.4.3.2 Sizing The Month:

The sizing process involves evaluating all 12 months of the year to determine which one is the most challenging or unfavorable in terms of solar energy availability.

This determination is based on a ratio known as the Relative Irradiance Efficiency (RIE), calculated as follows:

$$RIE = \frac{\text{Solar Irradiance } (G_{jm}(\beta))}{\text{Required hydraulic Energie } (E_h)} \quad (I.11)$$

Where:

$G_{jm}(\beta)$: is the daily solar irradiance for a specific inclination β .

E_h : is the daily required hydraulic energy for pumping.

The principle is to calculate RIE for each month and each inclination β . The month with the minimum RIE value is considered the most unfavorable because it has the lowest ratio of solar energy to hydraulic energy.

Conversely, the sizing month with the optimal inclination is the one with the highest RIE value, indicating the best match between available solar energy and the system's pumping needs [31].

I.4.3.3 Sizing of PV Generator:

Peak power of the PV generator under standard measurement conditions (1000 W/m² and 25°C):

$$P_C = \eta_g \cdot A \cdot G_{cs} \quad (I.12)$$

P_C : Output power under CSM (W)

η_g : Generator efficiency at reference temperature (25°C)

A : Active surface of the generator (m²)

G_{cs} : Illuminance in CSM (1000 W/m²).

I.4.3.3.a. Daily electrical energy, E_e :

$$E_e = \eta_{PV} \cdot A \cdot G_{jm}(\beta) \quad (I.13)$$

η_{PV} : Average daily generator efficiency under operating conditions

$G_{jm}(\beta)$: Average daily irradiance on the module plane at β (kWh/m²/day).

Generator efficiency η_{PV} can be calculated using the expression:

$$\eta_{PV} = F_m \cdot \left[1 - \gamma \cdot (T_c - T_{c,ref}) \right] \cdot \eta_g \quad (I.14)$$

F_m : Coupling factor, defined as the ratio of electrical energy generated under operating conditions to the electrical energy that would be generated if the system operated at the maximum power point.

γ : Cell temperature coefficient. γ takes values between 0.004 and 0.005/°C for mono and polycrystalline silicon modules, and between 0.001 and 0.002 for amorphous silicon modules.

T_c : Average daily cell temperature during sunny hours.

Required electrical energy is related to hydraulic energy through the expression:

$$E_e = \frac{E_h}{\eta_{mp}} \quad (I.15)$$

E_h : Average monthly hydraulic energy (kWh)

η_{mp} : Motor-pump sub-system efficiency.

Peak power of the generator:

$$P_C = \frac{G_{CS}}{F_m \left[1 - \gamma (T_c - T_{c,ref}) \right] G_{jm}(\beta) \eta_{mp}} \cdot E_h \quad (I.16)$$

I.4.3.3.b. Sizing of the Motor

The motor must be capable of handling the peak power of the PV generator.

I.4.3.3.c. Sizing of the Pump

Peak flow rate Q (m³/h):

$$Q = \frac{3,6 \cdot P_h}{g \cdot h} \quad (\text{I.17})$$

P_h : Required hydraulic power (W)

h : Total manometric head (m)

g : Acceleration due to gravity (9.81 m/s²)

Where : **Ph = f(PC):**

$$P_h = P_c \cdot \eta_{mpp} \quad (\text{I.18})$$

P_c : Peak electrical power supplied by the PV generator (W)

η_{mpp} : Peak efficiency of the motor-pump sub-system.

I.5. Conclusion

This chapter on photovoltaic solar energy and PV pumping system sizing offers a thorough exploration of the principles, technologies, and methodologies involved in harnessing solar power for sustainable water pumping applications. It begins by elucidating the photovoltaic conversion process, delving into the intricacies of photovoltaic cells, and outlining the constitution of photovoltaic generators. The advantages and disadvantages of solar energy are meticulously detailed. The chapter further categorizes photovoltaic systems into standalone, hybrid, and grid-connected configurations, considering their respective utilities and adaptabilities. Notably, the introduction of solar photovoltaic pumping systems emphasizes their innovative and eco-friendly approach to addressing water supply needs, particularly in regions blessed with abundant sunlight but limited access to conventional electricity grids. The chapter culminates by elucidating the systematic approach to sizing PV pumping systems, encompassing critical steps such as assessing water requirements, calculating hydraulic energy demands, evaluating solar energy availability, and selecting suitable system components. Overall, this chapter equips readers with a comprehensive understanding of photovoltaic technology's pivotal role in sustainable water pumping solutions.

II Chapter 02 : Overview On Fault Diagnosis And Fault Tolerant Control

II.1. Introduction

This chapter offers a comprehensive overview of crucial topics within the domain of fault diagnosis and fault-tolerant control. It covers the foundational concepts of fault diagnosis, encompassing the classification and various types of faults. Additionally, it explores the diverse methods and approaches for detecting and diagnosing faults. Moreover, the chapter delves into the fundamental principles of fault-tolerant control, drawing a distinction between passive FTC and active FTC.

Importance of Fault Detection and Diagnosis (FDD)

Faults are rare events that occur at inconvenient times in the complex systems that permeate every aspect of modern life. Where the complex systems are found in automobiles, ships, planes, computers, and every industry such as distillation columns, nuclear power reactors, and chemical reactors. As long as these systems are continuously improving how comfortable and enjoyable our lives are, it is essential to operate them safely, efficiently, and reliably [32].

Considering the solar pumping system is a complex system, where it relies on the efficient conversion of sunlight into electricity, and faults in the system can cause a drop in energy output, reduce the overall efficiency, and lead to downtime and lost revenue [33][34].

Fault detection and diagnosis can help to identify potential problems early, allowing for preventative maintenance to be scheduled and extending the lifespan of the system [35].

In addition, the system may generate high voltages that can be dangerous if not properly maintained, and fault detection and diagnosis can help to identify potential safety hazards and prevent accidents. Fault detection and diagnosis can also optimize the performance of these systems by identifying and correcting inefficiencies, which can lead to improved energy output, reduced costs, and increased revenue [33][35]. For solar pumping systems, early detection of faults is especially important because they often operate in remote areas, making it difficult and costly to perform repairs.

Fault detection and diagnosis involve the use of sensors or monitoring techniques to detect changes or abnormalities in the system. This can include changes in temperature, pressure, or voltage. Fault diagnosis involves identifying the specific cause of the fault, which can include identifying defective parts, incorrect settings, or other issues. Fault-tolerant control, on the other hand, helps to ensure the system continues to operate safely and efficiently, even in the presence of faults. It involves reconfiguring the system in response to faults, providing redundancy, and isolating the fault to prevent it from causing further damage [34][36].

One example of a fault that can occur in a PV solar pumping system is a fault in the solar panels. If the panels become damaged or covered with debris, the system's efficiency can be significantly reduced, leading to decreased energy output. Fault detection and diagnosis can help to detect this issue and fault-tolerant control can reconfigure the system to maintain operation, such as by increasing the use of backup battery power or switching to a lower energy mode [34][37].

Another common fault in PV solar pumping systems is related to the electrical motor of the pump. A failure in the motor can lead to reduced output, overheating, or even permanent damage. Fault-tolerant control can help to manage the power flow of the malfunctioning motor to ensuring that water supply is maintained [38].

In addition, faults can also occur in the system's electronic components, such as the inverter or charge controller. Fault detection and diagnosis can detect these faults and fault-tolerant control can take corrective action, such as bypassing the faulty component and switching to a backup system [39].

Overall, the combination of fault detection and diagnosis and fault-tolerant control is crucial for ensuring the safe and reliable operation of PV solar pumping systems. It helps to minimize the impact of faults, reduce downtime, extend the lifespan of the system, increase efficiency, and minimize maintenance costs. By providing redundancy and the ability to reconfigure the system in response to faults, these measures can help to ensure that water supply and irrigation can continue even in the presence of system failures.

II.2. Basic Concepts of Fault Diagnosis (FD):

Fault diagnosis is the systematic process of identifying and determining the underlying cause of a fault or malfunction in a system, device, or process. It involves a careful analysis of symptoms or observed behaviors to pinpoint potential faults and subsequently narrow down the root cause of the fault through a process of elimination or testing [40][41].

The primary objectives of Fault Detection and Diagnosis (FDD) are to monitor the system continuously and provide insights into the abnormal behavior exhibited by its components. The FDD procedure typically encompasses three fundamental steps:

- **Symptoms:**

Symptoms serve as indicators that something is amiss within the system. These indicators can manifest as abnormal readings, illuminated warning lights, unusual sounds, or other deviations from expected behavior. Recognizing and cataloging symptoms constitute the initial phase of fault diagnosis.

- **Fault Detection:**

Fault detection entails the use of sensors or similar monitoring techniques to identify changes or anomalies within the system. These deviations may manifest as alterations in temperature, pressure, voltage, or other measurable parameters. The goal is to detect any departure from the system's normal operating state.

- **Fault Identification:**

Fault identification involves the process of pinpointing the specific cause of the fault. This could encompass identifying defective components, incorrect system settings, or other issues that might lead to the observed abnormal behavior. It aims to determine the exact source of the problem.

After that the following steps are mandatory:

➤ **Fault Isolation:**

Fault isolation revolves around identifying which particular component or subsystem within the system is responsible for the detected fault. This can be achieved through a process of elimination, where potential culprits are ruled out systematically. Alternatively, more advanced diagnostic techniques may be employed for precise localization of the fault.

➤ **Repair or Corrective Action:**

Once the fault has been successfully diagnosed and the root cause is identified, appropriate corrective actions can be taken. These actions may involve replacing faulty components, adjusting system settings, or conducting other necessary repairs to rectify the issue and restore normal system operation.

➤ **Validation and Testing:**

Following the implementation of corrective actions, it is imperative to validate that the fault has been fully resolved. This validation process typically involves comprehensive testing of the system to ensure that it is functioning as expected. It serves as a crucial step to confirm that the fault has been effectively addressed and the system is operating reliably.

II.3. Fault classification and Types

Faults are unwelcome occurrences that can disrupt the seamless operation of complex industrial systems at various levels. To address and rectify these disruptions effectively, it is crucial to classify faults based on their origin and characteristics. Illustrated in Figure (II.1) is an open-loop dynamic system comprising three essential components: an actuator, a plant dynamic, and a sensor, all governed by inputs $u(t)$ and measured outputs $y(t)$. When diagnosing faults within dynamic systems, a comprehensive understanding of all potential causes for alarms or false alarms is essential. Actuators, components or parameters of the plant dynamics, and sensors all exhibit susceptibility to faults that may compromise the system's performance and reliability. Furthermore, to ensure that alarms are triggered only when necessary, it is imperative to consider the influence of system noise, often referred to as unknown input, as well as measurement noise in the fault diagnosis process [32][40][41][42].

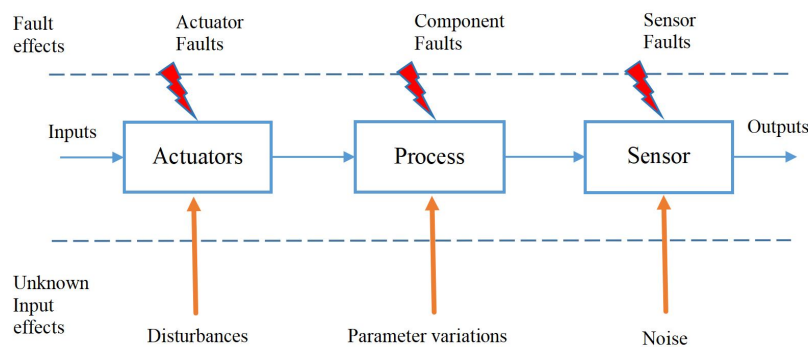


Figure II.1 : Fault type a effects in system.

II.3.1. Based on the Occurrence's Location:

Faults can be categorized into three primary types based on their physical location within a system: component faults, actuator faults, and sensor faults.

II.3.1.1 Actuator Faults:

These faults represent a partial or complete loss of control action. A total actuator fault, for instance, can occur due to issues like wiring damage, shortcuts, or foreign objects in the actuator, resulting in no actuation despite applied inputs. Partial actuator faults may produce only a fraction of the expected actuation due to factors such as hydraulic or pneumatic leakage or voltage fluctuations.

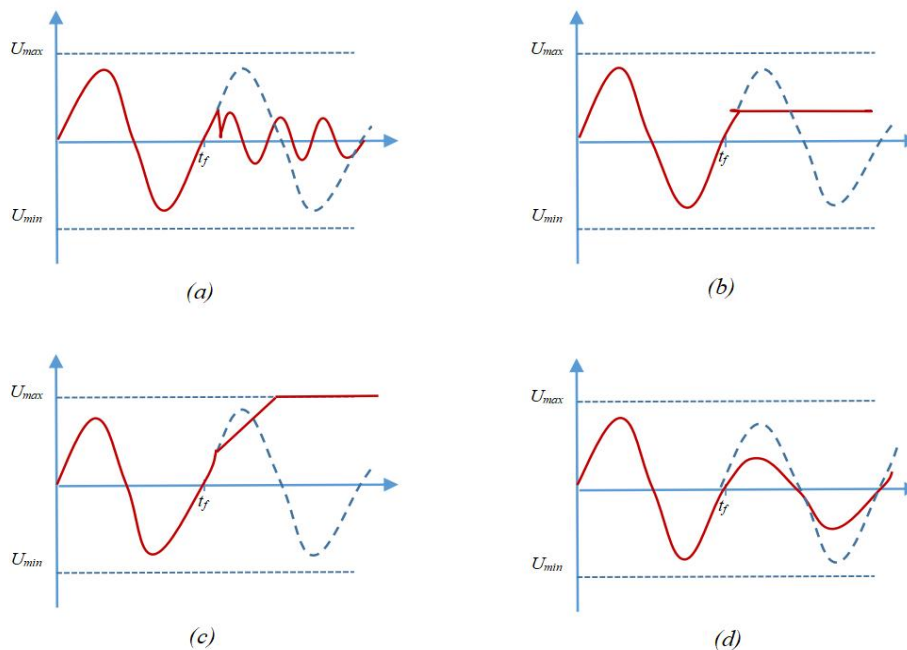


Figure II.2 : Common types of actuator faults: (a) floating trim, (b) lock-in-place, (c) hard-over failure, and (d) loss of effectiveness.

II.3.1.2 Sensor Faults:

Sensor faults involve incorrect readings from sensors and can be further divided into partial and total categories. Total sensor faults result in readings unrelated to the measured physical parameter due to issues like broken wires or lost contact with the surface. Partial sensor faults may still produce some useful information but can introduce inaccuracies, such as reduced gain, biased measurements, or increased noise.

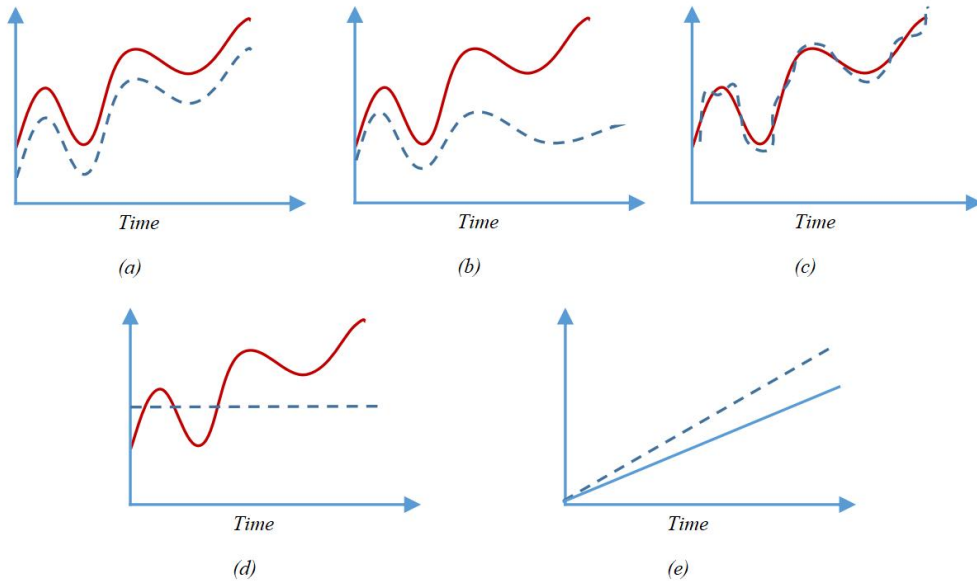


Figure II.3 : Common types of sensor faults: (a) bias, (b) drift, (c) performance degradation (or loss of accuracy), (d) sensor freezing, and (e) calibration.

II.3.1.3 Component Faults:

These are faults within the components of a complex system that do not fall into the sensor or actuator categories. Component faults often involve changes in parameters, such as damping constants, often caused by structural damage. They frequently lead to alterations in the dynamic behavior of nonlinear complex systems and are among the most commonly encountered types in fault diagnosis.

II.3.2. Based on the Behavior of Fault:

Faults can also be classified based on their time profiles, with three main categories: abrupt, incipient, and intermittent faults. Abrupt faults are nearly instantaneous and can result in severe equipment damage but are relatively easier to detect. Incipient faults develop slowly over time, often involving time-varying changes in system parameters, making them challenging to detect due to their gradual nature. Intermittent faults manifest at specific time intervals or under certain operating conditions, not consistently.

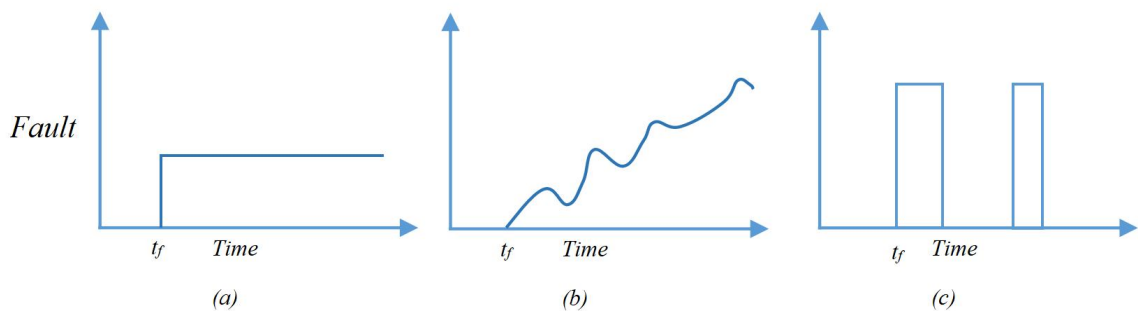


Figure II.4 : Types of faults based on behavior: (a) Abrupt fault, (b) Incipient fault, and (c) Intermittent fault.

II.3.3. Based on the Way Faults are Modeled:

Faults are further categorized as additive or multiplicative. Additive faults are used to represent component faults within the system, while sensor and actuator faults are typically multiplicative in nature. Additive faults involve an additional term that can influence system inputs or outputs and are commonly addressed through Fault-Tolerant Control (FTC). Multiplicative faults, on the other hand, are modeled as changes in parameter matrices, impacting the system's behavior. These distinctions are essential for effectively addressing and mitigating different types of faults.

II.3.4. Unknown Inputs:

It's critical to distinguish between faults and unknown inputs in a system. Unknown inputs refer to undesirable or unacceptable elements that are not errors but should be avoided to ensure proper system functioning. These inputs can manifest as environmental disturbances, unexpected changes in process variables during operation, or process/measurement noise. Significant unknown inputs can lead to system malfunctions or failures, and differentiating them from faults is crucial for accurate fault diagnosis and control.

II.4. Classification of fault detection and diagnosis methods

In realm of fault detection and diagnosis methods there is several methods and approaches.

II.4.1. Model-based approaches:

Refer to techniques that rely on mathematical models of the system being monitored. These models are typically derived from a deep understanding of the system's physical principles, behavior, and dynamics. The central idea behind model-based FDD is to compare the actual behavior of the system, as measured by sensors, with the expected behavior predicted by the mathematical model. Any discrepancies between the observed and predicted behavior are used as indicators of faults or anomalies within the system [43][44][45].

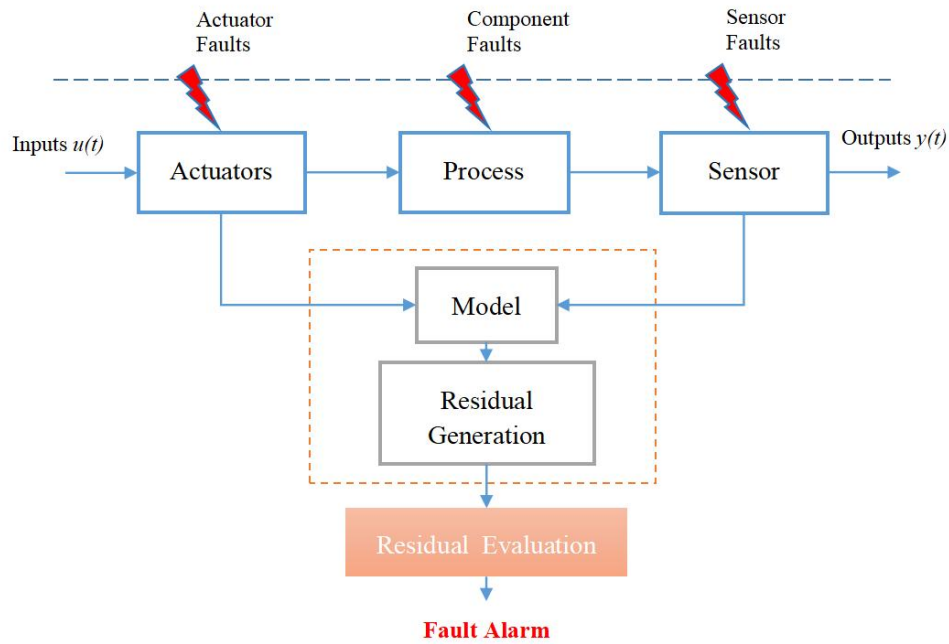


Figure II.5 : Model-based approaches.

Some of the basic elements and characteristics of model-based FDD are as follows:

Mathematical Models: Model-based FDD relies on mathematical equations or models that describe how the system should behave under normal operating conditions. These models can be simple, such as linear equations, or highly complex, involving differential equations, state-space representations, or other mathematical formalisms.

System Understanding: Building accurate models requires a deep understanding of the system's physics, dynamics, and interactions. Engineers and researchers use their knowledge of the system's components, operating principles, and expected behaviors to formulate these models.

Residual Analysis: In model-based FDD, the primary diagnostic tool is residual analysis. Residuals are the differences between the predicted behavior (as per the model) and the actual behavior of the system. Large or unexpected residuals indicate potential faults or deviations from normal operation.

Fault Detection: Model-based FDD can detect the presence of faults by monitoring the residuals. When a fault occurs, it often leads to discrepancies between the model's predictions and actual sensor measurements, causing the residuals to exceed predefined thresholds.

Fault Isolation: In addition to detecting faults, model-based FDD can sometimes isolate the specific component or subsystem that is responsible for the fault. By analyzing how the residuals change across different sensors and system components, it may be possible to pinpoint the exact source of the anomaly.

Fault Identification: In some cases, model-based FDD can also identify the nature or type of fault, such as whether it's a sensor fault, actuator fault, or a fault in a specific component. This identification helps in determining the appropriate corrective action.

Advantages: Model-based FDD is advantageous when there is a well-established understanding of the system's behavior and when it is feasible to develop accurate mathematical models. It can provide early detection of faults, reduce false alarms, and offer insights into fault causes.

Challenges: Model-based FDD can be challenging when the system's behavior is highly nonlinear, or when the models become too complex to handle in real-time. Developing and maintaining accurate models can also be resource-intensive.

II.4.2. Signal-based approaches:

It focus on analyzing sensor signals directly, without relying on detailed mathematical models of the system. These methods are particularly useful when the system's behavior is complex, poorly understood, or difficult to model accurately. Instead of modeling the system's dynamics, signal-based FDD techniques monitor sensor data and look for patterns, anomalies, or deviations from expected behavior that may indicate the presence of faults [46].

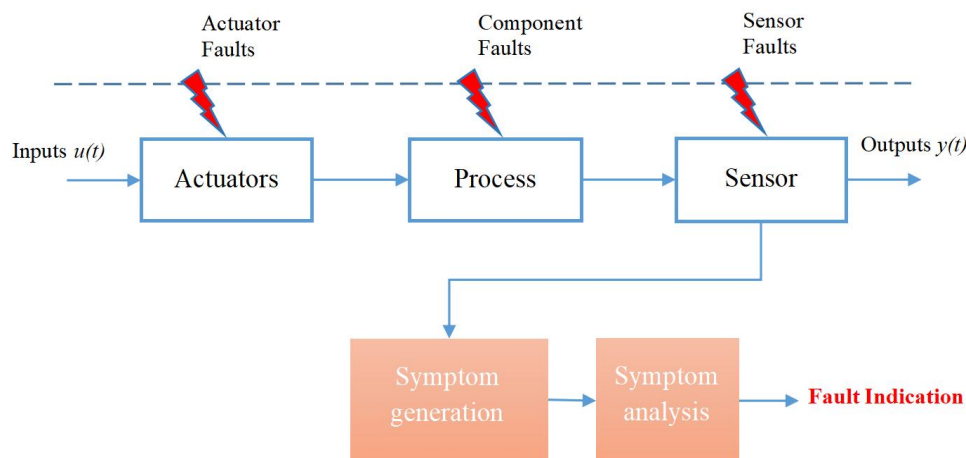


Figure II.6 : Signal-based approaches.

The following are some of the fundamental elements and characteristics of signal-based FDD:

Data-Driven Analysis: Signal-based FDD relies on historical or real-time sensor data to detect and diagnose faults. This data can include measurements of various system variables such as temperature, pressure, voltage, flow rates, or any relevant sensor readings.

Feature Extraction: One of the key steps in signal-based FDD is feature extraction, where specific characteristics or features of the sensor signals are calculated or derived.

These features could include statistical parameters (mean, standard deviation), frequency domain analysis (e.g., Fourier transforms), or other relevant metrics.

Baseline Comparison: Signal-based approaches often involve comparing the extracted features of the current sensor data with a baseline or reference dataset representing normal or healthy system behavior. Deviations from this baseline can be indicative of faults or anomalies.

Thresholding and Alarms: Thresholds or statistical bounds are set for each feature to determine when a signal deviation is significant enough to trigger an alarm. When the values of one or more features exceed these thresholds, an alarm is raised to signal a potential fault.

Pattern Recognition: Advanced signal-based FDD methods may employ machine learning and pattern recognition techniques to identify fault patterns in the sensor data. This can involve training algorithms to recognize specific fault signatures from historical data.

Fault Detection: Signal-based approaches are primarily focused on fault detection, alerting operators or control systems when deviations from normal behavior occur. These deviations serve as early warnings of potential issues within the system.

Data Fusion: In complex systems with multiple sensors, signal-based FDD often involves data fusion, where data from various sensors are combined to improve fault detection and reduce false alarms.

Advantages: Signal-based FDD is advantageous when accurate mathematical models are difficult to develop, or when the system behavior is highly nonlinear or dynamic. It can be effective in detecting a wide range of faults and is particularly suited for data-rich environments.

Challenges: Signal-based FDD may struggle with noisy data or variations in operating conditions. It may also face challenges in pinpointing the specific source or nature of a fault without additional information.

II.4.3. Knowledge-based approaches:

In the context of (FDD) rely on expert knowledge, rules, or heuristics to identify and diagnose faults within a system. These approaches are often used when there is a wealth of domain-specific knowledge available about the system and its potential faults. Knowledge-based FDD combines human expertise with computational methods to make informed decisions about the presence, nature, and causes of faults [47][48].

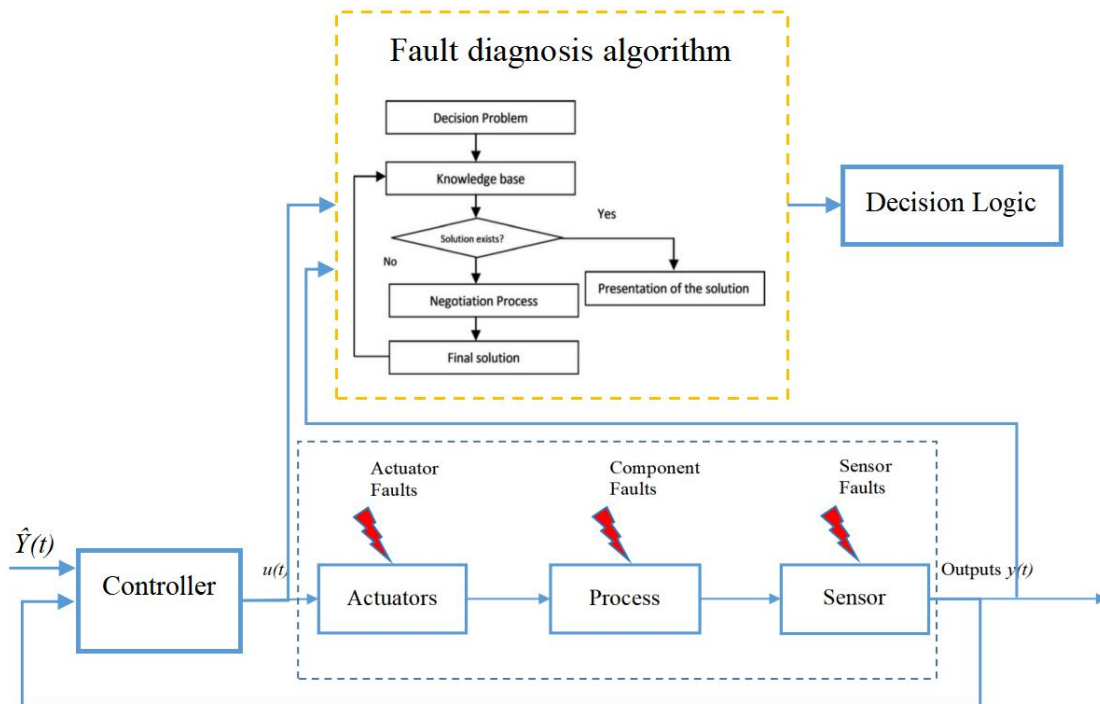


Figure II.7 : Knowledge-based approaches.

The key characteristics and aspects of knowledge-based FDD are:

Expert Knowledge: Knowledge-based FDD leverages the expertise of domain specialists or engineers who have an in-depth understanding of the system being monitored. These experts provide rules, guidelines, or knowledge bases that describe how the system should behave and how to detect and diagnose faults.

Rule-Based Systems: One common implementation of knowledge-based FDD is through rule-based systems. These systems consist of a set of rules that relate sensor measurements, symptoms, and observations to specific fault conditions. When certain conditions are met, the corresponding rule is triggered, indicating the presence of a fault.

Knowledge Bases: Knowledge-based FDD systems often include extensive knowledge bases that store information about the system's components, expected behaviors, potential fault modes, and diagnostic procedures. These knowledge bases are used to make informed decisions during fault diagnosis.

Inference Engines: Inference engines or reasoning mechanisms are employed to apply the rules and knowledge from the knowledge base to the current data from the system. The engine evaluates the data and draws conclusions about the presence and nature of faults.

Heuristics and Expert Judgment: Knowledge-based FDD can also incorporate heuristics and expert judgment. These are informal rules or guidelines based on the experience and intuition of domain experts. Heuristics help guide the diagnostic process.

Fault Diagnosis: Knowledge-based approaches are proficient at diagnosing faults and identifying their causes. They can provide information not only about the presence of a fault but also about its origin and potential implications.

Explanatory Capability: Knowledge-based FDD often offers explanations or recommendations for fault mitigation and corrective actions. This explanatory capability aids operators and maintenance personnel in understanding the issues and making informed decisions.

Advantages: Knowledge-based FDD is valuable when there is a substantial body of expert knowledge available, and it can be particularly effective in diagnosing complex or rare faults. It also provides interpretability and explanations for its diagnoses.

Challenges: Knowledge-based FDD depends on the quality and completeness of the knowledge base, which may require continuous updates and maintenance. It may struggle with novel or unforeseen faults that are not covered by existing rules.

II.4.4. Hardware-based:

(FDD) methods involve the use of dedicated hardware components and sensors to monitor the performance and condition of a system or equipment. These approaches are particularly useful when real-time and continuous monitoring is essential, and they often provide a high level of accuracy and reliability in detecting faults and anomalies [49]. Here are some key characteristics and aspects of hardware-based FDD:

Sensor Systems: Hardware-based FDD typically relies on a network of sensors strategically placed within the system or equipment under surveillance. These sensors continuously measure various parameters such as temperature, pressure, voltage, current, vibration, or other relevant variables.

Data Acquisition: Sensor data is collected and processed by specialized hardware devices or data acquisition systems. These systems are responsible for sampling, digitizing, and transmitting the sensor data to processing units.

Real-time Monitoring: One of the advantages of hardware-based FDD is its ability to provide real-time monitoring of the system's condition. This enables the immediate detection of faults as they occur or even before they manifest into critical issues.

Redundancy: Redundant sensors and hardware components may be used to ensure fault tolerance within the monitoring system itself. Redundancy helps maintain monitoring functionality even in the presence of sensor failures.

Diagnostics Algorithms: Hardware-based FDD systems often incorporate diagnostic algorithms that analyze sensor data in real-time. These algorithms can detect deviations from expected behavior and identify potential faults.

Alarm Generation: When a fault or anomaly is detected, hardware-based FDD systems can generate alarms or alerts to notify operators, maintenance personnel, or control systems. These alarms trigger appropriate actions to address the issue.

Distributed Monitoring: In complex systems, multiple sensors and monitoring devices may be distributed throughout various components or subsystems. This distributed approach allows for comprehensive system-wide monitoring.

Integration: Hardware-based FDD systems can be integrated with other control and automation systems to facilitate coordinated responses to faults. For example, they can trigger safety shutdowns or initiate backup systems.

Applications: Hardware-based FDD finds applications in a wide range of industries, including manufacturing, aerospace, automotive, energy, and healthcare. It is particularly valuable in critical systems where the consequences of faults can be severe.

Maintenance Planning: Continuous monitoring provided by hardware-based FDD allows for condition-based maintenance. Maintenance activities can be scheduled when they are most needed, minimizing downtime and reducing costs.

Challenges: Hardware-based FDD can be expensive to implement, especially in complex systems with numerous sensors. It also requires careful calibration, regular maintenance, and a robust data analysis infrastructure.

II.4.5. History-based:

(FDD) methods rely on historical data and patterns to identify faults and anomalies within a system. These approaches analyze the system's past behavior and compare it to current data to detect deviations that may indicate the presence of faults [49]. Here are key characteristics and aspects of history-based FDD:

Historical Data Collection: History-based FDD begins by collecting and storing historical data from sensors and system measurements. This historical data provides a baseline of normal system behavior.

Data Analysis: Analytical techniques, statistical methods, and machine learning algorithms are applied to historical data to identify typical patterns, trends, and statistical properties of the system's behavior under normal operating conditions.

Pattern Recognition: History-based FDD relies on pattern recognition to identify deviations from historical norms. This can involve statistical process control charts, time series analysis, or more advanced machine learning models.

Alarm Thresholds: Thresholds or statistical bounds are established based on historical data to define acceptable variations in system behavior. When current data exceeds these thresholds, it triggers an alarm or alert.

Change Detection: History-based FDD monitors for changes in the statistical properties of data, such as mean, variance, or distribution shape. Significant changes may indicate the presence of a fault or anomaly.

Time-Series Analysis: Time-series data, which captures how system variables change over time, is a fundamental component of history-based FDD. Techniques like autoregressive models or moving averages can be used to analyze time-series data for deviations.

Feature Extraction: Historical data can also be used to extract features or statistical parameters that describe the system's behavior, such as mean, standard deviation, skewness, or kurtosis.

Learning Algorithms: Machine learning algorithms, including supervised and unsupervised learning techniques, can be employed to model normal system behavior based on historical data and detect anomalies that deviate from this learned model.

Training and Validation: To build accurate models of normal behavior, history-based FDD methods often require training periods during which the system's behavior is monitored and learned. Validation data may be used to assess model performance.

Alarm Generation: When deviations from historical norms are detected, history-based FDD systems generate alarms or alerts to notify operators or control systems of potential issues.

Advantages: History-based FDD is valuable for detecting gradual or slowly developing faults that may not be apparent through real-time monitoring alone. It is data-driven and can adapt to changes in system behavior over time.

Challenges: Accurate history-based FDD depends on having sufficient historical data, and it may not be as effective for rapidly changing or transient faults. It may also require continuous updates and retraining to account for system evolution.

II.4.6. Hybrid approaches:

In the context of fault detection and diagnosis (FDD) refer to methods that combine multiple FDD techniques or strategies to enhance fault detection and diagnosis capabilities. These approaches leverage the strengths of different FDD methods to improve accuracy, robustness, and overall performance [40][41][50]. Where the key characteristics and aspects of hybrid FDD approaches are:

Integration of Multiple Methods: Hybrid FDD combines two or more FDD techniques, such as model-based, signal-based, knowledge-based, or history-based methods. These methods may complement each other by addressing different aspects of fault detection and diagnosis.

Diversity in Data Sources: Hybrid approaches may utilize data from various sources, including sensors, historical records, expert knowledge, and mathematical models. By combining diverse data sources, they aim to provide a more comprehensive view of system behavior.

Sequential or Parallel Execution: Hybrid FDD methods can be implemented in a sequential or parallel manner. In sequential execution, different FDD methods are applied one after another, with each method serving as a backup if the previous one fails. In parallel execution, multiple FDD methods run simultaneously, and their results are combined or voted upon to make decisions.

Complementary Information: Each FDD method within a hybrid approach provides unique insights and advantages. For example, model-based methods excel at understanding system dynamics, while signal-based methods are effective at capturing real-time anomalies. Knowledge-based methods provide expert guidance, and history-based methods capture long-term trends and patterns.

Enhanced Fault Detection: Hybrid FDD can improve fault detection by reducing false alarms and increasing sensitivity to faults. When multiple methods independently flag a potential fault, the likelihood of a true fault occurrence is higher.

Fault Isolation and Identification: Hybrid approaches can enhance the capability to isolate the source of a fault and identify its nature. By cross-referencing results from different methods, it becomes easier to pinpoint the specific component or subsystem responsible for a fault.

Robustness: Combining multiple FDD methods can make the system more robust against uncertainties, sensor failures, or modeling inaccuracies. When one method faces challenges, others can compensate.

Adaptability: Hybrid FDD systems can adapt to changing system conditions or evolving fault patterns. By integrating diverse techniques, they can adjust their strategies to remain effective over time.

Implementation Challenges: Developing and deploying hybrid FDD systems can be complex and resource-intensive. It requires careful integration of different algorithms, data sources, and decision-making processes.

Performance Evaluation: Assessing the performance of hybrid FDD approaches often involves validating their effectiveness through testing and simulation, considering factors such as fault detection rates, false alarm rates, and fault identification accuracy.

Applications: Hybrid FDD is applied in various industries, including manufacturing, aerospace, automotive, energy, and healthcare, where reliability and safety are critical.

The various fault detection and diagnosis (FDD) methods and approaches differ in their fundamental strategies. Model-based approaches rely on mathematical models of the system to predict and compare expected behavior with real data. Signal-based approaches analyze sensor data directly, focusing on detecting patterns or anomalies. Knowledge-based methods use expert domain knowledge and predefined rules for decision-making. Hardware-based FDD involves dedicated sensors and real-time data acquisition. History-based FDD analyzes historical data for trends and deviations. Hybrid approaches combine multiple methods to enhance reliability and accuracy [32][40][41][43].

II.5. Fault Tolerant Control (FTC)

In the realm of control systems engineering, the concept of Fault Tolerant Control (FTC) has emerged as a crucial solution to address the vulnerability of complex technological systems to faults and malfunctions. These faults can range from minor component failures to critical sensor errors, and their occurrence can pose significant risks to the overall functionality, stability, and safety of industrial processes and systems. In this section, we delve into the fundamental concepts, classifications, and key approaches in the field of FTC [51].

II.5.1. The Need for FTC

Traditional control theory assumes ideal conditions, where all components function flawlessly and precisely. However, real-world systems often deviate from these ideal conditions due to various factors, including wear and tear, environmental conditions, and unforeseen component failures. The cumulative effects of these faults can jeopardize the stability and performance of control systems. Robust control theories, while effective to a certain extent, may not always provide a sufficient solution to address the dynamic challenges posed by faults in complex systems [40][41][43].

II.5.2. Classification of FTC

FTC schemes can be broadly categorized into two main approaches: passive FTC and active FTC.

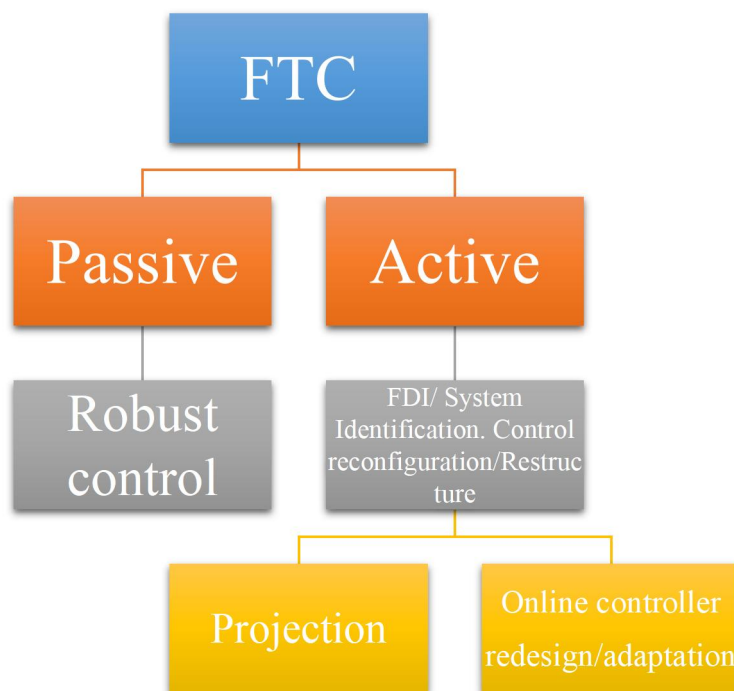


Figure II.8 : Classification of FTC.

II.5.2.1 Passive FTC

In passive FTC, the focus is on designing control systems that are robust against predefined fault scenarios. These scenarios are considered during the initial design and manufacturing phase. Passive FTC relies on redundancy and robust compensators to mitigate the effects of faults. While this approach provides a level of fault tolerance, it has inherent limitations. One of the key challenges in passive FTC is the extreme dependency on hardware redundancy. Although redundancy can enhance system reliability, it comes at the cost of increased production expenses, size, and weight.

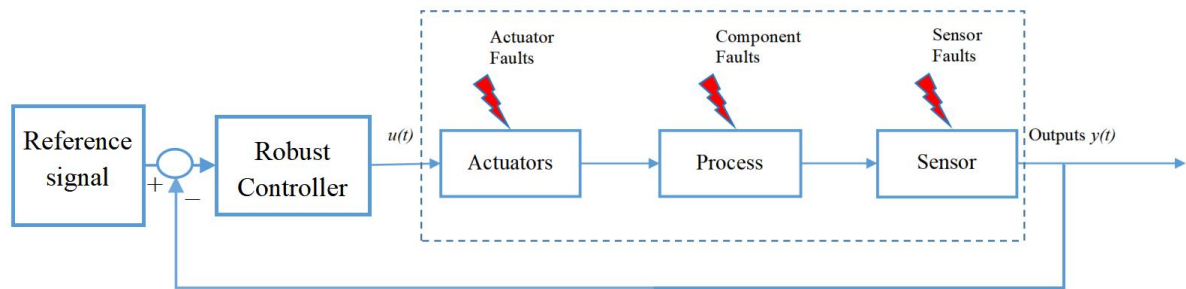


Figure II.9 : Architecture of the passive FTC.

Furthermore, passive FTC strategies are conservative, as they aim to ensure system stability under various scenarios, potentially sacrificing optimal performance in normal conditions. This approach may not be suitable for situations where a high level of performance is required even in the presence of faults.

II.5.2.2 Active FTC

Active FTC, on the other hand, takes a more dynamic and adaptive approach. It reacts to detected faults in real-time and reconfigures control actions to maintain stability and performance. Active FTC can be seen as an adaptive control scheme that responds actively to fault events. It can use pre-computed control laws or synthesize new ones on-the-fly based on fault information. This approach is more versatile and can potentially achieve better performance than passive FTC [35].

Key factors for the effectiveness of active FTC include the accuracy of fault detection, robustness to imperfect fault information, and the speed of fault recovery. Active FTC systems typically consist of three main steps: detection, supervision, and control.

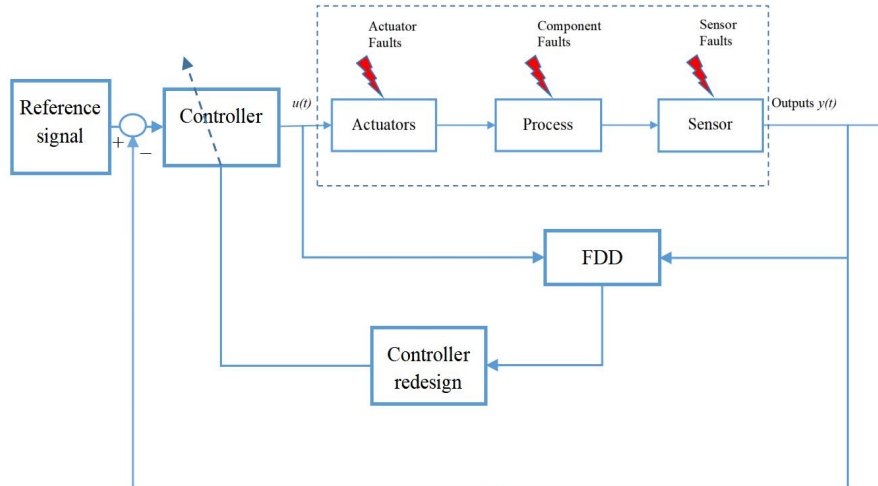


Figure II.10 : Architecture of the active FTC.

II.5.3. Fundamental Mechanisms in FTC

FTC schemes rely on two fundamental mechanisms: Fault Detection and Isolation (FDI) and Reconfiguration Control (RC). FDI is responsible for detecting and locating faults within the system, while RC is responsible for reconfiguring the control actions to compensate for the faults. These mechanisms are often treated separately, but their interaction and influence on each other remain areas of ongoing research [51][52].

II.5.4. Challenges and Considerations

Both passive and active FTC approaches have their own challenges and considerations. Passive FTC relies heavily on hardware redundancy, leading to increased costs and complexity. It assumes that the system will maintain stability under predefined fault scenarios, which may not cover all possible fault conditions. Additionally, passive FTC strategies tend to be conservative, prioritizing robustness over optimal performance.

Active FTC, while more adaptable, requires accurate fault detection, robustness to imperfect fault information, and swift fault recovery. The accuracy of the FDI unit is critical in ensuring the effectiveness of active FTC. It also demands a high level of integration between the detection, supervision, and control phases.

In conclusion, FTC has emerged as a vital field in control systems engineering to ensure the reliability, safety, and performance of complex technological systems in the face of faults and malfunctions. Understanding the distinctions between passive and active FTC, as well as the interplay between FDI and RC mechanisms, is essential for designing effective fault-tolerant control systems tailored to specific applications and requirements.

II.6. Conclusion

In Chapter 2, "Overview on Fault Diagnosis and Fault Tolerant Control," we embarked on a comprehensive exploration of the fundamental concepts and methodologies underlying

Chapter 02 : Overview On Fault Diagnosis And Fault Tolerant Control Chapter

fault detection, diagnosis, and fault-tolerant control (FTC). This chapter elucidated the paramount importance of fault detection and diagnosis in ensuring the robustness and reliability of complex systems, such as photovoltaic (PV) pumping systems. We also delved into the core principles and mechanisms of FTC, a crucial facet of ensuring system resilience in the face of faults.

Throughout this chapter, we laid the groundwork for a deeper understanding of fault detection, diagnosis, and fault-tolerant control. where it covers the foundational concepts of fault diagnosis, encompassing the classification and various types of faults. Additionally, it explores the diverse methods and approaches for detecting and diagnosing faults. Moreover, the chapter delves into the fundamental principles of fault-tolerant control, drawing a distinction between passive FTC and active FTC. The knowledge and insights gained from this exploration are instrumental in the subsequent chapters, where we delve into the applications and implementation of these techniques in the context of PV pumping systems. By comprehending the intricacies of fault management, we are better equipped to enhance the reliability and efficiency of these systems and tackle the challenges posed by faults head-on.

III Chapter 03 : PV Pumping System Modeling and Control

III.1. Introduction

Chapter 3, titled "PV Pumping System Modeling and Control," is a pivotal section in our exploration of photovoltaic pumping systems. This chapter follows a structured approach to dissect the system's intricate components and functions. We commence with a detailed introduction to our proposed system, encompassing photovoltaic panels, a boost converter, buck-boost converter for battery management, a three-phase inverter, an induction motor, and a centrifugal pump. Following this, we delve into the vital realm of system modeling, breaking down each component's behavior. Subsequently, we explore the system's control strategies, touching upon Maximum Power Point Tracking (MPPT) techniques, voltage control, battery management, inverter control using Sinusoidal Pulse Width Modulation (SPWM), as well as induction machine control via scalar control technique.

III.2. Proposed system description

The proposed system is a meticulously designed configuration with a purposeful choice of components to optimize energy utilization and enhance overall efficiency in a PV-based pumping system. At its core, photovoltaic panels (PV) are connected to a Boost converter, controlled by Maximum Power Point Tracking (MPPT) algorithms. This choice ensures that the PV system operates at its peak performance by tracking the maximum power point of the solar panel, thereby harnessing the maximum available solar energy. This not only increases energy harvest but also significantly reduces energy wastage, making it a vital choice in the system.

In addition, the system incorporates a battery connected to a buck-boost converter, serving the purpose of efficient energy storage and management. The buck-boost converter optimizes the battery charging and discharging process, ensuring that energy is stored and used effectively. This integration enhances system reliability and resilience, providing a stable energy supply even during periods of low sunlight.

Both the Boost and buck-boost converters are interconnected to a DC-Bus, facilitating seamless energy transfer between components. The DC-Bus control ensures efficient energy routing and minimizes energy losses during conversion, which is critical for maintaining high system efficiency.

The DC-Bus then connects to a three-phase inverter, which, in turn, feeds power to an induction motor. The choice of an induction motor offers benefits such as high reliability, low maintenance requirements, and suitability for continuous operation. It is coupled with a centrifugal pump, which is commonly used for water pumping applications due to its efficiency and reliability.

Furthermore, familiar control techniques such as Pulse Width Modulation (PWM) and scalar control are applied to the inverter, enabling control of the motor's speed. This ensuring that the centrifugal pump operates at its best capacity while minimizing energy consumption.

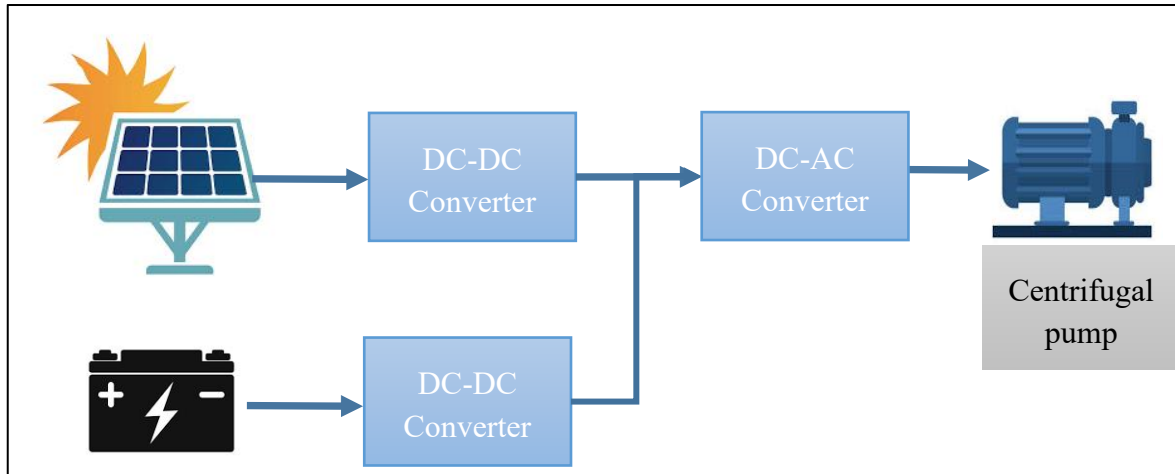


Figure III.1 : Proposed system description.

In summary, the purposeful choice of components in this system results in several notable benefits. It maximizes energy capture through MPPT, enhances energy storage and management with the battery and converters, minimizes energy losses with DC-Bus control, and ensures reliable and efficient water pumping with the induction motor and centrifugal pump. This integrated system offers improved energy harvesting, enhanced system reliability, and increased overall system efficiency, making it a sustainable and efficient solution for various water pumping applications.

III.3. System Modeling

III.3.1. Photovoltaic (PV) Modeling

III.3.1.1 PV Generator Modeling

The primary component of the PV generator is the photovoltaic cell, in which the direct conversion of solar radiation into electrical current occurs through a process called the photovoltaic effect. Several mathematical models have been developed to represent the nonlinear behavior of semiconductor junctions, Known as the ideal PV cell model and the a real PV cell model [53][54].

III.3.1.2 Ideal PV cell model

A photovoltaic cell can be described simply as an ideal current source that produces a current I_{ph} proportional to the incident light power, in parallel with a diode corresponding to the p-n junction area of the PV cell.

$$I = I_{ph} - I_d \quad (III.1)$$

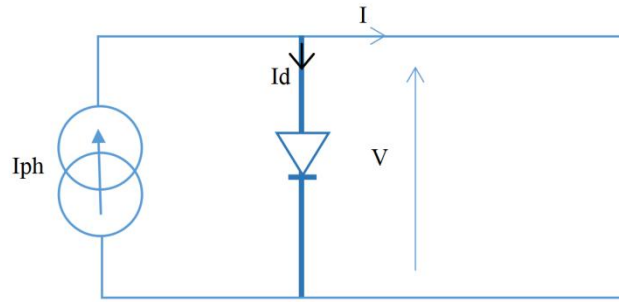


Figure III.2 : Ideal photovoltaic cell model.

For an ideal PV generator, the voltage across the resistor is equal to that across the diode [33]:

$$V=V_d \quad (III.2)$$

The diode being a non-linear element, its I-V characteristic is given by the relation:

$$I_d = I_s \left[\exp\left(\frac{qV}{nKT}\right) - 1 \right] \quad (III.3)$$

So the relation (III.1) will be:

$$I = I_{ph} - I_s \left[\exp\left(\frac{qV}{nKT}\right) - 1 \right] \quad (III.4)$$

Where :

I :Output current (A).

I_d : Diode current (A).

I_s : Reverse saturation current of the diode (A).

I_{ph} : Photo-current (A).

V : Output voltage (V).

k : Boltzmann constant (1,38e-23 J/K).

n : Quality factor of the diode.

q : Charge of the electron (1.6 10^e-19 C).

T : PN junction temperature in (K).

III.3.1.3 Real PV cell model

The previous photovoltaic model does not explain all the phenomena present during the conversion of light energy.

In reality, there is a voltage loss at the output, as well as leakage currents [53][54]. Therefore, this voltage loss is modeled by a series resistance R_s and the leakage currents are

modeled by a parallel resistance R_p , such that (R_p) tends towards infinity if the leakage currents (I_p) are not mentioned.

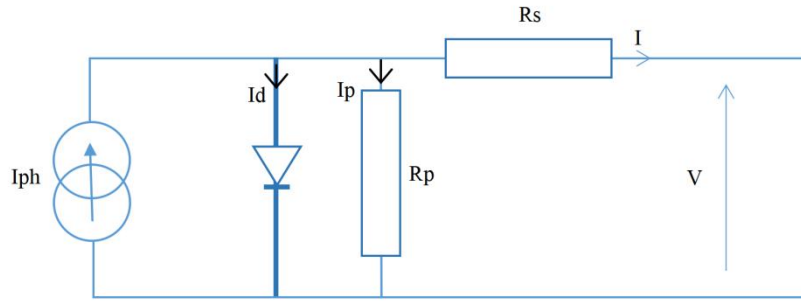


Figure III.3 : Real photovoltaic cell model.

The voltage V across the cell is reduced to:

$$V = V_d - I \cdot R_s \quad (III.5)$$

Where :

V_d : Voltage across the diode (V).

R_s :Series resistance (Ω).

The behavior of this cell is described by the following electrical equation:

$$I = I_{ph} - I_d - I_p \quad (III.6)$$

The current in the diode is given by:

$$I_d = I_s \left[\exp \left(\frac{q V_d}{nKT} \right) - 1 \right] = I_s \left[\left(\frac{q V + R_s \cdot I}{nKT} \right) - 1 \right] \quad (III.7)$$

The current passing through the resistor is given by :

$$I_p = \left(\frac{V_d}{R_p} \right) = \left(\frac{V + R_s \cdot I}{R_p} \right) \quad (III.8)$$

So the expression of the characteristic $I(V)$ is :

$$I = I_{ph} - I_s \left[\left(\frac{q V + R_s \cdot I}{nKT} \right) - 1 \right] - \left(\frac{V + R_s \cdot I}{R_p} \right) \quad (III.9)$$

If we set N_s the number of cells connected in series and N_p the number of cells connected in parallel, we obtain a photovoltaic generator whose model is presented in Figure (III.4).

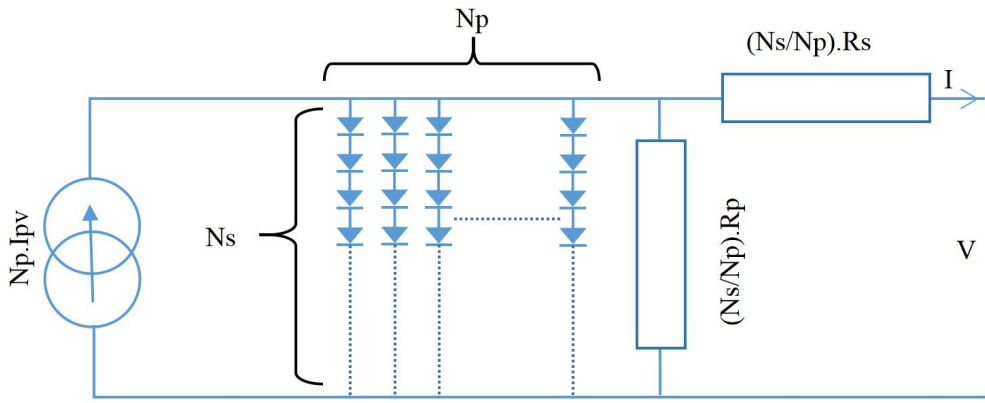


Figure III.4 : Asymptotic electrical diagram of a photovoltaic module.

For modeling, the photocurrent I_m of the PV panel given by the equation:

$$I_m = N_{pp}I_{pn} - N_{pp}I_s \left(\exp \left[\frac{\left(V + \frac{N_{ss}}{N_{pp}} R_s \cdot I \right)}{V_T N_{ss}} \right] - 1 \right) \quad (III.10)$$

Where:

N_{ss} : Number of modules connected in series.

N_{pp} : Number of modules connected in parallel.

And the panel current:

$$I = I_m - \frac{V + \frac{N_{ss}}{N_{pp}} R_s \cdot I}{\frac{N_{ss}}{N_{pp}} R_p} \quad (III.11)$$

III.3.2. Converters Modeling

Converter modeling is a fundamental aspect of understanding and analyzing the behavior of electrical power converters in various applications. Below, we provide brief descriptions of models for three commonly used converters: the Boost Converter Model, the Buck-Boost Converter Model, and the Three-Phase Inverter Model.

III.3.2.1 Boost Converter Model

The Boost Converter is a DC-DC power converter that steps up the input voltage to a higher output voltage. It typically consists of a power switch (a transistor, MOSFET, IGBT), an inductor, a diode, and a capacitor. The mathematical model of a Boost Converter involves equations that describe the relationships between input voltage, output voltage, inductor current, and duty cycle (control signal)[55][56].

The operation of a Boost converter can be divided into two distinct phases depending on the state of the switch S:

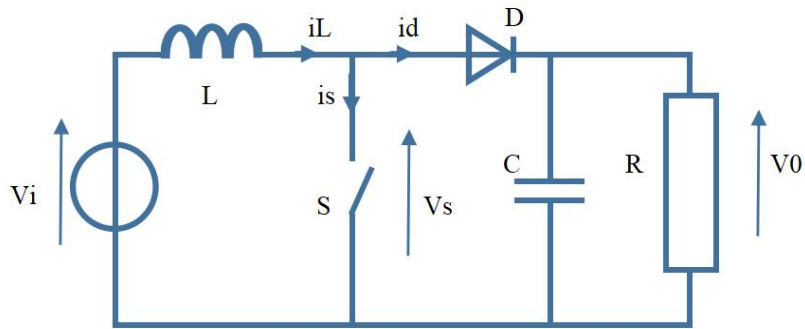


Figure III.5 : Boost Converter.

a. For the first period d.Ts:

An energy accumulation phase: when the switch S is closed (on state), this causes the current to increase in the inductor and therefore the storage of a quantity of energy in the form of magnetic energy. Diode D is then blocked and the load is then disconnected from the power supply.

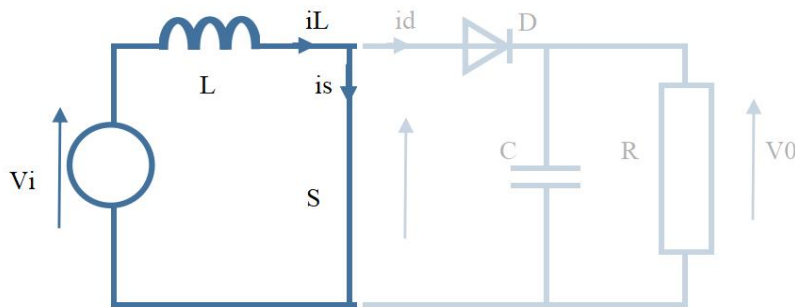


Figure III.6 : Boost Converter (ON state)

$$\frac{d i_L}{dt} = \frac{V_s}{L} \quad ; \quad -i_s = i_c = \frac{V_s}{R} \quad (III.12)$$

$$\frac{d U_c}{dt} = \frac{d V_s}{dt} = \frac{1}{C} i_c = \frac{-1}{C} i_s = \frac{-V_s}{R C} \quad (III.13)$$

b. For the second period (1-d)T:

When the switch is open, the inductance is then in series with the generator and its e.m.f. is added to that of the generator (boost effect). The current passing through the inductor then passes through the diode D, the capacitor C and the load R. This results in a transfer of the energy accumulated in the inductor towards the capacitance .

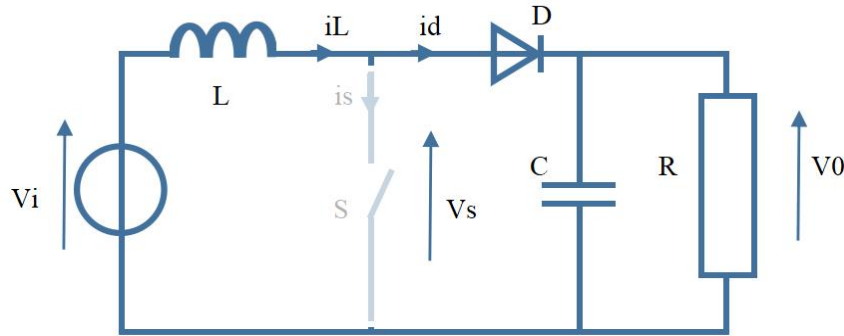


Figure III.7 : Boost Converter (OFF state)

$$\frac{d i_L}{dt} = \frac{V_e - V_s}{L} \quad (III.14)$$

$$\frac{dV_s}{dt} = \frac{i_c}{c} = \frac{i_e - i_s}{c} = \frac{i_e \frac{V_s}{R}}{c} = \frac{i_e R - V_s}{Rc} \quad (III.15)$$

To find a dynamic representation valid for the **entire period Ts**, we use:

$$\frac{d i_L}{dt} = \frac{1}{L} (V_e - V_s(1 - d)) \quad (III.16)$$

$$\frac{dV_s}{dt} = \frac{1}{Rc} (i_e.R(1 - d) - V_s) \quad (III.17)$$

III.3.2.2 Buck Converter Model:

A Buck Converter, also referred to as a step-down converter, is a DC-DC power converter designed to reduce the input voltage to a lower output voltage.

Much like the Boost Converter, the mathematical model of a Buck Converter encompasses equations that establish relationships between the input voltage, output voltage, inductor current, and duty cycle (control signal)

The essential part is the inductor, which alternates from load (reducing voltage, supplied by the generator, available to the downstream circuit) to source (providing voltage while the generator is switched off) [55][57]. Operation can be divided into two phases depending on the state of switch S:

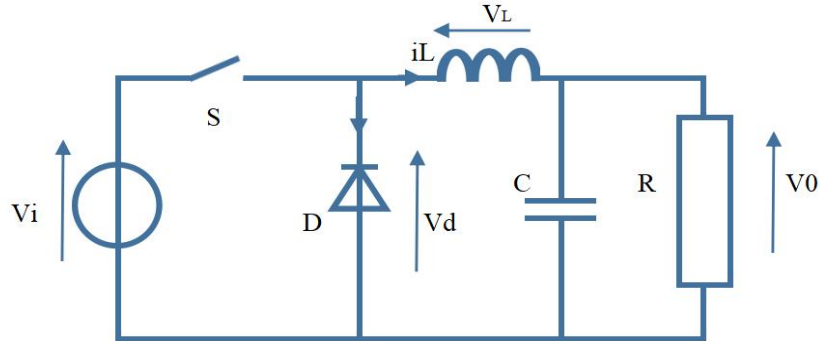


Figure III.8 : Buck Converter

a. For the first period $d.T_s$:

$$\frac{d i_L}{dt} = \frac{V_e - V_s}{L} \quad (III.18)$$

$$\frac{dV_s}{dt} = \frac{ic}{c} = \frac{ie.R - V_s}{Rc} \quad (III.19)$$

When close the switch S. The current supplied by the generator, initially zero, increases linearly and passes through the inductor. The inductance opposes this increase in current, producing an opposite voltage, and it stores the received energy in magnetic form.

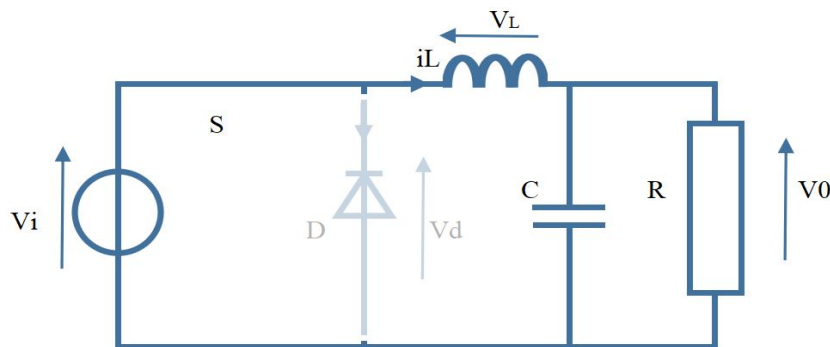


Figure III.9 : Buck Converter (ON state).

The diode being reverse biased with the voltage V_i of the generator, no current passes through it.

b. For the second period (1-d)T:

$$\frac{d i_L}{dt} = \frac{V_s}{L} \quad (III.20)$$

$$\frac{dV_s}{dt} = \frac{i_e \cdot R - V_s}{R_c} \quad (III.21)$$

The switch is open. The generator is switched off, no more current flows through it. The diode turns on to ensure continuity of current in the inductor. The current passing through the inductor decreases. The inductance opposes this reduction in current, producing a voltage which puts it in a source situation for the downstream circuit, using the magnetic energy stored in the previous phase.

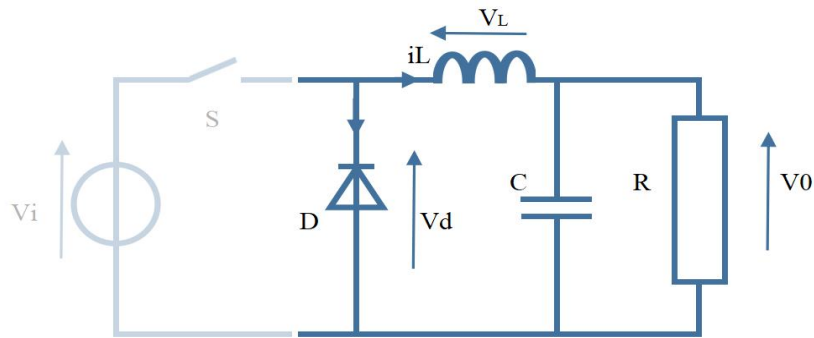


Figure III.10 : Buck Converter (OFF state).

To find a dynamic representation valid for the **entire period Ts**, we use:

$$\frac{d i_L}{dt} = \frac{V_e - V_s}{L} \cdot d + \frac{-V_s}{L} (1 - d) = \frac{1}{L} (V_e \cdot d - V_s) \quad (III.22)$$

$$\frac{dV_s}{dt} = \frac{(i_e \cdot R - V_s)}{R_c} \cdot d + \frac{(i_e \cdot R - V_s)}{R_L} (1 - d) = \frac{i_e \cdot R - V_s}{R_c} \quad (III.23)$$

III.3.2.3 Buck-Boost Converter Model:

The Buck-Boost Converter is another DC-DC converter that can both step up and step down the input voltage to obtain the desired output voltage. It is commonly used for battery charging, voltage regulation, and power inversion [55][58].

The operation of a Buck-Boost converter can be divided into two configurations depending on the state of the switch S:

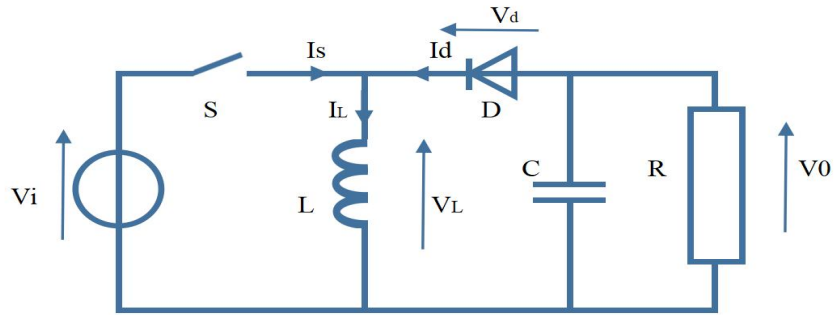


Figure III.11 : Buck-boost Converter

a. For the first period $d \cdot Ts$:

In the on state, the switch S is closed, thus leading to an increase in the energy stored in the inductor.

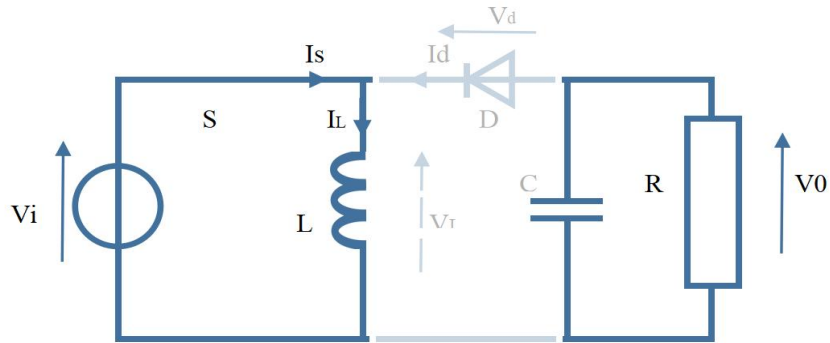


Figure III.12 : Buck-boost Converter (ON state).

$$\frac{d i_L}{dt} = \frac{V_i}{L} \tag{III.24}$$

$$\frac{dV_c}{dt} = \frac{i_c}{c} = \frac{-i_s}{c} = \frac{-V_s}{Rc} \tag{III.25}$$

b. For the second period $(1-d)T$:

In the blocked state, switch S is open. Inductance is related to charge and capacitance. This results in a transfer of the energy accumulated in the inductance to the capacitance and the charge.

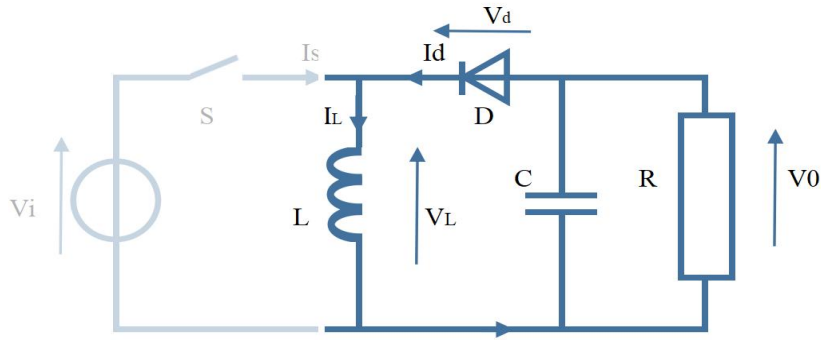


Figure III.13 : Buck-boost Converter (OFF state).

$$\frac{d i_l}{d t} = \frac{V_s}{L} \quad (III.26)$$

$$\frac{d V_s}{d t} = \frac{i_c}{c} = \frac{-i_l - i_s}{c} = \frac{-i_e . R - V_s}{R c} \quad (III.27)$$

To find a dynamic representation valid for the **entire period Ts**, we use:

$$\frac{d i_l}{d t} = \frac{V_e}{L} . d + \frac{V_s}{L} (1 - d) = \frac{1}{L} (V_e . d + V_s (1 - d)) \quad (III.28)$$

$$\frac{d V_s}{d t} = \frac{-V_s}{R c} . d + \frac{(i_e . R - V_s)}{R c} (1 - d) = \frac{1}{R c} (-i_e . R . (1 - d) - V_s) \quad (III.29)$$

III.3.2.4 Three-Phase Inverter Model

The Three-Phase Inverter is used to convert DC power into three-phase AC power, commonly used in motor control and variable-speed drive applications. The model for a Three-Phase Inverter involves equations that describe the generation of sinusoidal output voltages based on the modulation technique used, such as Space Vector Pulse Width Modulation (SVPWM) or Sinusoidal Pulse Width Modulation (SPWM) [59]. In general, the PWM control technique makes it possible to define the control times of the switches. There are two types of this technique:

- Voltage control by sine-triangle PWM.
- Current control by hysteresis PWM.

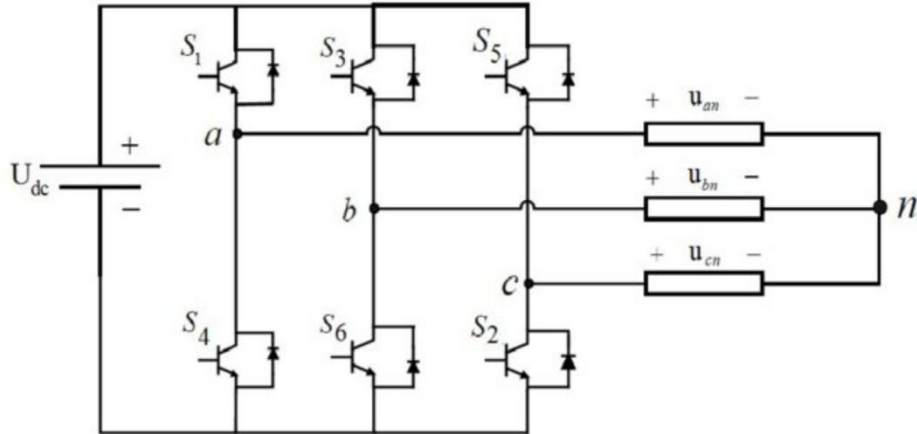


Figure III.14 : Three-Phase Inverter.

The complexes voltages are obtained from the inverter outputs:

$$U_{ab} = V_{an} - V_{bn} = U_0(S_a - S_b) \quad (III.30)$$

$$U_{bc} = V_{bn} - V_{cn} = U_0(S_b - S_c) \quad (III.31)$$

$$U_{ca} = V_{cn} - V_{an} = U_0(S_c - S_a) \quad (III.32)$$

The voltages V_{an}, V_{bn} et V_{cn} form a balanced three-phase voltage system, so:

$$V_{an} + V_{bn} + V_{cn} = 0 \quad (III.33)$$

From (III.30) and (III.32) we get:

$$V_{an} = \frac{U_0}{3}(2S_a - S_b - S_c) \quad (III.34)$$

From (III.30) and (III.31) we get:

$$V_{bn} = \frac{U_0}{3}(-S_a + 2S_b - S_c) \quad (III.35)$$

From (III.31) and (III.32) we get:

$$V_{cn} = \frac{U_0}{3}(-S_a - S_b + 2S_c) \quad (III.36)$$

So in matrix form we will have:

$$\begin{bmatrix} V_{an} \\ V_{bn} \\ V_{cn} \end{bmatrix} = \frac{U_0}{3} \begin{bmatrix} 2 & -1 & -1 \\ -1 & 2 & -1 \\ -1 & -1 & 2 \end{bmatrix} \begin{bmatrix} S_a \\ S_b \\ S_c \end{bmatrix} \quad (\text{III.37})$$

III.3.3. Induction Machine Modeling

An Induction Machine Model is a mathematical representation or simulation of the behavior and characteristics of an induction motor. Modeling such motors is crucial for understanding their performance, designing control systems, and predicting their behavior under different operating conditions.

III.3.3.1 Operating principle of the asynchronous machine

Let us assume that a stator made up of three coils with axes offset by 120° and supplied by a balanced three-phase network, creates in the motor air gap a magnetic field rotating at the synchronism speed:

$$\Omega_s = \frac{\omega_s}{P} \quad (\text{III.38})$$

A rotor, swept by this rotating field, is therefore the seat of a magnetomotive force which will give rise to currents; the rotor is therefore subjected to electromagnetic Laplace forces, all of these forces create a driving torque which drives the rotor in rotation [60].

The rotor rotates in the same direction as the rotating field, but its rotation speed must necessarily be lower than that of the rotating field $\Omega_s > \Omega$ so that there is this variation in flux necessary for the operation of the machine.

The relative speed of the wave with respect to the stator is given by:

$$\Omega = \Omega_s - \Omega_r \quad (\text{III.39})$$

where :

$$\begin{cases} \Omega = \frac{\omega}{P} \\ \Omega_r = \frac{\omega_r}{P} \end{cases} \quad (\text{III.40})$$

III.3.3.2 Simplifying assumptions

The asynchronous machine presents very complicated phenomena which intervene in its operation, such as magnetic saturation, eddy current, etc. These phenomena have very difficult mathematical formulas although their influence on the machine is negligible [60].

Therefore, we assume certain simplifying hypotheses to model the asynchronous machine:

- Air gap of uniform thickness.
- Magnetic saturation, hysteresis, eddy current are neglected.
- The resistance does not vary with temperature; the Skin effect (Kelvin effect) is negligible.
- The magnetomotive force created by the machine windings at the air gap has a sinusoidal distribution.
- The power supply is provided by a symmetrical three-phase voltage system
- These hypotheses imply that:
 - Flows are additive.
 - The self-inductances are constant.
 - The mutual inductance varies in a sinusoidal manner.

III.3.3.3 Asynchronous machine Equations

The asynchronous machine can be represented by a diagram given in Figure (III.15). The stator is made up of three windings offset by 120° in space, crossed by three variable currents forming a balanced three-phase system.

The rotor can be modeled, like the stator, by three windings offset by 120° in space, but they are short-circuited.

The three stator windings and the three rotor windings are noted, respectively, (A, B, C) and (a, b, c). The angle θ is the angle that the rotor makes as it rotates relative to the stator.

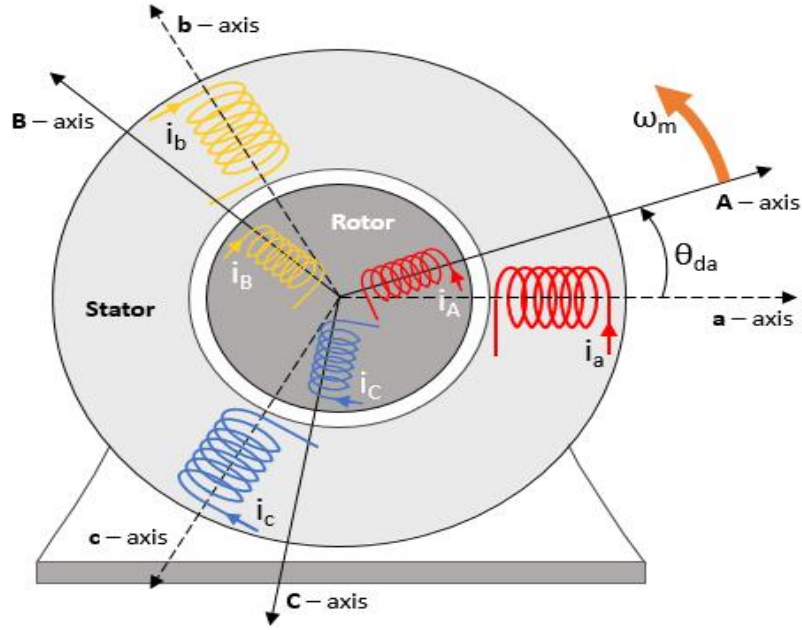


Figure III.15 : Three-phase model of the asynchronous machine [].

III.3.3.3.a. Electrical equations

The windings of the three stator phases are offset in space by an angle of $\frac{2\pi}{3}$ and also those of the rotor and can be represented as shown. The rotor phases are short-circuited on themselves. θ is the electrical angle between the axis of the stator phase (A) and the rotor phase (a). By applying Ohm's generalized law to each phase of the stator (respectively rotor), we will have the following voltage equations:

$$\begin{cases} [V_s]_{abc} = [R_s][I_s]_{abc} + \frac{d}{dt}[\phi_s]_{abc} \\ [V_r]_{abc} = [R_r][I_r]_{abc} + \frac{d}{dt}[\phi_r]_{abc} \end{cases} \quad (III.41)$$

Where:

$$[V_s]_{abc} = [V_{sa} V_{sb} V_{sc}]^T ; [\phi_s]_{abc} = [\phi_{sa} \phi_{sb} \phi_{sc}]^T ; [I_s]_{abc} = [I_{sa} I_{sb} I_{sc}]^T \quad (III.42)$$

And :

$$[V_r]_{abc} = [V_{ra} V_{rb} V_{rc}]^T ; [\phi_r]_{abc} = [\phi_{ra} \phi_{rb} \phi_{rc}]^T ; [I_r]_{abc} = [I_{ra} I_{rb} I_{rc}]^T \quad (III.43)$$

And:

$$[R_s] = \begin{bmatrix} R_s & 0 & 0 \\ 0 & R_s & 0 \\ 0 & 0 & R_s \end{bmatrix} ; [R_r] = \begin{bmatrix} R_r & 0 & 0 \\ 0 & R_r & 0 \\ 0 & 0 & R_r \end{bmatrix} \quad (III.44)$$

$[R_s]$: Matrix of stator resistances.

$[R_r]$: Matrix of rotor resistances.

III.3.3.3.b. Magnetic equations

The hypotheses, presented previously, lead to an inductance matrix which establishes the linear relationships between the totalized flows and the currents:

$$\begin{cases} [\phi_s]_{abc} = [L_s][I_s]_{abc} + [M_{sr}][I_r]_{abc} \\ [\phi_r]_{abc} = [L_r][I_r]_{abc} + [M_{rs}][I_s]_{abc} \end{cases} \quad (\text{III.45})$$

where :

$$[L_s] = \begin{bmatrix} l_s & m_s & m_s \\ m_s & l_s & m_s \\ m_s & m_s & l_s \end{bmatrix} ; [L_r] = \begin{bmatrix} l_s & m_s & m_s \\ m_s & l_s & m_s \\ m_s & m_s & l_s \end{bmatrix} \quad (\text{III.46})$$

$$[M_{sr}] = [M_{rs}]^T = M \cdot \begin{bmatrix} \cos \theta & \cos(\theta - \frac{4\pi}{3}) & \cos(\theta - \frac{2\pi}{3}) \\ \cos(\theta - \frac{2\pi}{3}) & \cos \theta & \cos(\theta - \frac{4\pi}{3}) \\ \cos(\theta - \frac{4\pi}{3}) & \cos(\theta - \frac{2\pi}{3}) & \cos \theta \end{bmatrix} \quad (\text{III.47})$$

$[L_s]$: Stator inductance matrix.

$[L_r]$: Rotoric inductance matrix.

M : Maximum mutual inductance between stator phase and rotor phase

III.3.3.3.c. Mechanical equation

For study the dynamic characteristics, we introduce the following equation of motion:

$$J \frac{d\Omega}{dt} = C_{em} - C_r - F\Omega \quad (\text{III.48})$$

The stator and rotor of the asynchronous machine exhibit electrical and magnetic isotropy, which implies that only the mutual inductance matrix $[M_{sr}]$ is a function of position θ . The coefficients of equations (III.45) and (III.47) are therefore variable, the analytical resolution of the system becomes practically difficult, hence the adaptation of a change of basis on the physical quantities (voltage, current and flux) independent of the position θ , this passage is called Park transformation.

III.3.3.3.d. Park transformation applied to the three-phase IM

The Park transformation can be applied as a change of base to currents, voltages, and fluxes involving the angle between the axis of the windings and the axes “d” and “q”.

Thus, the stator windings A, B, C and the rotor windings a, b, c are replaced respectively by two stator windings d_s, q_s and two rotor windings d_r, q_r . Figure (III.16) allows us to define the various frames of reference and the spatial relationships that link them [60].

d : the direct axis and q : the quadrature axis.

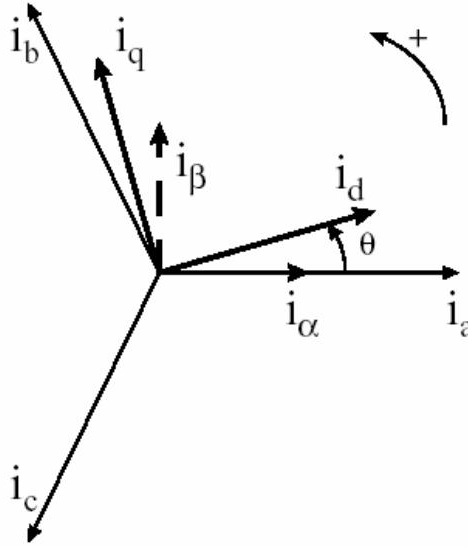


Figure III.16 : Angular registration of axis systems in space.

We notice in figure (III.16) that θ_s and θ_r are naturally linked to θ by the rigid relation:

$$\theta = \theta_s - \theta_r \quad (\text{III.49})$$

And consequently :

$$\frac{d\theta}{dt} = \frac{d\theta_s}{dt} - \frac{d\theta_r}{dt} \quad (\text{III.50})$$

In the initial Park transform, we define a transformation matrix as follows:

$$[p(\theta_s)] = \sqrt{\frac{2}{3}} \begin{bmatrix} \cos \theta_s & \cos(\theta_s - \frac{2\pi}{3}) & \cos(\theta_s + \frac{2\pi}{3}) \\ -\sin \theta_s & -\sin(\theta_s - \frac{2\pi}{3}) & -\sin(\theta_s + \frac{2\pi}{3}) \\ \frac{1}{\sqrt{2}} & \frac{1}{\sqrt{2}} & \frac{1}{\sqrt{2}} \end{bmatrix} \quad (\text{III.51})$$

And its inverse is defined by:

$$[p(\theta_s)]^{-1} = \sqrt{\frac{2}{3}} \begin{bmatrix} \cos \theta_s & -\sin \theta_s & \frac{1}{\sqrt{2}} \\ \cos(\theta_s - \frac{2\pi}{3}) & -\sin(\theta_s - \frac{2\pi}{3}) & \frac{1}{\sqrt{2}} \\ \cos(\theta_s + \frac{2\pi}{3}) & -\sin(\theta_s + \frac{2\pi}{3}) & \frac{1}{\sqrt{2}} \end{bmatrix} \quad (\text{III.52})$$

The Park transform generally allows the transition from the three-phase system by a, b, c to a two-phase system d, q whatever the electrical or electromagnetic quantities (flux, current and voltage). The transformation of the stator quantities is thus defined by :

$$\begin{aligned} [i_{dqo}] &= [p(\theta_s)][i_{abc}] \\ [V_{dqo}] &= [p(\theta_s)][V_{abc}] \\ [\phi_{dqo}] &= [p(\theta_s)][\phi_{abc}] \end{aligned} \quad (\text{III.53})$$

O : the homopolar axis.

The matrix $[p(\theta_s)]$ represents the transformation matrix applied to the stator.

The transformation of the rotor quantities is obtained by replacing the index (s) by the index (r).

We define :

$$\begin{aligned} \omega_{sp} &= \frac{d\theta_s}{dt} \quad \text{and} \quad \omega_{rp} = \frac{d\theta_r}{dt} \\ \omega_{sp} &= \omega + \omega_{rp} \end{aligned} \quad (\text{III.54})$$

ω_{sp} : Park reference speed relative to the stator.

ω_{rp} : Park reference speed relative to the rotor.

III.3.3.3.e. Flux equations

The stator flux equation is of the form:

$$[\phi_s]_{abc} = [L_s][I_s]_{abc} + [M_{sr}][I_r]_{abc} \quad (\text{III.55})$$

After applying the Park transform becomes:

$$[p(\theta_s)]^{-1}[\phi_s]_{dqo} = [L_s][p(\theta_s)]^{-1}[I_s]_{dqo} + [M_{sr}][p(\theta_s)]^{-1}[I_r]_{dqo} \quad (\text{III.56})$$

Multiplying equations (III.55) by $[p(\theta_s)]$ we obtain:

$$[\phi_s]_{dqo} = [p(\theta_s)][L_s][p(\theta_s)]^{-1}[I_s]_{dqo} + [p(\theta_s)][M_{sr}][p(\theta_s)]^{-1}[I_r]_{dqo} \quad (\text{III.57})$$

After the development we get:

$$[p(\theta_s)][L_s][p(\theta_s)]^{-1} = \begin{bmatrix} l_s - m_s & 0 & 0 \\ 0 & l_s - m_s & 0 \\ 0 & 0 & l_s + 2m_s \end{bmatrix} \quad (\text{III.58})$$

$$[p(\theta_s)][M_{sr}][p(\theta_s)]^{-1} = \frac{3}{2}M. \begin{bmatrix} 1 & 0 & 0 \\ 0 & 1 & 0 \\ 0 & 0 & 0 \end{bmatrix} \quad (\text{III.59})$$

So the expressions for the stator flux in the Park frame are:

$$\begin{cases} \phi_{sd} = L_s i_{sd} + M_{sr} i_{rd} \\ \phi_{sq} = L_s i_{sq} + M_{sr} i_{rq} \\ \phi_{so} = L_{so} i_{so} \end{cases} \quad (\text{III.60})$$

where :

$L_s = l_s - m_s$: Stator cyclic inductance.

$M_{sr} = \frac{3}{2}M$: Cyclic mutual inductance.

$L_{so} = l_s + 2m_s$: Stator homopolar inductance.

For the rotor flux equations we find the same result with change of index "s" by "r".

$$\begin{cases} \phi_{rd} = L_r i_{rd} + M_{rs} i_{sd} \\ \phi_{rq} = L_r i_{rq} + M_{rs} i_{sq} \\ \phi_{ro} = L_{ro} i_{ro} \end{cases} \quad (\text{III.61})$$

$L_r = l_r - m_r$: Rotor cyclic inductance.

$L_{ro} = l_r + 2m_r$: Rotor homopolar inductance.

III.3.3.3.f. Definitive equation of the IM in Park reference frame

If the system is balanced, the 3rd equations (homopolar component) are zero and useless.

$$\begin{cases} V_{sd} = R_s i_{sd} + \frac{d\phi_{sd}}{dt} - \omega_{sp} \phi_{sq} \\ V_{sq} = R_s i_{sq} + \frac{d\phi_{sq}}{dt} - \omega_{sp} \phi_{sd} \\ V_{rd} = R_r i_{rd} + \frac{d\phi_{rd}}{dt} - \omega_{rp} \phi_{sq} = 0 \\ V_{rq} = R_r i_{rq} + \frac{d\phi_{rq}}{dt} - \omega_{rp} \phi_{rd} = 0 \end{cases} \quad (\text{III.62})$$

$$\begin{cases} \phi_{sd} = L_s i_{sd} + M_{sr} i_{rd} \\ \phi_{sq} = L_s i_{sq} + M_{sr} i_{rq} \\ \phi_{rd} = L_r i_{rd} + M_{rs} i_{rd} \\ \phi_{rq} = L_r i_{rq} + M_{rs} i_{rq} \end{cases} \quad (\text{III.63})$$

III.3.3.4 Reference Choice

On désigne par $\omega_s = \frac{d\theta_s}{dt}$, la vitesse angulaire des axes d, q dans le repère statorique et par $\omega_r = \frac{d\theta_r}{dt}$, la vitesse angulaire des axes d, q dans le repère rotorique.

There are different possibilities concerning the choice of the orientation of the axes d, q which depend on the objectives of the application

- Axes rotating at rotor speed ($\theta_r = 0$): study of stator quantities.
- Axes linked to the stator ($\theta_s = 0$): for the study of rotor quantities,
- Axes attached to the rotating field: study for the control.

The design of vector control by flow orientation requires choice (c) and the action models depend on the position of the marker in relation to the various axes of the flow.

We denote by $\omega_s = \frac{d\theta_s}{dt}$: the angular speed of the axes d, q in the stator frame, and by $\omega_r = \frac{d\theta_r}{dt}$: the angular speed of the axes d, q in the rotor frame.

III.3.3.4.a. Reference frame linked to the stator

This frame of reference is noted (α, β) , it translates into the conditions:

$$\frac{d\theta_s}{dt} = \omega_{sp} = 0 \quad ; \quad \omega_{rp} = -\omega$$

Hence the electrical equations:

$$\left\{ \begin{array}{l} V_{s\alpha} = R_s i_{s\alpha} + \frac{d\phi_{s\alpha}}{dt} \\ V_{s\beta} = R_s i_{s\beta} + \frac{d\phi_{s\beta}}{dt} \\ V_{r\alpha} = R_r i_{r\alpha} + \frac{d\phi_{r\alpha}}{dt} + \omega \phi_{s\beta} = 0 \\ V_{r\beta} = R_r i_{r\beta} + \frac{d\phi_{r\beta}}{dt} + \omega \phi_{r\alpha} = 0 \end{array} \right. \quad (\text{III.64})$$

III.3.3.4.b. Reference frame linked to the rotor

This frame of reference is denoted (X, Y) , it is translated by the equations:

$$\frac{d\theta_r}{dt} = \omega_{rp} = 0 \quad ; \quad \frac{d\theta_s}{dt} = \omega_{sp} = \omega$$

Hence the electrical equations:

$$\left\{ \begin{array}{l} V_{sX} = R_s i_{sX} + \frac{d\phi_{sX}}{dt} - \omega \phi_{sY} \\ V_{sY} = R_s i_{sY} + \frac{d\phi_{sY}}{dt} - \omega \phi_{sX} \\ V_{rX} = R_r i_{rX} + \frac{d\phi_{rX}}{dt} = 0 \\ V_{rY} = R_r i_{rY} + \frac{d\phi_{rY}}{dt} = 0 \end{array} \right. \quad (\text{III.65})$$

III.3.3.4.c. Reference frame linked to the rotating field

This frame of reference is noted (d, q) , it results in the conditions:

$$\frac{d\theta_s}{dt} = \omega_{sp} = \omega_s \quad ; \quad \frac{d\theta_r}{dt} = \omega_{rp} = \omega_r \quad ; \quad \omega = \omega_s - \omega_r$$

Where: ω_r is the pulsation of the slip.

So the electrical equations are written:

$$\left\{ \begin{array}{l} V_{sd} = R_s i_{sd} + \frac{d\phi_{sd}}{dt} - \omega_s \phi_{sq} \\ V_{sq} = R_s i_{sq} + \frac{d\phi_{sq}}{dt} - \omega_s \phi_{sd} \\ V_{rd} = R_r i_{rd} + \frac{d\phi_{rd}}{dt} - \omega_r \phi_{sq} = 0 \\ V_{rq} = R_r i_{rq} + \frac{d\phi_{rq}}{dt} - \omega_r \phi_{rd} = 0 \end{array} \right. \quad (\text{III.66})$$

The advantage of using this frame of reference is to have constant quantities in steady state. It is then easier to regulate it.

In our work we will opt for this frame of reference.

III.3.4. Centrifugal pump modeling

The operation of a centrifugal pump involves three parameters, head, flow and speed. The pumping head is the sum of the static head and the dynamic head [61]

In this application, the hydraulic power of the centrifugal pump is given by:

$$P_h = R_{mp} \cdot P_{ele} = \rho \cdot Q \cdot h \cdot g \quad (\text{III.67})$$

where :

P_h : Hydraulic power to the fluid by the pump (W); ;

P_{ele} : Electric power of the asynchronous motor (W) ;

R_{mp} : Pump set efficiency (%) ;

g : Acceleration of gravity (9.81 m/s²) ;

ρ : Density of water (1000 Kg/m³) ;

Q : Volume flow (m³/s) ;

h : Total manometric height that the pump could satisfy (m).

The centrifugal pump opposes a resisting torque T_r :

$$T_r = K_r \cdot \Omega^2 \quad (\text{III.68})$$

where :

Ω : Speed of the asynchronous motor (rad/s).

K_r : Proportionality coefficient [(Nm/ (rad.s-1)²)] which is expressed by the following equation:

$$K_r = \frac{P_n}{\Omega_n^3} \quad (\text{III.69})$$

P_n : Rated power of the asynchronous motor (W).

Ω_n : Rated speed of the asynchronous motor (rad/s).

III.3.5. Storage modeling

Given the great diversity of battery cell types and the very varied number of parameters involved, a very empirical representation of the behavior of the battery can be established [62] [63].

The storage system used in a photovoltaic installation is a lead-acid storage battery.

In this study, we can calculate the storage capacity based on the power produced by the photovoltaic generator and the requested load.

III.3.5.1 Battery charging model

When the PV generator power is greater than the load, the batteries are in the state of charge, the capacity of the batteries at time t can be described by:

$$C_{Bat}(t) = C_{Bat}(t-1) \cdot (t - \sigma) + (P_{pv}(t) - P_L(t)/\eta_{inv}) \cdot \eta_{Bat} \quad (III.70)$$

$C_{Bat}(t)$ et $C_{Bat}(t-1)$: are the quantities of charging and discharging of the batteries at time (t) and $(t-1)$ respectively.

σ : is the hourly rate of spontaneous charging.

P_{pv} : is the power of the PV generator.

P_L : is the load requested at time t .

η_{inv} and η_{Bat} : are the efficiencies of the inverter and the battery successively.

III.3.5.2 Battery discharge model

If this is the case where the load demand is greater than the power produced, the capacity of the batteries in time t can be described as follows:

$$C_{Bat}(t) = C_{Bat}(t-1) \cdot (t - \sigma) + (P_L(t)/\eta_{inv} - P_{pv}(t)) \quad (III.71)$$

At any time, the quantity of battery charge is subject to the following constraints:

$$C_{Batmin} \leq C_{Bat}(t) \leq C_{Batmax} \quad (III.72)$$

The maximum battery capacity takes the value of the nominal battery capacity ($C_{Batmax} = C_{Batmin}$), and the minimum capacity is determined by the depth of charge (DOD):

$$C_{Batmin} = DOD \cdot C_{Bat \cdot N} \quad (III.73)$$

The maximum state of charge (SOC) value is equal to 1, and the minimum is determined by the maximum depth of discharge.

$$SOC_{min} = 1 - DOD \quad (III.74)$$

Relying on the properties of manufacturers, the service life of batteries can be extended to the maximum if DOD takes the values of 30-50%.

III.3.5.3 Battery voltage

The relationship between voltage, current and state of charge is described by the electrical diagram in Figure (III.17)

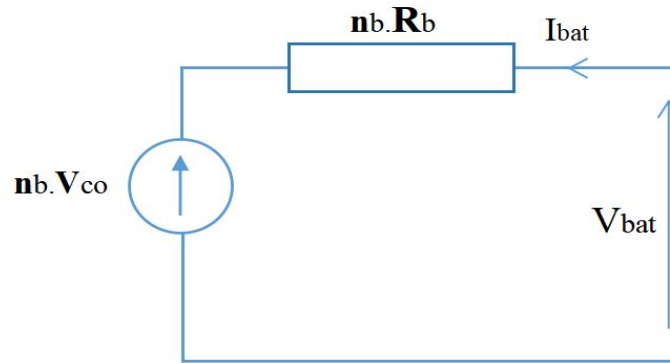


Figure III.17 : Battery electrical diagram.

For n batteries in series, we can write the equation:

$$v_{bat}(t) = n_b \cdot V_{co}(t) + n_b \cdot I_{bat}(t) \cdot R_{bat}(t) \quad (III.75)$$

$V_{bat}(t)$: is the open circuit voltage at time t .

$R_{bat}(t)$: is the internal battery resistance in Ohms.

The open circuit voltage is expressed as the following equation in terms of the state of charge function:

$$V_{co}(t) = V_F + b \cdot \log (SOC(t)) \quad (III.76)$$

where:

V_F : electromotive force ; b : is an empirical constant.

The variation in the internal resistance of a battery $R_{bat}(t)$, is mainly due to two components, namely, the electrode resistance $R_{\acute{e}lectrode}$ and the electrolyte resistance $R_{\acute{e}lectrolyte}$.

$$R_{bat}(t) = R_{\acute{e}lectrode} + R_{\acute{e}lectrolyte}$$

The variation of $R_{\acute{e}lectrode}$ et $R_{\acute{e}lectrolyte}$ as a function of the SOC state of charge can be expressed by:

$$R_{\acute{e}lectrode} = r_1 + r_2 \cdot (SOC(t)) R_{\acute{e}lectrolyte} = [r_3 - r_4 \cdot (SOC(t))]^{-1} \quad (III.77)$$

where:

r_1 , r_2 , r_3 and r_4 are empirical constants, these constants have different values for the charge and discharge mode.

III.3.5.4 Battery current

When the power of the PV generator is greater than the load, the batteries are in the charging mode, the battery charging current at time t can be described by:

$$I_{Bat} = \frac{P_{pv}(t)}{V_{bat}(t)} - \frac{E_L(t)/\eta_{inv}}{V_{bat}(t)} \quad (III.78)$$

When the power of the PV generator cannot meet the load demand, the discharge current of the batteries is:

$$I_{Bat} = \frac{E_L(t)/\eta_{inv}}{V_{bat}(t)} - \frac{P_{pv}(t)}{V_{bat}(t)} \quad (III.79)$$

III.4. System Control

III.4.1. Maximum Power Point

Maximum Power Point Tracking (MPPT) is a crucial control technique used in photovoltaic (PV) systems to maximize the power output from solar panels. MPPT algorithms ensure that the PV system operates at the point where it extracts the maximum available power from the solar irradiance. Here, I'll explain two common MPPT algorithms: Perturb and Observe (P&O) and Incremental Conductance (INC).

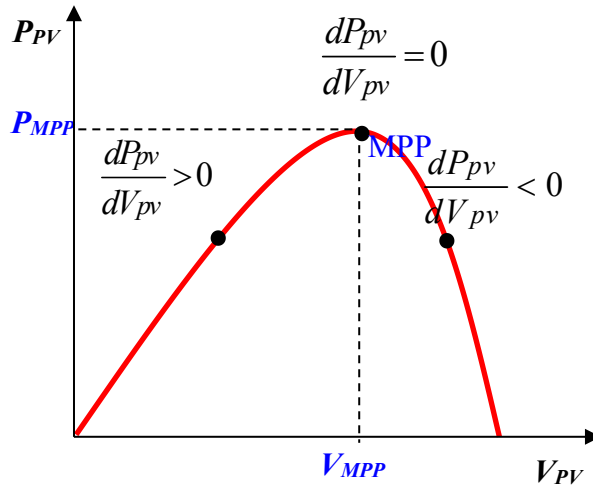


Figure III.18 : Maximum Power Point.

III.4.1.5 Perturb and Observe (P&O)

Perturb and Observe is one of the most widely used MPPT algorithms. It works by continuously perturbing (changing) the operating point of the PV system and observing the resulting change in power output [64]. Here's how P&O works:

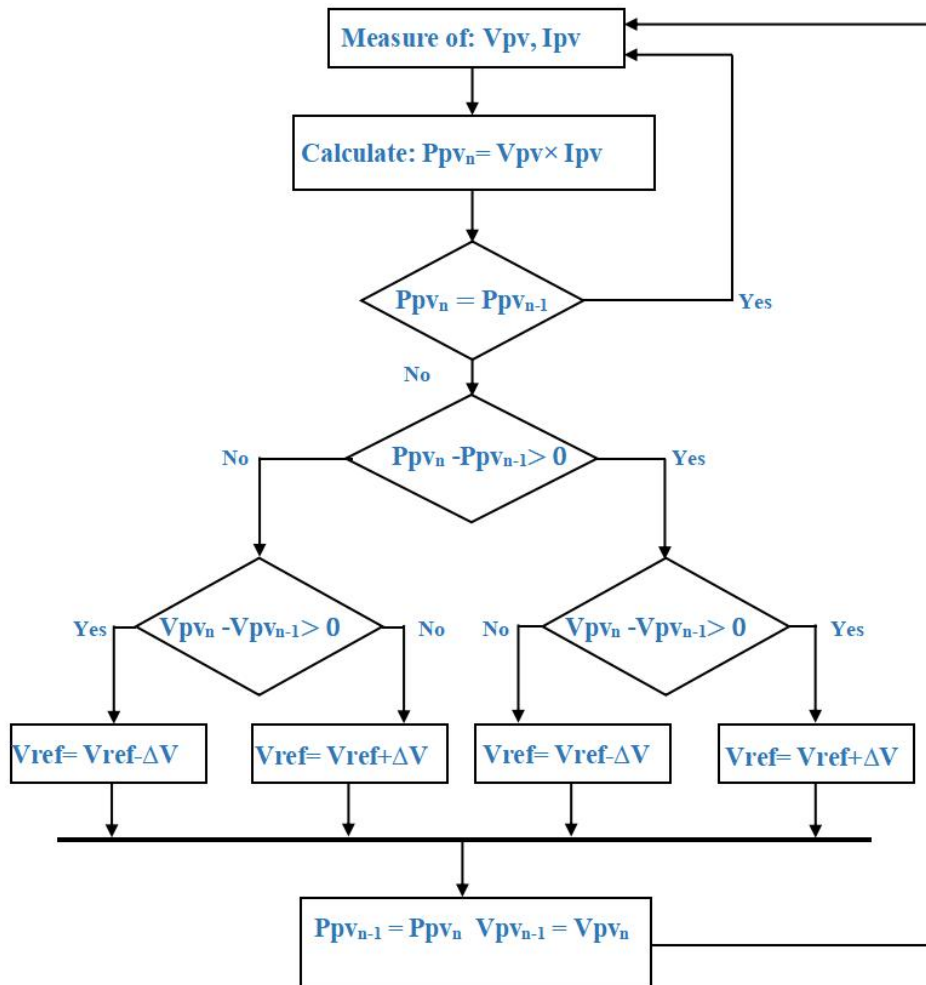


Figure III.19 : Perturb and Observe.

The controller starts at an initial operating point (usually the point where the system last operated or some predefined value).

It perturbs the operating point by increasing or decreasing the system's voltage or current slightly.

It then observes whether this perturbation increases or decreases the power output.

Based on this observation, the controller adjusts the operating point further in the same direction if power output increased, or in the opposite direction if power output decreased.

This process continues iteratively until the controller converges to the maximum power point (MPP), where the power output is maximized.

P&O is relatively simple and works well in many situations. However, it can oscillate around the MPP in rapidly changing or low-irradiance conditions.

III.4.1.6 Incremental Conductance (INC)

Incremental Conductance is another popular MPPT algorithm, known for its ability to track the MPP accurately, especially under varying irradiance and temperature conditions [65]. Here's how INC works:

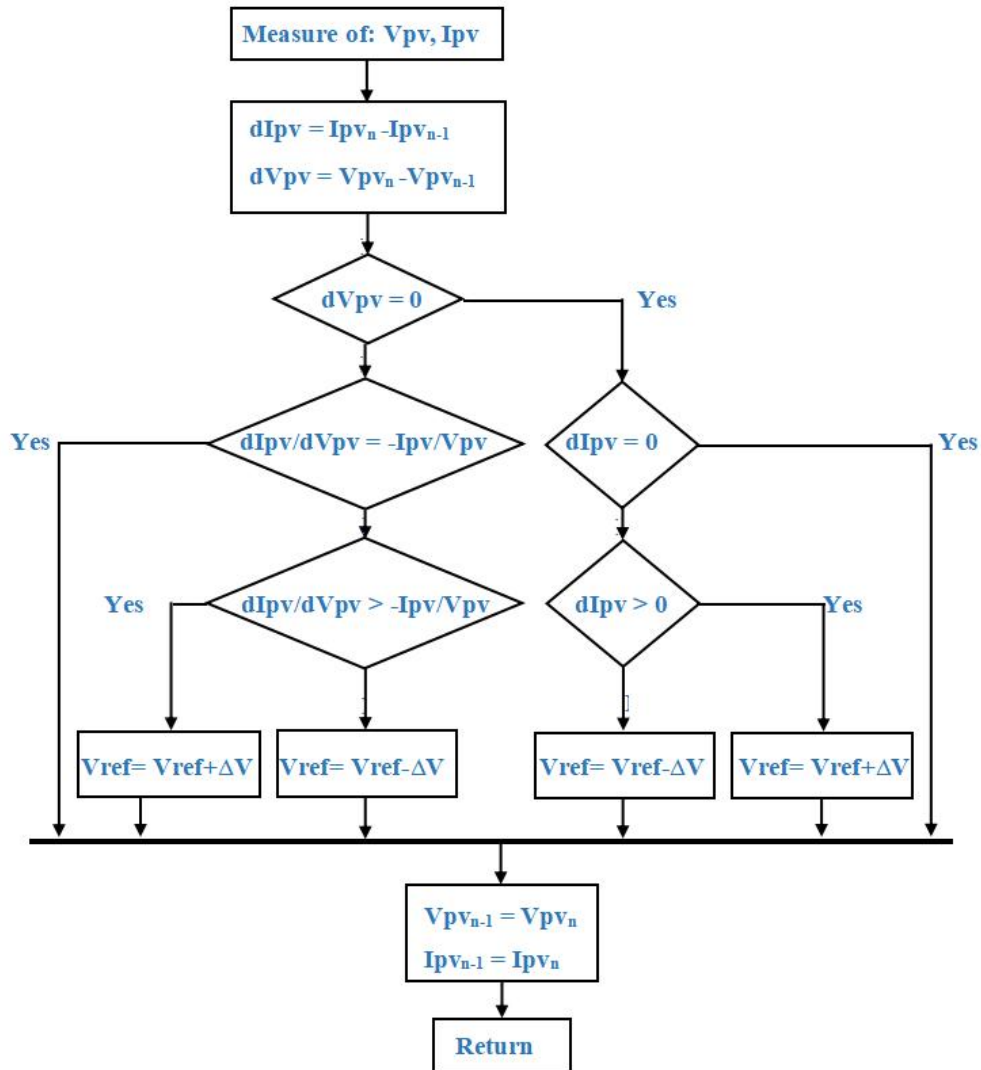


Figure III.20 : Incremental Conductance.

It calculates the incremental change in power (dP) and incremental change in voltage (dV) for the current operating point.

Then, it calculates the instantaneous conductance (G), which is the ratio of dP to dV .

If G matches the negative of the conductance at the previous operating point (indicating that $dP/dV = -dI/dV$), it means the system is close to the MPP.

If G is greater (indicating that the system is on the left side of the MPP), the voltage is adjusted in one direction to approach the MPP.

If G is smaller (indicating that the system is on the right side of the MPP), the voltage is adjusted in the opposite direction to approach the MPP.

This process continues until the controller converges to the MPP.

Incremental Conductance is known for its fast and accurate tracking of the MPP, making it suitable for environments with rapidly changing irradiance and temperature conditions. However, it is computationally more intensive than P&O.

Both P&O and INC MPPT algorithms aim to ensure that a photovoltaic system operates efficiently and extracts the maximum available energy from sunlight, improving the overall performance and energy yield of PV systems. The choice between these algorithms depends on the specific application and the environmental conditions in which the PV system operates.

III.4.2. DC-Bus Control (Vdc)

In the context of a PV pumping system, DC-Bus (Vdc) control assumes a pivotal role, serving as the linchpin that connects the system's key components. This specialized DC-Bus control mechanism orchestrates the interface between the Boost converter of the photovoltaic (PV) system and the 3-phase inverter, while also managing the Buck-Boost converter of the battery system, all in service of efficiently powering the electrical pump.

Much like its broader applications, DC-Bus control in this context revolves around several critical functions. Firstly, it meticulously regulates the DC link voltage, ensuring that it remains at a predetermined reference level. This voltage regulation is crucial to maintaining the stability and efficiency of the entire system, as deviations from the desired voltage can lead to suboptimal performance or even system instability [66][67].

Moreover, DC-Bus control plays a key role in managing the energy storage component, the battery in this case. It oversees the charging and discharging cycles of the battery to ensure that the DC link voltage remains within the specified range. By doing so, it safeguards against overcharging or deep discharging of the battery, thus prolonging its lifespan and optimizing its performance [66][67].

Additionally, the DC-Bus control system in a PV pumping system boasts rapid dynamic response capabilities. This responsiveness enables it to swiftly adapt to changes in load demand or input conditions, ensuring that the electrical pump receives the power it needs precisely when it's required. Such dynamic control is essential for maintaining system stability and minimizing voltage fluctuations, which can be particularly critical in water pumping applications.

Lastly, the effective coordination of the Boost converter, 3-phase inverter, and Buck-Boost converter by the DC-Bus control system optimizes the energy conversion processes within the system. This optimization translates into increased energy efficiency, reduced power losses, and an overall enhancement in the performance and reliability of the PV pumping system.

In conclusion, within the realm of PV pumping systems, DC-Bus (Vdc) control emerges as the central nervous system, seamlessly connecting the Boost converter, 3-phase inverter, and Buck-Boost converter to efficiently power the electrical pump. Its multifaceted functions encompass voltage regulation, energy storage management, dynamic response to load changes, and the optimization of energy conversion processes. By doing so, DC-Bus control ensures that the system operates at peak efficiency, delivering reliable and sustainable water pumping solutions in a variety of environmental conditions.

III.4.3. Battrey management & control

Within the PV pumping system, the intricate coordination between the Boost converter of the PV system and the Buck-Boost converter of the battery plays a pivotal role in maintaining a stable DC link voltage (V_{dc}) on the DC-Bus. The Boost converter, under the guidance of Maximum Power Point Tracking (MPPT) control, optimizes power extraction from the photovoltaic panels by perpetually tracking voltage and current, thus identifying the ideal operational point for maximum power output. Simultaneously, the Buck-Boost converter meticulously manages voltage and energy flow, ensuring that V_{dc} remains within the prescribed range. Its precise charge and discharge control algorithms govern parameters such as charging currents, voltage limits, and discharge rates to avert overcharging or deep discharging of the battery, safeguarding its longevity. Together, these converters provide a dependable and well-regulated power supply to the electrical pump, bolstering efficiency and reliability. This synergy between efficient power utilization and systematic energy management extends component lifespans and guarantees consistent pump performance across a spectrum of environmental conditions [63][68][69].

III.4.4. Inverter Control

Three-phase inverters employ modulation techniques to control the switching of semiconductor devices (usually MOSFETs or IGBTs) in the inverter bridge. often PWM which stands for Pulse Width Modulation. It is a modulation technique used in electronics to control the average voltage or power delivered to a load, typically a motor, light, or other device. PWM is widely employed because of its effectiveness in regulating power and achieving precise control over various applications [59][70].

In PWM, a continuous signal, typically a square wave, is generated with a fixed frequency. The key parameter that varies is the width of the "on" or "high" part of the signal, known as the duty cycle. The duty cycle represents the fraction of time during one cycle that the signal is in the "on" state, and it's expressed as a percentage[59][70].

By adjusting the duty cycle of the PWM signal, we can control the average power delivered to the load. When the duty cycle is higher, more power is delivered, and when it's lower, less power is delivered. This control method is especially useful for applications where fine-grained control of speed, intensity, or voltage is required.

Two predominant types of PWM control techniques exist for Three-Phase Inverters:

III.4.4.1 Voltage Control by Sine-Triangle PWM

This technique involves the comparison of a sinusoidal reference waveform (representing the desired output voltage) with a triangular waveform. The resulting comparison signal modulates the switching times of the inverter's power switches to generate the required three-phase AC output voltage waveform. Voltage control through Sine-Triangle PWM ensures that the output closely mimics the desired sinusoidal waveform, making it suitable for applications demanding high-quality voltage output [59][70].

III.4.4.2 Current Control by Hysteresis PWM

In contrast, this technique prioritizes the control of current flow within the inverter. It operates by comparing the actual current with a reference hysteresis band. If the current exceeds this band, the switching signals are adjusted to regulate the current within the desired range. Current control using Hysteresis PWM is particularly useful in applications where maintaining precise control over the motor's current is essential, as it can offer rapid and robust current regulation [70].

III.4.5. Induction machine control

Induction motor open-loop control finds its application in the context of PV pumping systems, where the primary objective is to regulate the speed and performance of the induction motor responsible for driving the pump. In this setup, open-loop control is employed to manage the motor's speed without the need for feedback from sensors to measure its actual performance.

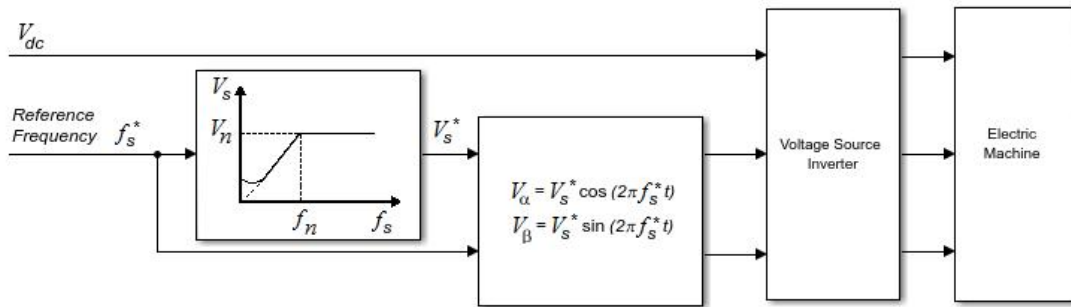


Figure III.21 : Scaler Control.

One of the fundamental aspects of this control strategy lies in adjusting the voltage and frequency supplied to the induction motor. Through a variable frequency drive (VFD) or motor controller, the voltage and frequency levels are manipulated to achieve the desired motor speed. This control technique often maintains a constant voltage-to-frequency (V/f) ratio, ensuring that the motor operates smoothly [71][72].

In the PV pumping system, open-loop control operates under certain assumptions about the load placed on the motor. It assumes a relatively consistent and known load, which may be appropriate for applications with relatively stable operating conditions. However, it's essential to recognize that open-loop control cannot adapt to variations in the load, which could arise due to changes in sunlight intensity, pump head, or other factors.

One of the advantages of employing open-loop control in PV pumping systems is its simplicity and cost-efficiency. It doesn't necessitate the installation of speed or position sensors, making it an economical choice for applications where precise speed control is not the foremost priority. This makes it suitable for scenarios where a certain degree of speed variation can be accommodated without compromising the system's overall functionality.

However, it's crucial to acknowledge the limitations of open-loop control in PV pumping systems. It cannot account for fluctuations in motor performance due to factors such

as variable sunlight, temperature changes, or mechanical wear on the pump. As a result, while it may suffice for certain applications with relatively stable operating conditions, it may not be suitable for scenarios where precise and adaptive control of the motor's speed is essential.

In summary, induction motor open-loop control serves as a pragmatic solution within PV pumping systems, offering a cost-effective means of regulating motor speed without the need for complex feedback systems. Its suitability depends on the specific requirements of the application and the degree of precision necessary for effective pump operation in variable environmental conditions.

III.5. Conclusion

Throughout this chapter, we delved deep into the intricacies of system modeling, beginning with the PV array itself. The mathematical models developed for PV panels allowed us to capture the behavior of these energy sources under varying environmental conditions, enabling accurate predictions of energy generation. Additionally, we explored the modeling of key components such as converters, induction motors, and centrifugal pumps. These models elucidated the dynamic interactions between these components, paving the way for a comprehensive understanding of the entire system.

The chapter also unveiled the intricacies of system control, emphasizing the pivotal role of control strategies in optimizing system performance. We explored Maximum Power Point Tracking (MPPT) techniques like P&O and INC, which are instrumental in ensuring that the PV array operates at its peak efficiency. Further, we delved into the control of various components, including Vdc control, battery management, inverter control (SPWM and SVPWM), and induction machine control (scalar control). Each of these control strategies was presented with clarity, providing a roadmap for implementing and fine-tuning control algorithms in PV pumping systems.

In conclusion, Chapter 3 has equipped us with a robust foundation in PV pumping system modeling and control. The acquired knowledge will serve as a cornerstone for the subsequent chapters, where we will explore fault diagnosis and fault-tolerant control techniques specific to PV pumping systems. By understanding the system's intricacies and mastering control strategies, we are better poised to address the unique challenges posed by fault management in these systems and enhance their reliability and efficiency in real-world applications.

IV Chapter 04 : PV Pumping System Fault Modeling and Simulation

IV.1. Introduction

This chapter delves into the realm of PV pumping system faults simulation, aiming to investigate and understand the impact of faults on the performance and reliability of these systems. Faults, whether in the converters or the induction motor, can occur due to various reasons, including environmental conditions, wear and tear, or manufacturing defects. The ability to simulate these faults and assess their consequences is vital for system designers, operators, and maintenance personnel.

In this chapter, we will explore the generation and simulation of faults within PV pumping systems. The focus will be on two critical components: converters and induction motors. Converter faults, such as open switch and short switch faults, can disrupt the power conversion process, while induction motor faults, including stator and rotor faults, can compromise the system's ability to efficiently pump water. By systematically studying these faults and their effects through simulation, we aim to provide valuable insights into fault detection, mitigation, and maintenance strategies for PV pumping systems.

IV.2. Fault Modeling and Faults Generation in Simulation

Before we explore the effects of faults, it's essential to establish a framework for modeling and generating these faults in our simulation.

IV.2.1. Converters Fault

In the realm of PV pumping systems, where the efficient conversion and control of electrical energy are vital, the occurrence of converter switch faults, including open-circuit and short-circuit switch faults, can have significant implications for system performance and reliability [73][74][75][76].

IV.2.1.1 Open-Circuit Switch Fault

An open-circuit switch fault in a DC-DC or DC-AC converter within a PV pumping system occurs when one or more semiconductor switches fail to close properly, interrupting the flow of electrical current. This malfunction can disrupt the energy transfer process and result in decreased system efficiency. In a DC-DC converter, for example, an open-circuit fault could hinder the efficient conversion of DC power from the PV panels to the desired voltage level for the pump, leading to reduced water pumping capacity. Similarly, in a DC-AC converter, such a fault might prevent the generation of the required AC power for the motor. Open-circuit switch faults can be attributed to various factors, including component aging, manufacturing defects, or excessive stress during operation.

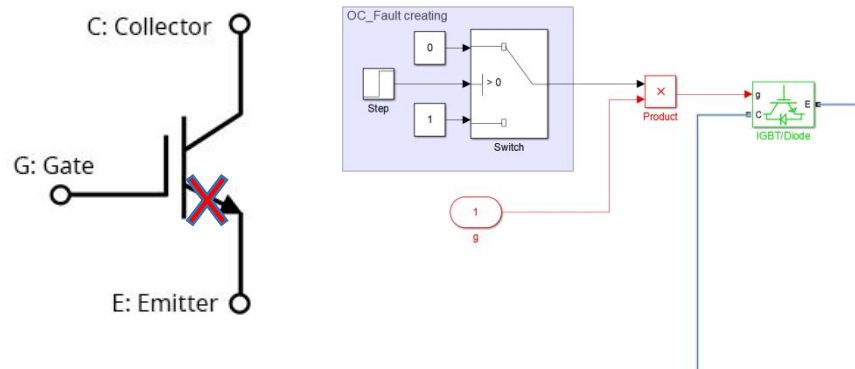


Figure IV.1 : Open-Circuit Switch Fault

IV.2.1.2 Short-Circuit Switch Fault

Conversely, a short-circuit switch fault in a DC-DC or DC-AC converter entails an unintended electrical connection between the high and low sides of the converter. This fault can result in excessive current flow, potentially damaging the semiconductor switches and other components within the converter. In the context of a PV pumping system, a short-circuit switch fault can lead to overcurrent conditions that may compromise the safety and longevity of the converter and connected equipment. Additionally, it can cause significant disruptions in the water pumping process, impacting the system's overall performance.

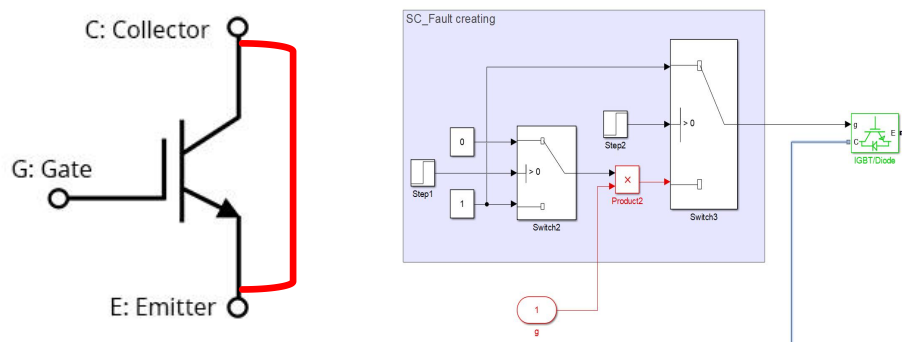


Figure IV.2 : Short-Circuit Switch Fault

For the simulation, the open switch faults are created by opening the switch of the converter, by a "zero" control signal, or can be given without the respective control line, thus the switch becomes in the off state. On the other hand, the short switch faults are created by connecting its Collector with its Emitter, or can be given by a "ones" control signal.

Mitigating the impact of these switch faults in a PV pumping system is crucial. Implementing protective measures, such as overcurrent and overvoltage protection devices, can help detect and isolate faults promptly. Additionally, regular inspection

and maintenance can help identify early signs of switch degradation or open-circuit faults. Advanced converter designs may also incorporate redundant switches or fault-tolerant control strategies to ensure continued operation even in the presence of switch faults, thereby enhancing system reliability.

In summary, open-circuit and short-circuit switch faults in DC-DC and DC-AC converters within PV pumping systems can jeopardize system performance and equipment safety. Proactive measures, including protective devices and fault detection strategies, are essential to minimize the impact of these faults and maintain the reliable operation of the PV pumping system, crucial for delivering water in remote or off-grid locations.

IV.2.2. Induction Motor Fault

IV.2.2.1 Stator Fault

Electrical stator faults in induction motors predominantly involve issues within the stationary component of the motor. These faults encompass a spectrum of problems, including the degradation of winding insulation, phase imbalances, breakage or openings in the windings, and contamination of the stator windings. One frequently encountered stator fault involves insulation breakdown, which can lead to short circuits between winding turns or phases, thereby altering the resistance within the windings. This altered resistance may result in heightened current flow, overheating, and, if left unaddressed, the potential for catastrophic motor failure. Additionally, phase imbalances can disturb the equitable distribution of electrical load across the motor windings, resulting in inefficiencies and the risk of overheating [77][78][79].

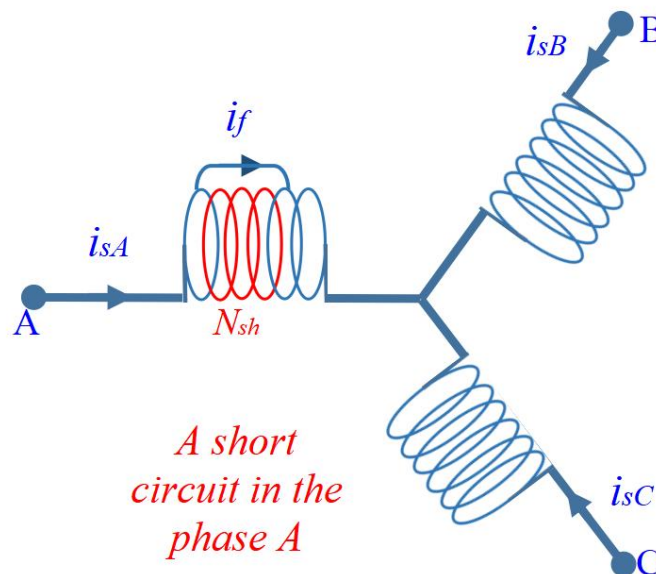


Figure IV.3 : Reduction in the number of turns by short-circuit effect.

The most common type of stator short circuit and which we will treat is the short circuit between turns. To model this fault we will assume that a number of turns n among those of a phase (phase 'a') is short-circuited, this section of short-circuited turns is defined by 'cc' which is introduced into the mathematical model governing the system studied as shown in Figure (IV.3), consequently the self-inductance and resistance of the faulty phase changes as well as the mutual inductance between this phase and all the other windings of the machine [52][60].

N_s is the number of turns in healthy mode of the asynchronous machine. A stator short circuit will lead to a decrease in the number of turns of the corresponding stator phase.

We can therefore define three coefficients cc_1 , cc_2 and cc_3 relating to the three phases of the machine as follows:

The number of useful turns for the three stator phases is then given by:

$$\begin{aligned} N_1 &= N_s - N_{cc1} = (1 - cc_1)N_s \\ N_2 &= N_s - N_{cc2} = (1 - cc_2)N_s \\ N_3 &= N_s - N_{cc3} = (1 - cc_3)N_s \end{aligned} \quad (IV.1)$$

The resistance of each phase is proportional to the number of useful turns. As a result of the reduction in the number of turns by short-circuit effect, this resistance decreases.

The new resistance matrix $[R_s]$ is rewritten as follows:

$$[R_s] = r_s \begin{bmatrix} (1 - cc_1) & 0 & 0 \\ 0 & (1 - cc_2) & 0 \\ 0 & 0 & (1 - cc_3) \end{bmatrix} \quad (IV.2)$$

IV.2.2.2 Rotor Fault

Electrical rotor faults in induction motors relate to issues within the motor's rotating component. These faults frequently involve problems with the rotor bars, such as breakage or damage, which can disrupt the smooth flow of electrical currents and lead to irregular motor performance, heightened vibrations, and overheating. Rotor faults can also emerge due to high starting currents, especially in scenarios where the motor undergoes frequent starts under heavy loads, inducing stress and potential rotor damage. Furthermore, faults associated with the rotor core, such as lamination shorts or open circuits, can detrimentally affect motor efficiency and

overall performance. Notably, rotor bar damage can significantly impact resistance by introducing higher resistive elements into the rotor circuit, causing disruptions in electrical current flow, elevated heat generation, and reduced motor efficiency [77][78][79].

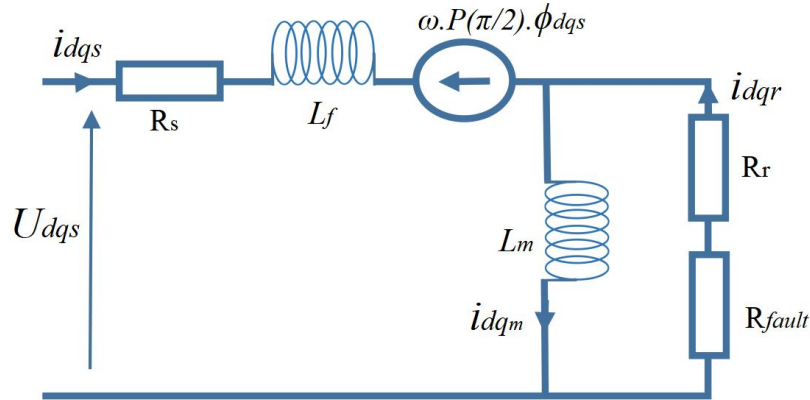


Figure IV.4 : broken bars rotor fault.

In broken bars model, the rotor defect results in an increase in the resistance of the elements presenting a defect. They do not lead to any modification of the rotor topology, but only certain elements of the matrix $[R_r]$ are modified. To do this, the simplest procedure consists of adding to the resistance matrix $[R_r]$ a new matrix $[R'_r]$ where the non-zero elements correspond to the faulty elements. In the case where the fault concerns bar k , the new rotor resistance matrix is written:

$$[R_{rf}] = [R_r] + [R'_r]$$

Where:

(IV.3)

$$[R_{rfdq}] = \begin{bmatrix} R_{rdd} & R_{rdq} \\ R_{rqd} & R_{rqq} \end{bmatrix}$$

In the case where we want to simulate the breakage of a bar or two or more bars, the only values that will change $R_{rdd}, R_{rdq}, R_{rqd}$ et R_{rqq} are those of the values of the broken bars which will be increased [52][60].

IV.3. System Simulation & Results (Healthy & Faulty Modes)

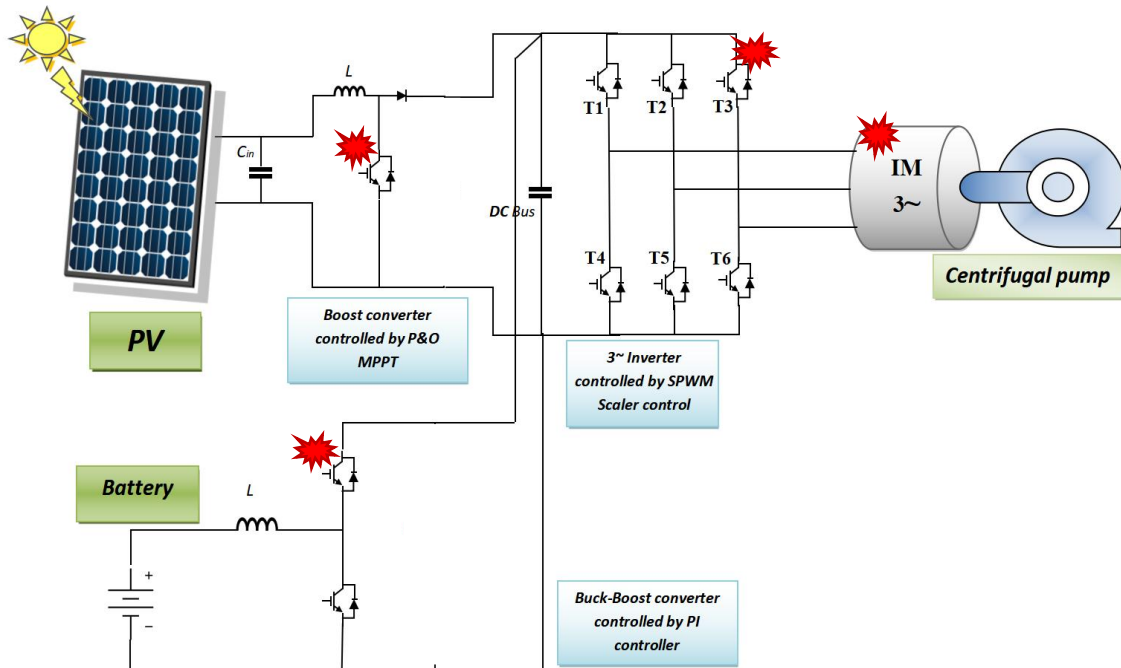
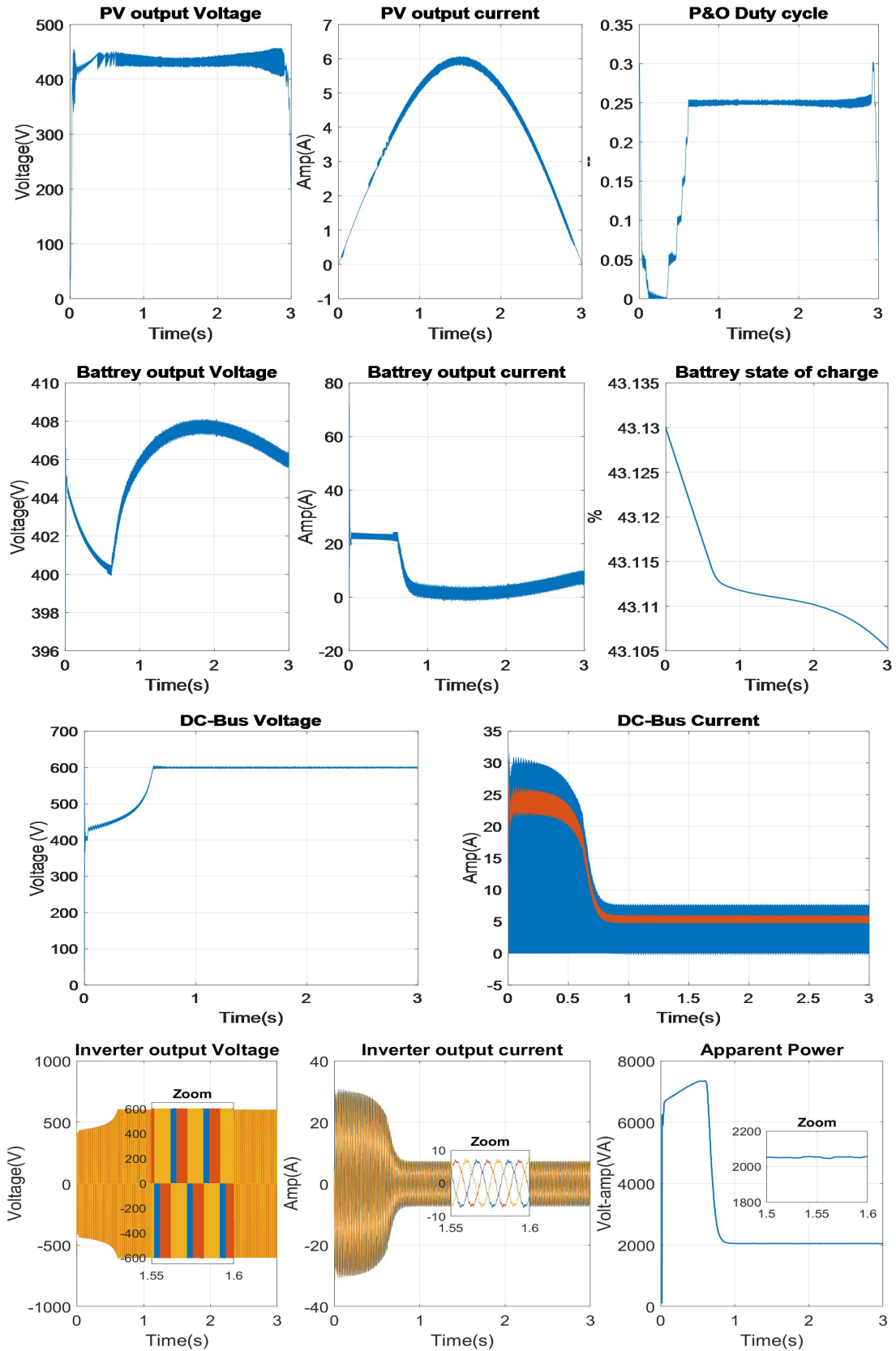


Figure IV.5 : Proposed system Faults.

In our exploration of PV pumping system faults simulation, we will systematically investigate eight critical fault scenarios that can impact system performance and reliability. These faults encompass both converter and induction motor components. Specifically, we will address two converter faults Open Switch Fault and Short Switch Fault examining their effects on Boost Converter and Buck-Boost Converter operation, as well as the consequences within the Three-Phase Inverter. In addition to converter faults, our analysis extends to induction motors, where we will delve into Stator Faults, including short circuits between turns, and Rotor Faults, encompassing the disruption caused by broken bars. By comprehensively studying these fault scenarios, we aim to provide valuable insights into the behavior and vulnerabilities of PV pumping systems, ultimately contributing to the development of more resilient and dependable water pumping solutions powered by renewable energy sources.

IV.3.1. Healthy Mode



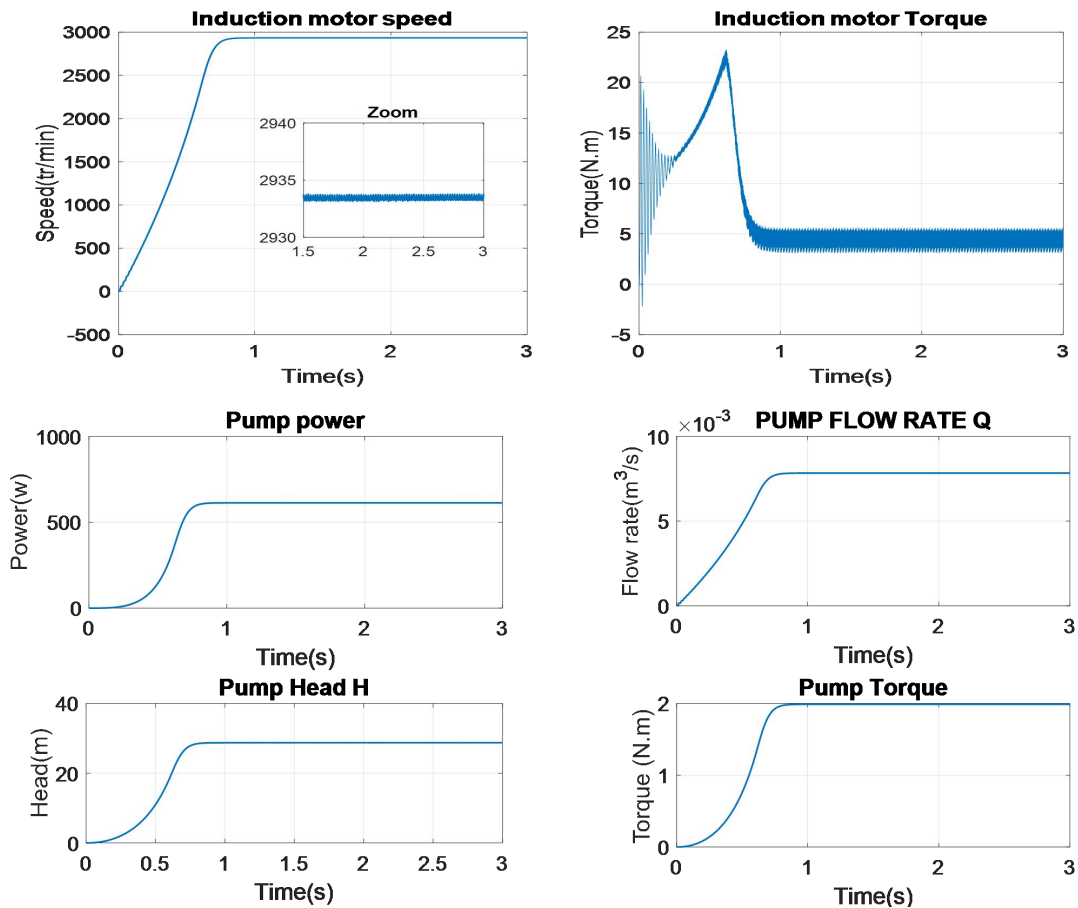


Figure IV.6 : Healthy Mode simulation results.

IV.3.2. Converters Fault effects

IV.3.2.1 Boost Converter Fault effects

IV.3.2.1.a. Open switch Fault

An Open Switch Fault in a Boost Converter within our PV pumping system with battery storage leads to a loss of Maximum Power Point Tracking (MPPT) functionality, significantly impacting system performance. This fault disrupts the converter's ability to regulate voltage effectively and track the maximum power point of the solar panels. Consequently, the PV system can no longer efficiently harvest solar energy, resulting in suboptimal energy conversion. The consequences include reduced energy output and inefficient battery charging.

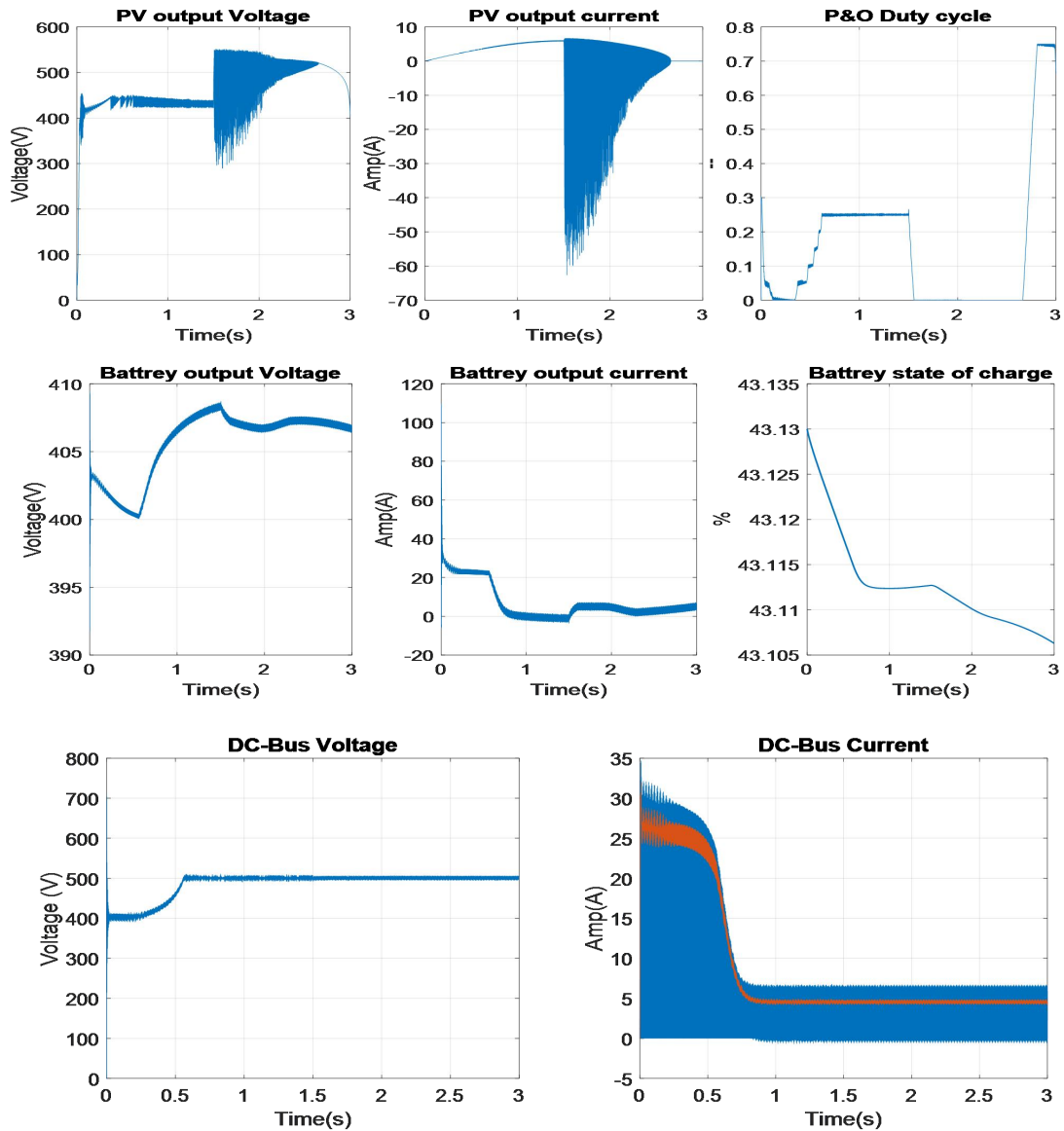


Figure IV.7 : Boost Converter Fault effects (Open switch Fault).

IV.3.2.1.b. Short switch Fault

A Short Switch Fault in a Boost Converter within a PV pumping system with a battery results in current flows through the short circuit which means the disconnection of the PV array power from the system and reliance solely on the battery to power the pump. Its notable that PV array functions on its I_{sc} ; to prevent further damage or safety hazards, the PV array should be disconnected. While this ensures continued water pumping, it places a heavy load on the battery, potentially depleting its charge rapidly and affecting the system's overall energy storage capacity.

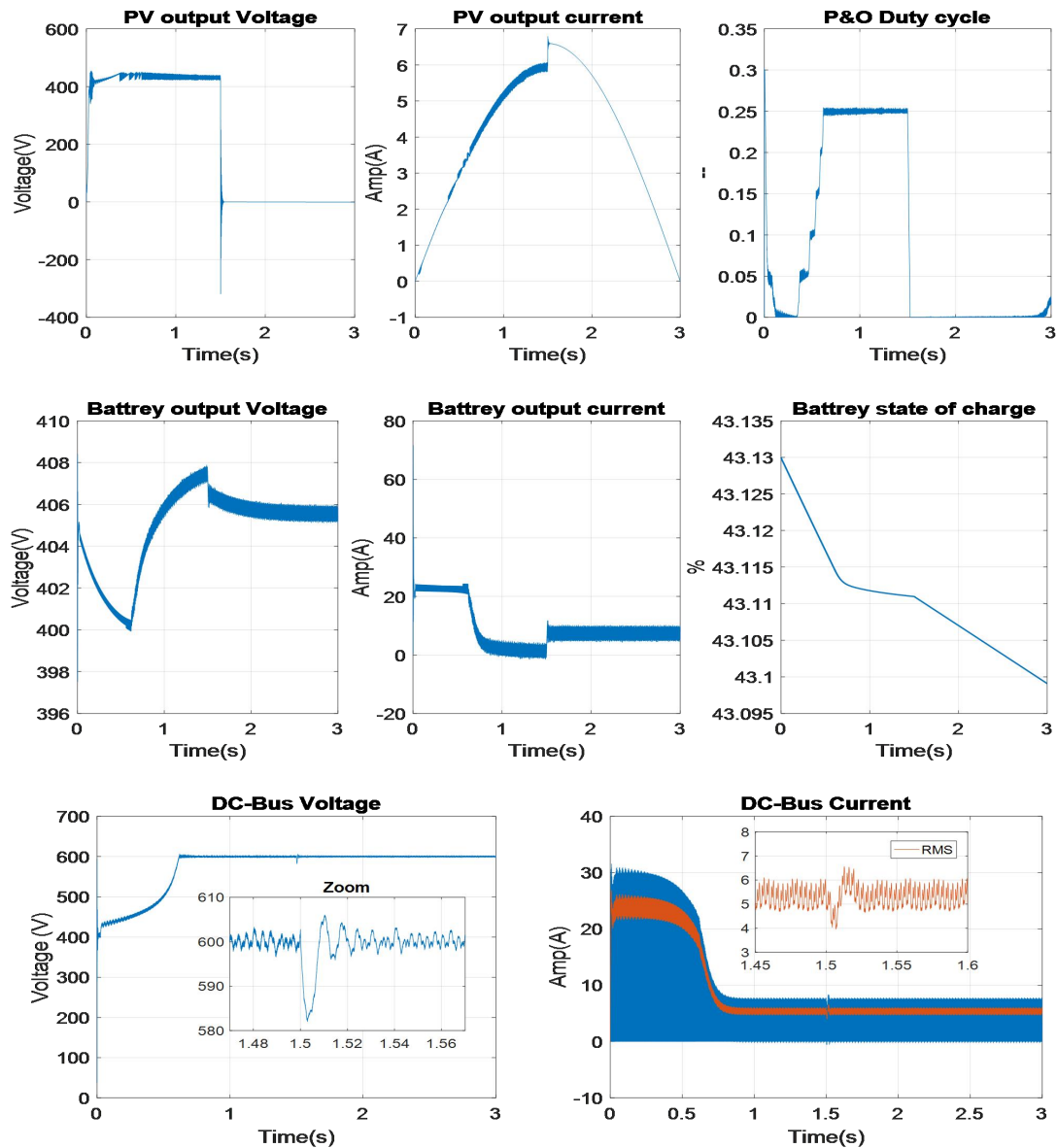


Figure IV.8 : Boost Converter Fault effects (short switch Fault).

IV.3.2.2 Buck-Boost Converter Fault effects

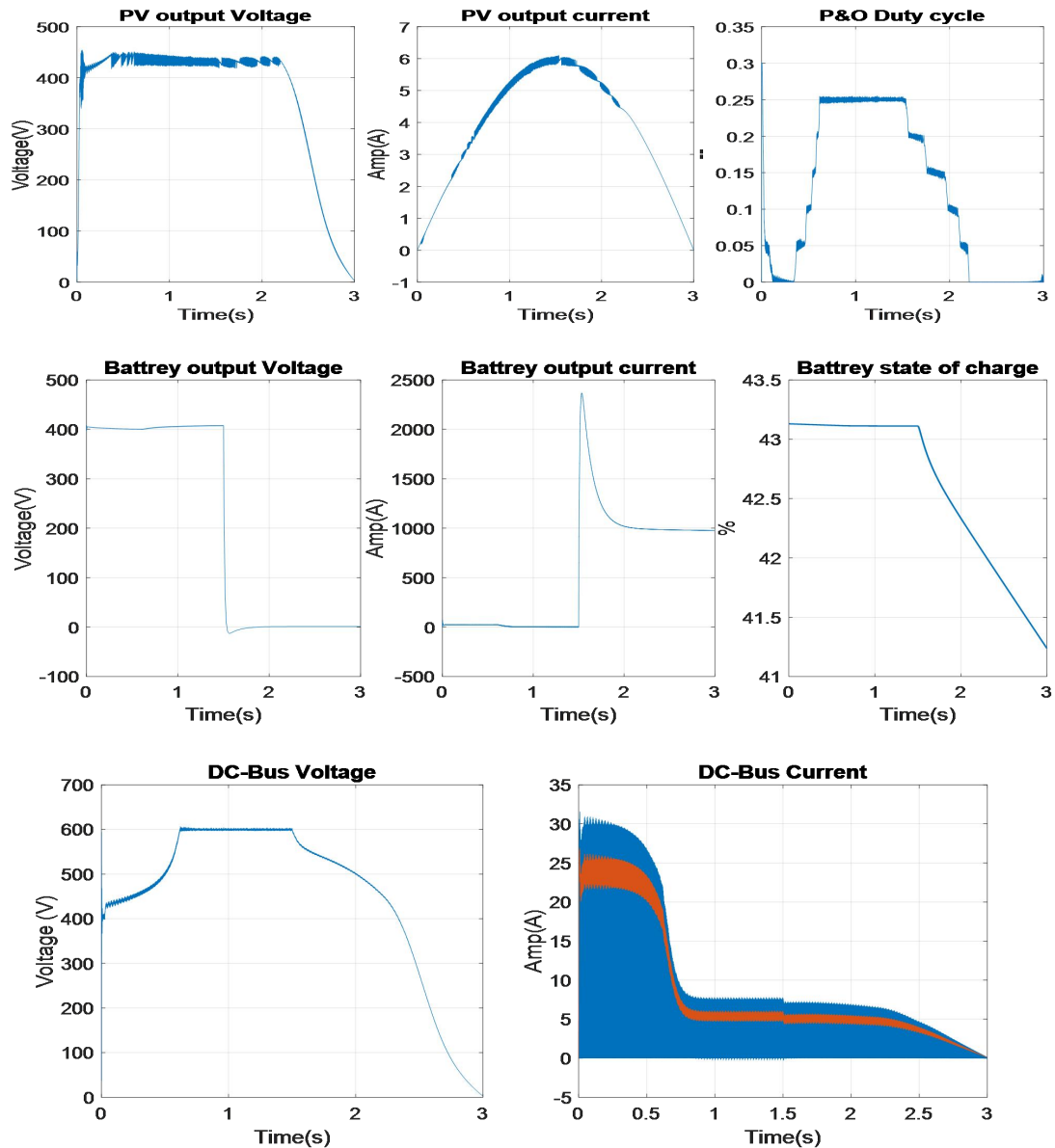
In our simulation, we considered a scenario where one of the switches in the Buck-Boost Converter was permanently in the OFF state, and the other was in a permanent ON state. This configuration resulted in distinct fault effects for each switch condition.

IV.3.2.2.a. Open switch Fault

The Buck-Boost Converter works as a boost converter, which means it increases the output voltage.

The power flow is dependent on the PV array, resulting in the pumping system primarily using power from the PV array. As a result, by the end of the day, when the sunset there will be no power to be distributed.

In the case of an open switch fault, a potentially dangerous condition arises as the current of the battery can become too high due to a short circuit. To prevent damage or overheating, it may be necessary to disconnect the battery.



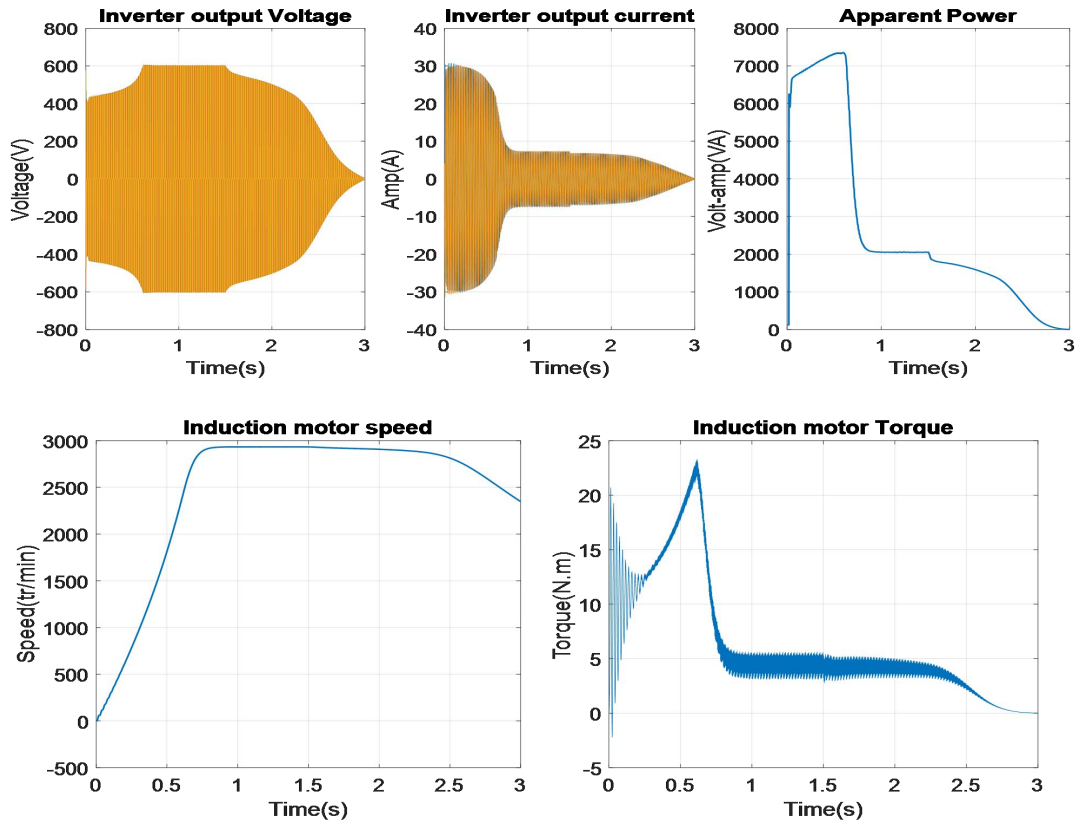


Figure IV.9 : Buck-Boost Converter Fault effects (Open switch Fault).

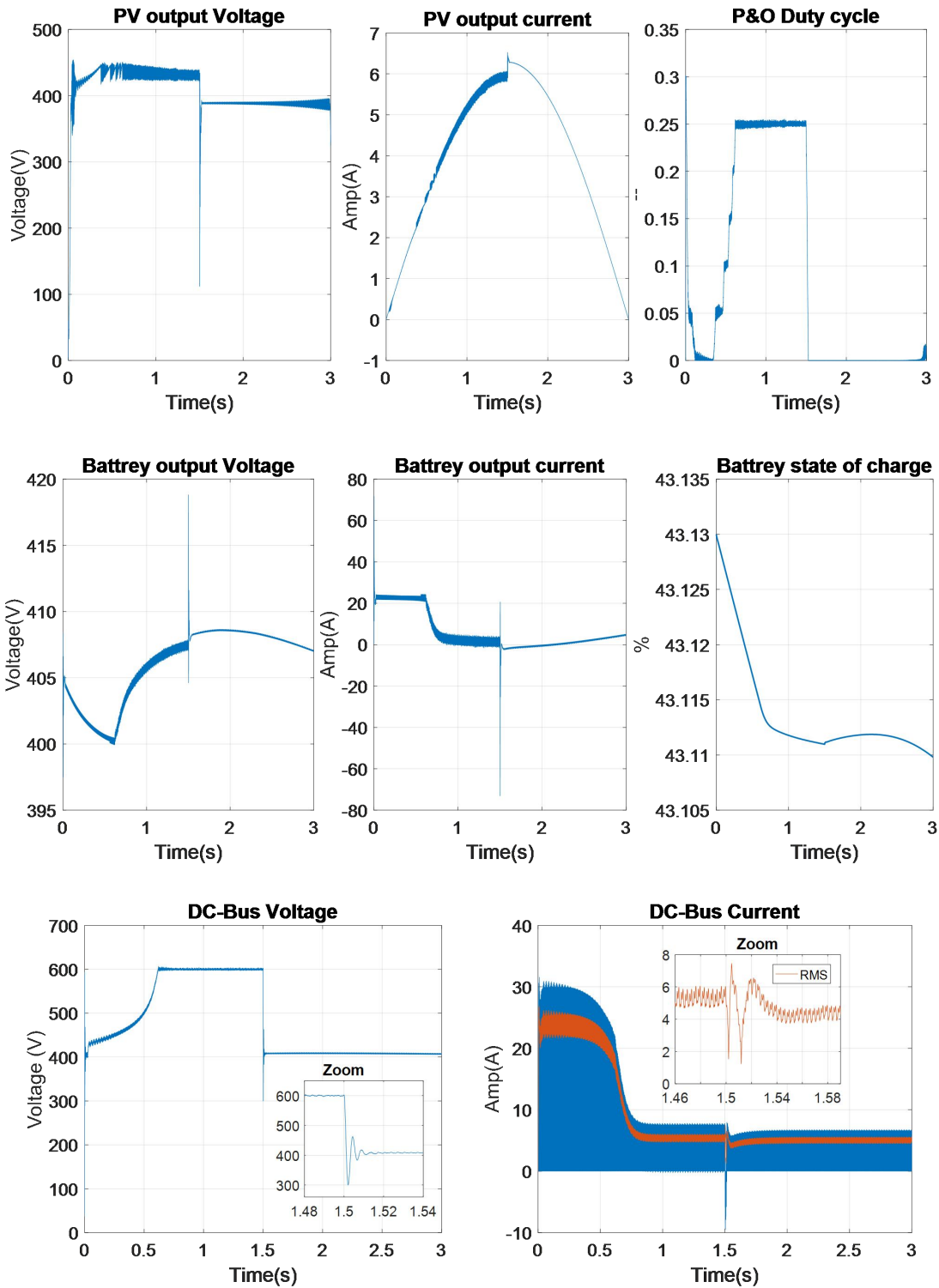
IV.3.2.2.b. Short switch Fault

In the event of a short switch fault, several effects can be observed:

The control of the DC-bus voltage may be compromised due to the short switch fault, causing the converter to operate differently from its intended function, which may result in a loss of voltage control.

The battery is primarily in a charging state, which is an accurate consequence of a short switch fault. The converter operates as a buck converter, reducing the output voltage and effectively charging the battery.

The PV output current may indeed approach the short-circuit current (I_{sc}) value. However, this outcome can potentially cause issues, especially if not managed properly, as the converter is trying to push a high current into the PV array. It's important to monitor and control this to prevent damage to the PV system.



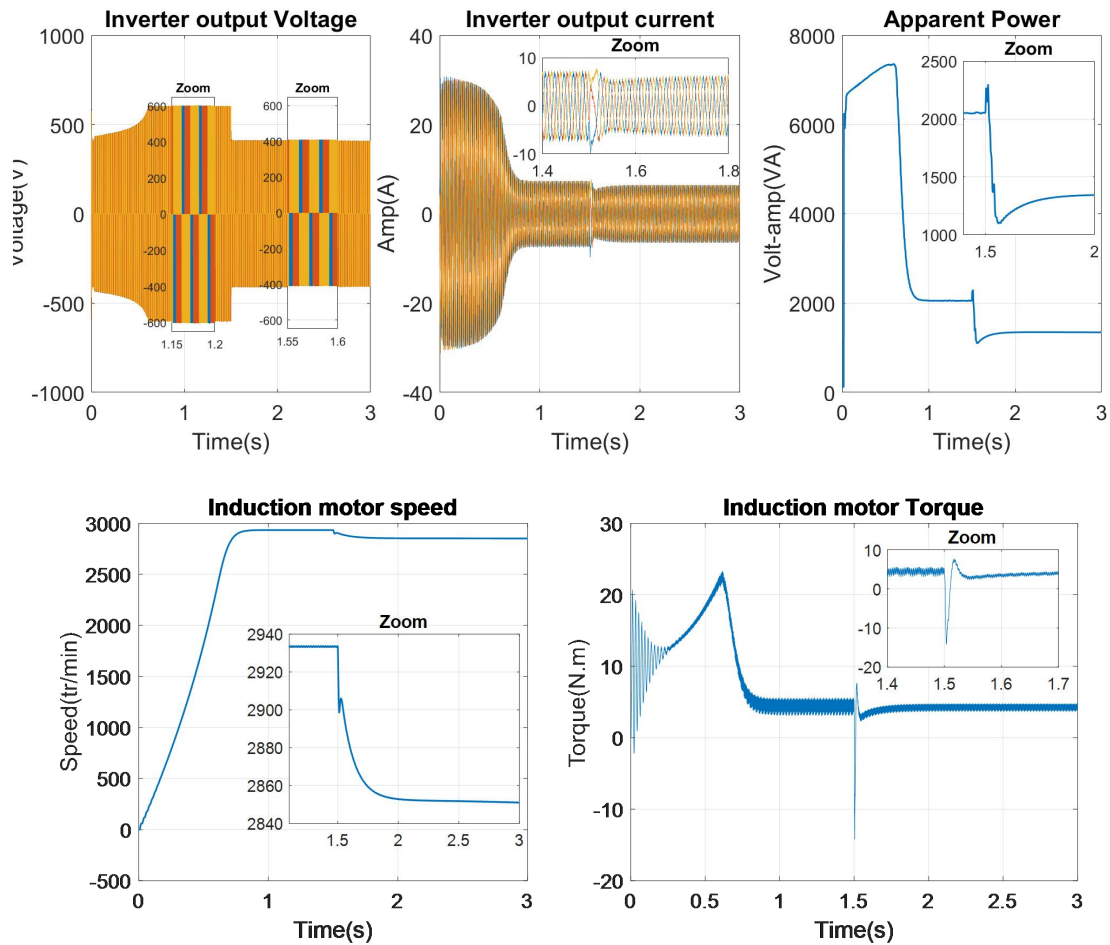


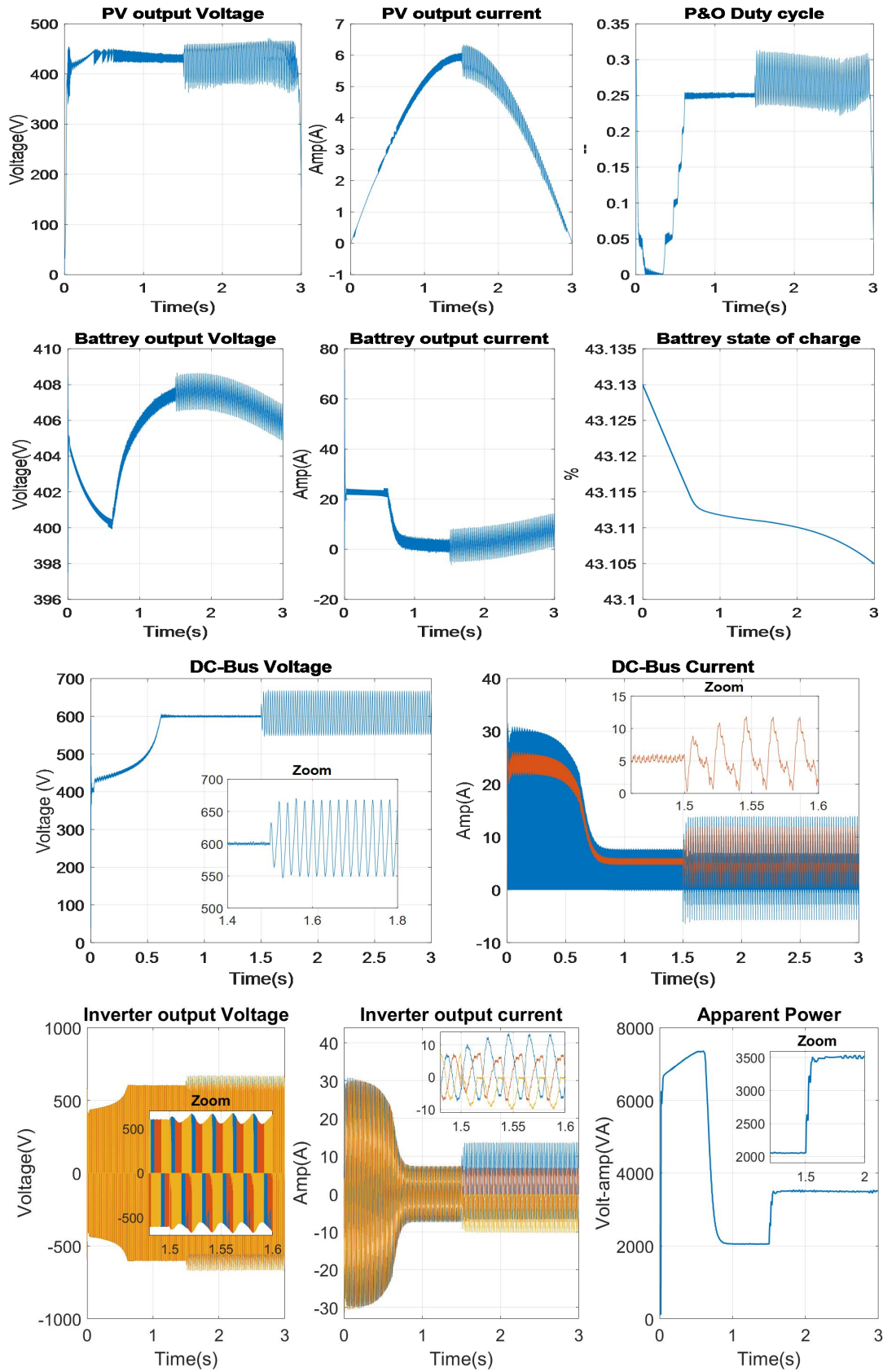
Figure IV.10: Buck-Boost Converter Fault effects (Short switch Fault).

IV.3.2.3 Three-Phase Inverter Fault effects

Both open switch and short switch faults in a Three-Phase Inverter can have significant and potentially detrimental effects on a PV pumping system. These effects range from unbalanced power delivery and operational disturbances to issues such as energy storage depletion, vibration, and even pump failure.

IV.3.2.3.a. Open switch Fault

In the event of an open switch fault within the inverter, several effects can be observed. Firstly, this fault may result in oscillations in PV voltage and current as well as DC-Bus voltage and current. This can introduce instability in the system's power supply and affect the overall performance of the pump. Additionally, the loss of half of one phase's output due to the fault leads to unbalanced power delivery, which can affect the pump's efficiency. Disturbances in the three-phase system's voltage and current waveforms may cause fluctuations in the pump's operation, potentially leading to performance issues and reduced water pumping capabilities.



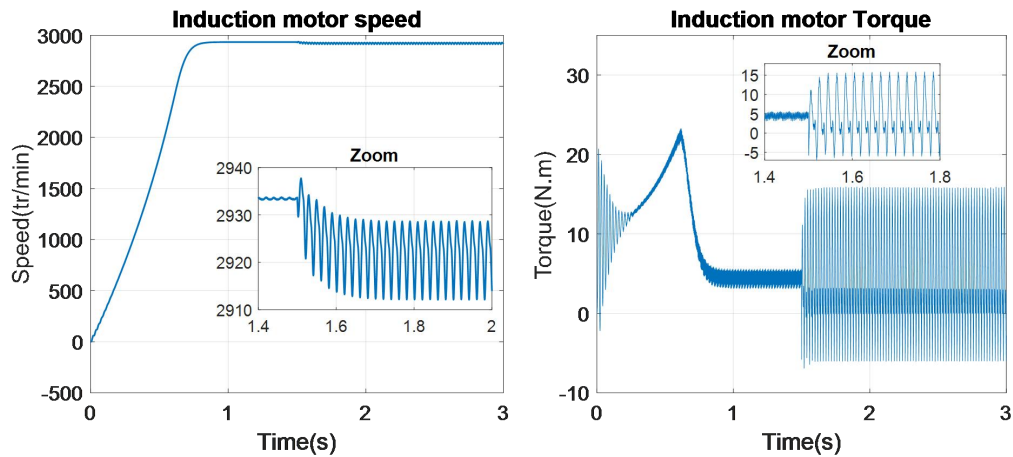
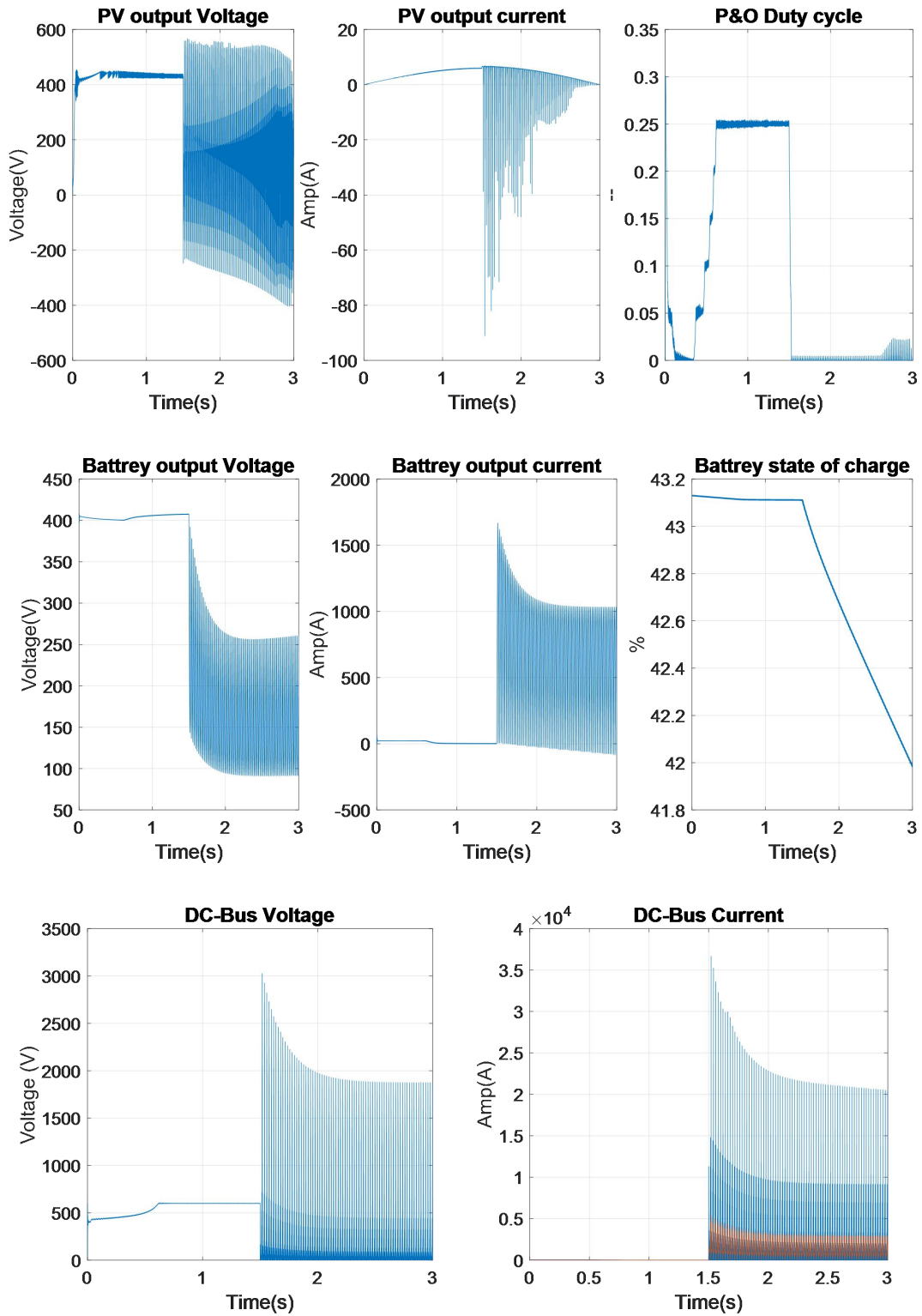


Figure IV.11 : Three-Phase Inverter Fault effects (Open switch Fault)

IV.3.2.3.b. Short switch Fault

On the other hand, a short switch fault in the Three-Phase Inverter can result in a different set of consequences. Distorted output voltage and current waveforms can significantly impact the operation of the pump. These waveform distortions can lead to issues such as overheating and inefficient pump operation. The high current levels associated with the short switch fault can not only cause potential damage to the inverter but also result in fluctuations in PV voltage and current, DC-Bus voltage and current, and battery voltage and current. As a result, the battery may start discharging, and the system's energy storage capacity may be compromised.

Furthermore, the increased oscillations in torque may lead to excessive vibration in the pump, potentially damaging the equipment and causing operational instability. The fault can even result in zero speed, rendering the pump unable to function effectively. Lastly, due to the disruption in the inverter's proper functioning, the system may consume more power than necessary, leading to inefficiencies and higher operational costs.



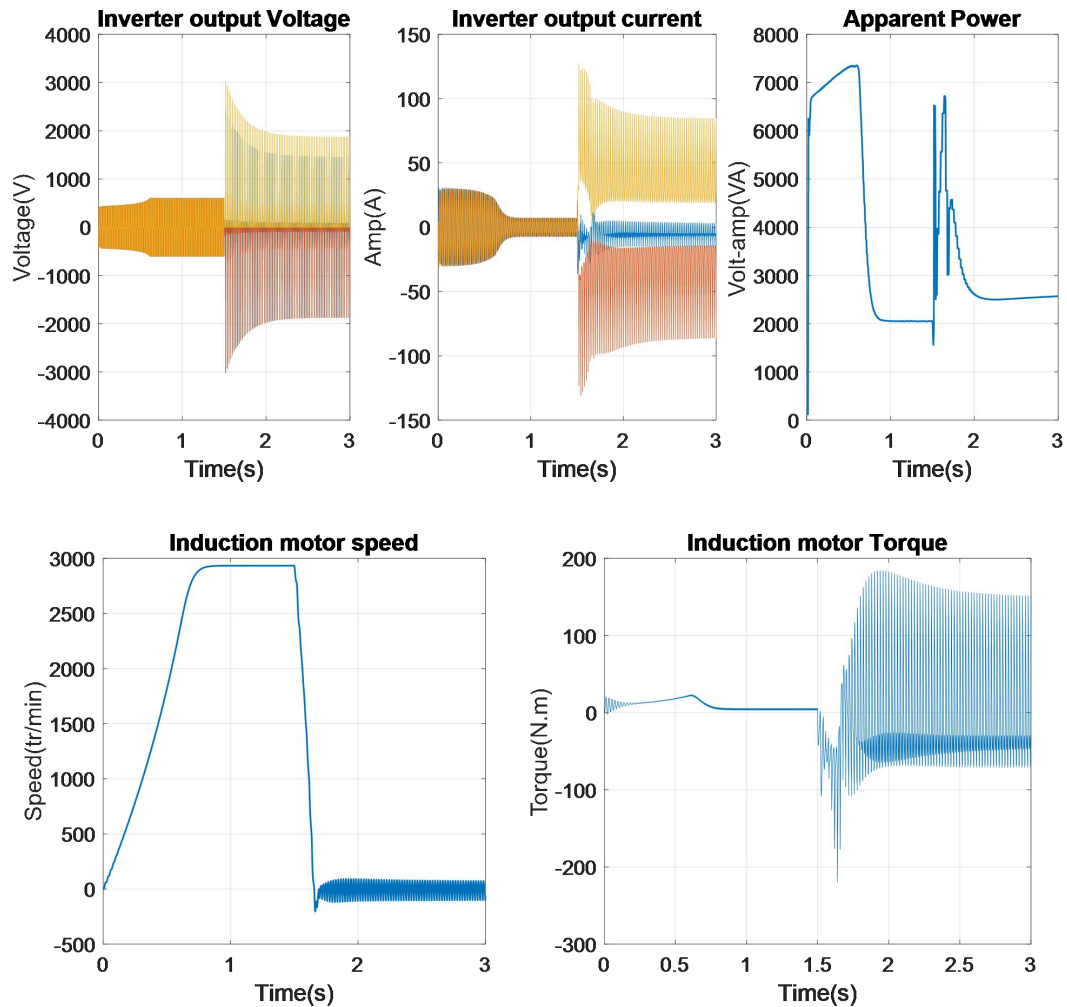


Figure IV.12 : Three-Phase Inverter Fault effects (Short switch Fault)

IV.3.3. Induction Motor Fault effects

IV.3.3.1 Stator Fault effects

Stator faults, such as winding shorts lead to reduced motor efficiency. This results in a decrease in the motor's ability to convert electrical power into mechanical power, leading to higher energy consumption for the same mechanical output. It also causes excessive current flow and increased copper losses, resulting in higher temperatures within the motor. Overheating can lead to insulation degradation and can be a precursor to more severe motor damage. In addition, Stator faults can lead to an imbalance in the magnetic field, causing increased vibration and noise in the motor. This can result in mechanical wear and reduced motor performance.

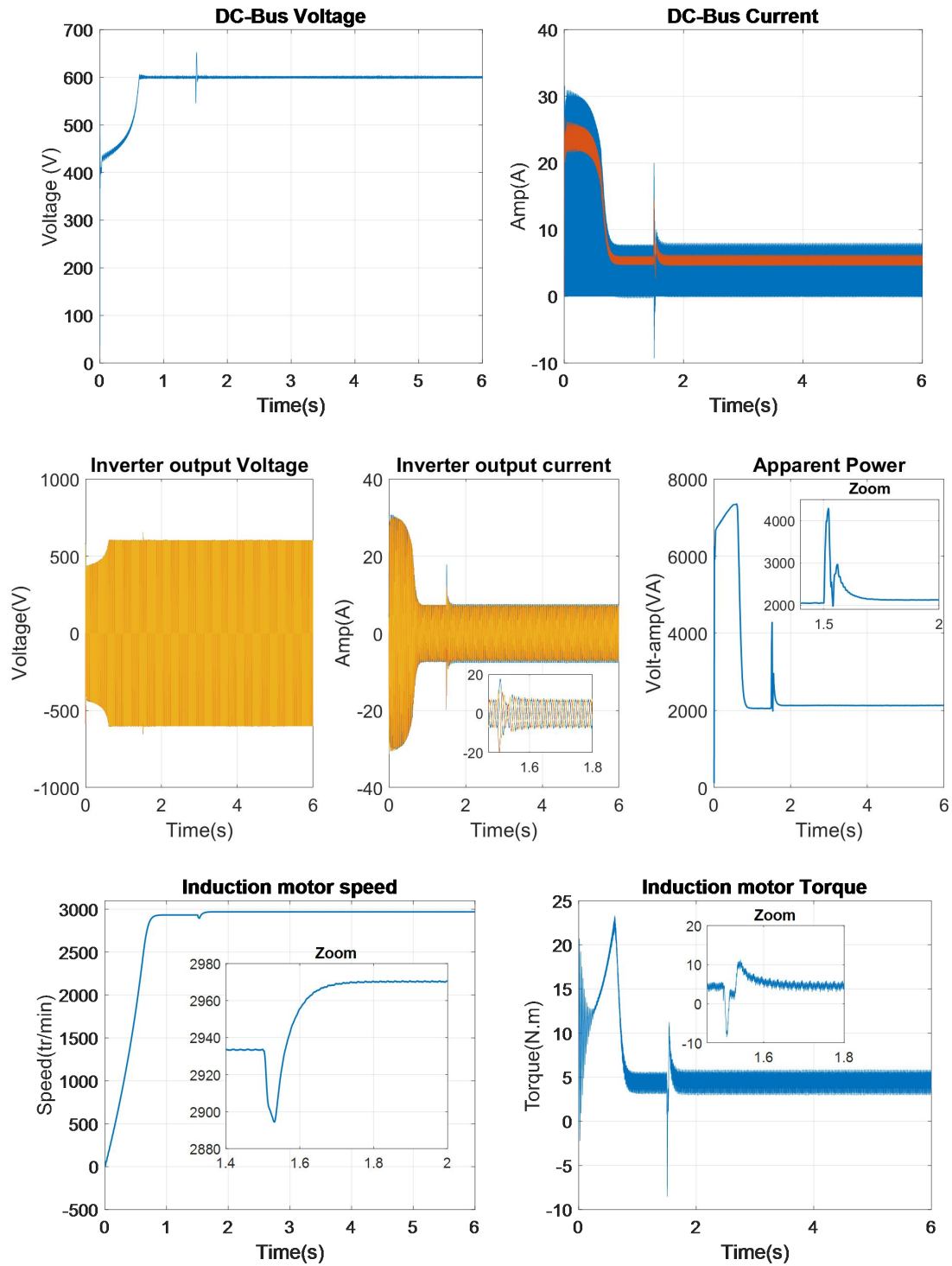


Figure IV.13 : Induction motor stator fault effects.

IV.3.3.2 Rotor Fault effects

Rotor faults, such as broken rotor bars or end-ring faults, can lead to unwanted effects, similar to stator faults. The motor may require more electrical power to

produce the same mechanical output. it increases the slip of the motor, which indicates a reduction in synchronous speed with oscliation and may lead to reduced motor performance. it also results in mechanical imbalances and increased vibration, leading to abnormal noise during motor operation. These vibrations can cause further damage to the rotor and other motor components.

Rotor faults can result in increased motor current and temperature, potentially leading to overheating and further damage to the rotor and stator. And also disrupt the symmetry of the magnetic field in the motor, leading to unbalanced operation and reduced motor efficiency.

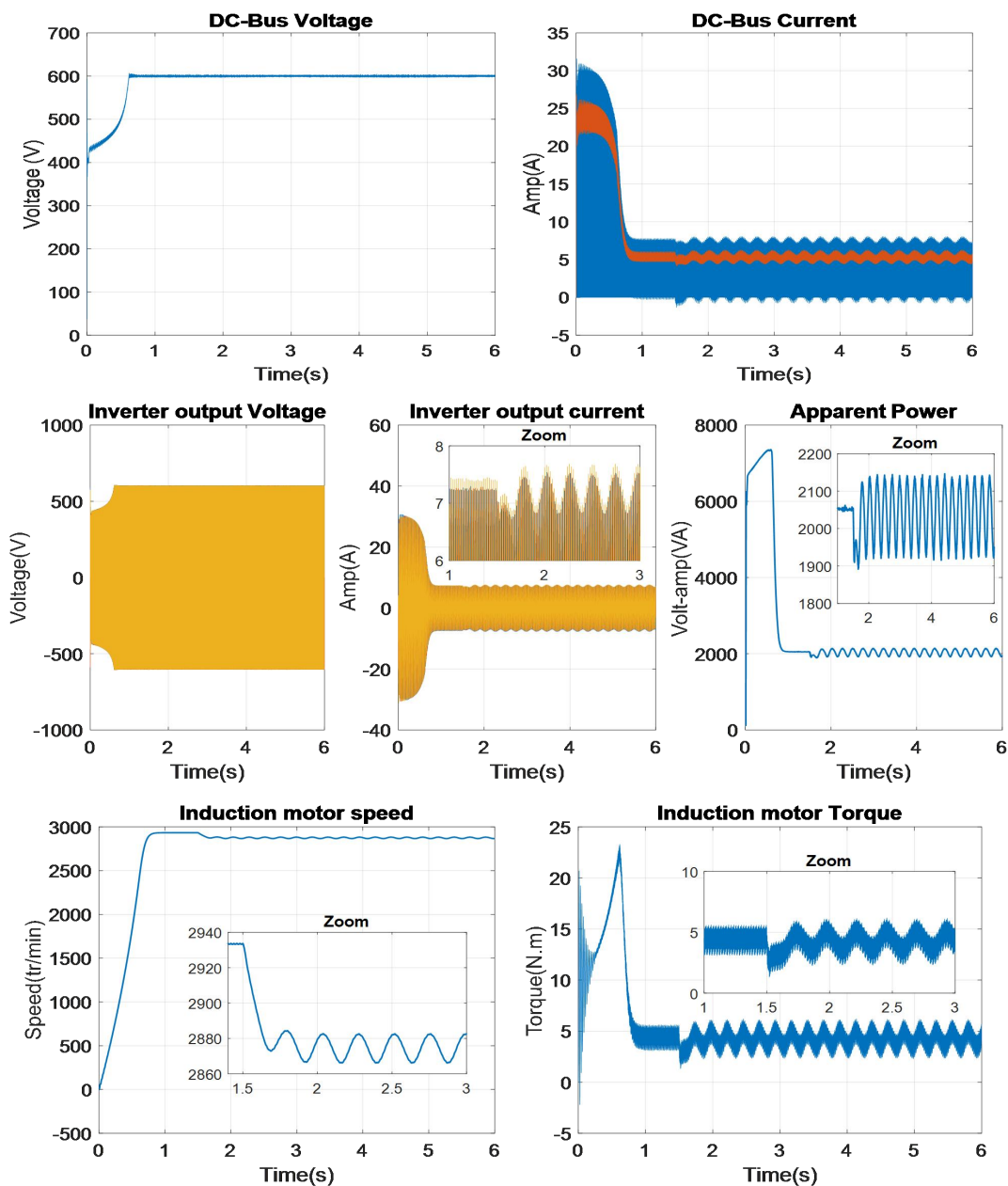


Figure IV.14 : Induction motor rotor fault effects.

IV.4. Conclusion

In this chapter, we embarked on a comprehensive exploration of PV pumping system fault modeling and simulation, aiming to shed light on the impact of faults on system performance and reliability. Faults within PV pumping systems can manifest in converters and induction motors due to various factors, including environmental conditions, wear and tear, and manufacturing imperfections. These faults, if left unaddressed, can disrupt water supply, reduce efficiency, and increase maintenance costs.

Our journey began with the establishment of a robust framework for fault modeling and fault generation within our simulation environment. For converter faults, encompassing open-circuit and short-circuit switch faults, we developed precise fault models to mirror real-world scenarios accurately. These models enabled us to understand the electrical consequences of such faults and evaluate potential countermeasures. Additionally, we implemented fault generation techniques to inject faults into the system dynamically, providing a controlled platform for observing their effects.

Moving forward, we dived into the realm of induction motor faults, focusing on stator and rotor faults. Stator faults, originating from insulation breakdown or winding defects, were modeled with precision to simulate their effects. These faults can lead to imbalanced currents, overheating, and efficiency degradation. In parallel, rotor faults, resulting from mechanical wear or manufacturing flaws, were meticulously studied. While less common, rotor faults can introduce mechanical imbalances and irregularities in motor behavior.

The insights gained from this chapter lay the foundation for subsequent investigations into fault detection, diagnosis, and tolerant control strategies. By understanding the intricacies and consequences of these faults, we empower system designers, operators, and maintenance personnel to implement effective strategies for fault detection, mitigation, and maintenance.

V Chapter 05: Fault Detection Using DWT-ANN

V.1. Introduction

Traditionally, fault detection has been tackled through a variety of methods, including statistical analysis, signal processing, and expert knowledge-based approaches. While these methods have their merits, they often face challenges when dealing with complex, non-linear, and multi-dimensional datasets.

In response to these challenges, this chapter introduces a cutting-edge approach that leverages the power of the Discrete Wavelet Transform (DWT) and Artificial Neural Networks (ANN) for fault detection. The DWT-ANN approach has gained prominence in recent years for its remarkable ability to address some of the most pressing issues in fault detection, such as early fault recognition, noise resilience, and pattern recognition in high-dimensional data.

The Discrete Wavelet Transform (DWT) : The DWT is a versatile signal processing technique that excels at capturing and representing both low and high-frequency components in a signal simultaneously. This characteristic is particularly advantageous when dealing with complex data streams, as it allows for the decomposition of signals into multiple levels of detail. The DWT has proven its efficacy in various domains, including image processing, speech recognition, and, crucially, fault detection. By decomposing signals into different scales, the DWT facilitates the extraction of informative features that can uncover subtle variations indicative of faults or anomalies [80][81][82].

Artificial Neural Networks (ANN) : Artificial Neural Networks, inspired by the human brain's neural architecture, have emerged as a reliable tool for complex pattern recognition and classification tasks. ANNs excel in learning intricate relationships within data, making them well-suited for modeling the intricacies of fault patterns in diverse systems. They offer the flexibility to handle both linear and non-linear data, adapt to varying fault scenarios, and learn from large datasets [83][84][85].

The DWT-ANN Synergy : The power of the DWT-ANN approach lies in the synergy between these two methodologies. The DWT effectively transforms complex data into a format suitable for ANN-based pattern recognition. It provides a hierarchical representation of the data that retains crucial information about transient fault patterns, even in the presence of noise or varying operating conditions. ANNs, on the other hand, excel at learning from these transformed data representations and making accurate fault predictions [86][87].

In this chapter, we will embark on a journey through the application of the DWT-ANN approach for fault detection. We will explore the essential steps in this process, provide insights into feature extraction using the DWT, delve into the intricacies of ANN model development, and illustrate its impact through our case study. By the end of this chapter, we will have a solid foundation to appreciate the transformative potential of the DWT-ANN methodology in the realm of fault detection.

V.2. DWT-ANN Fault Detection Framework

The DWT-ANN (Discrete Wavelet Transform-Artificial Neural Network) Fault Detection Framework is a comprehensive and advanced approach used in various industries, including engineering and manufacturing, for the early detection and detection of faults and anomalies in complex systems. This framework combines two essential components: the Discrete Wavelet Transform (DWT) for feature extraction and an Artificial Neural Network (ANN) for pattern recognition and classification. The DWT plays a critical role by decomposing the input data into multiple frequency scales, allowing it to capture both high and low-frequency components, which are often indicative of faults. The extracted features are then fed into an ANN, a machine learning model designed to learn and recognize patterns in the data. Through extensive training on labeled datasets, the ANN becomes capable of distinguishing between normal system behavior and various fault conditions. This framework offers the advantage of fault detection, increased reliability, and adaptability to various applications, making it a powerful tool for improving system performance and reducing downtime [88].

We can effectively utilize the DWT for feature extraction and train an ANN to detect faults in the system by following these steps:

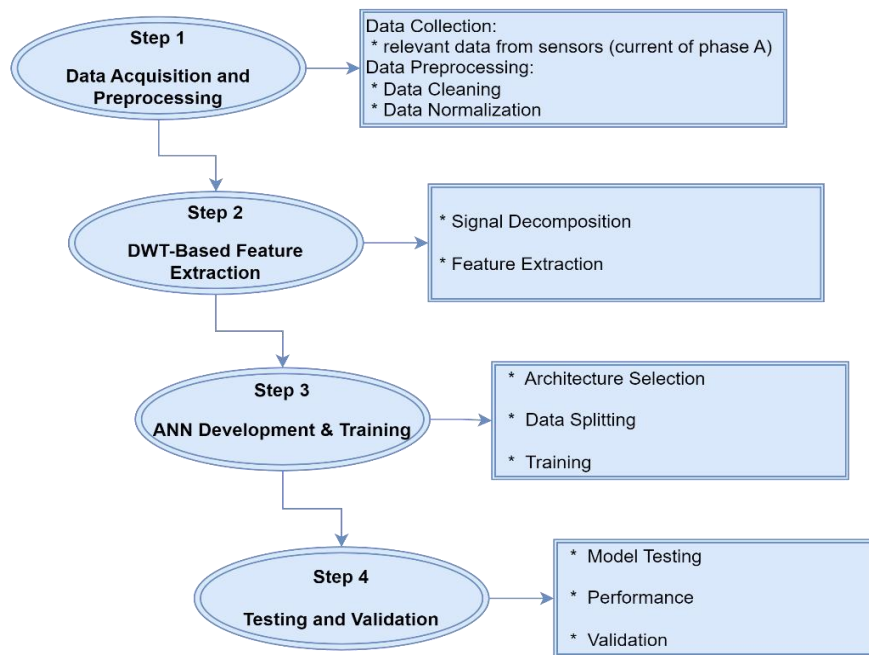


Figure V.1 : DWT-ANN Fault Detection Framework.

V.2.1. Data Collection and Preprocessing

Data collection and preprocessing play pivotal roles in preparing sensor data for analysis. In our specific scenarios, we initiate the process by collecting phase A

current data over a 3-second interval. Subsequently, we employ preprocessing techniques to enhance the data quality. This involves eliminating transition periods, isolating fault occurrences, and retaining only the final second of recorded data. Furthermore, we incorporate a normalization step to ensure uniformity in sampling intervals, data structure, and timestamps.

The utilization of phase A current as a primary indicator in our fault detection system for a PV pumping system, employing the DWT-ANN approach, offers a cost-effective and streamlined solution. By concentrating on a single sensor, we significantly reduce both acquisition and maintenance expenses while simplifying system setup and data management. This approach particularly benefits scenarios with budget constraints. Its true strength lies in early fault detection, enabling proactive interventions to prevent further damage and extend the lifespan of system components.

Despite the focus on monitoring a single parameter, the insights derived from this approach extend to the broader system, offering a comprehensive view of system health and performance.

V.2.1.1 Data Collection

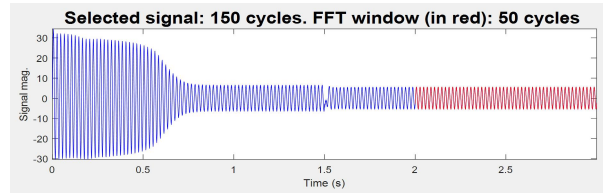
First, we will begin by setting up the data collection system to capture phase A current data from sensors. Then, Ensure that the data collection process records the current signal for a duration of 3 seconds, capturing the necessary information for subsequent analysis.

Table V.1 : Collected data of Phase A current

Healthy	<p>Selected signal: 150 cycles. FFT window (in red): 50 cycles</p>	THD = 4.09 %
Fault 1 Boost (OC)	<p>Selected signal: 150 cycles. FFT window (in red): 50 cycles</p>	THD = 4.07 %
Fault 2 Boost (SC)	<p>Selected signal: 150 cycles. FFT window (in red): 50 cycles</p>	THD = 4.96 %

Fault 3

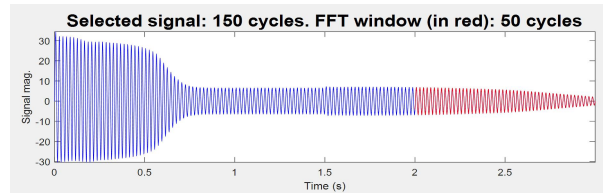
Buck-Boost
(OC)



THD = 3.43 %

Fault 4

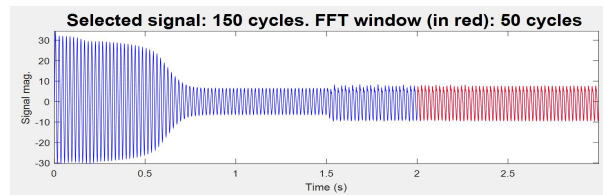
Buck-Boost
(SC)



THD = 24.22 %

Fault 5

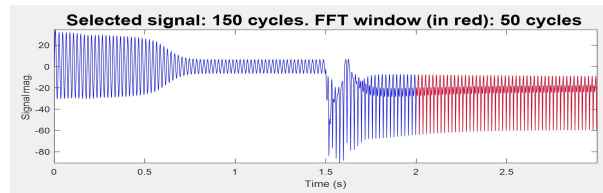
3~Inverter
(OC)



THD = 23.92 %

Fault 6

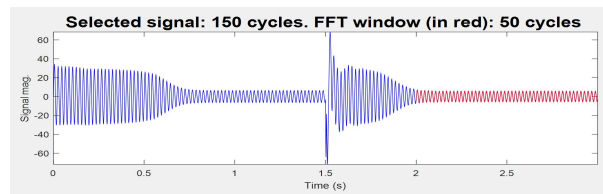
3~Inverter
(SC)



THD = 129.57 %

Fault 7

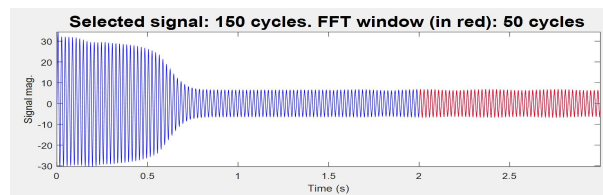
Stator Fault



THD = 4.05 %

Fault 8

Rotor Fault



THD = 4.28 %

V.2.1.2 Data Preprocessing

Data Cleaning: After data collection, the first preprocessing step involves cleaning the data. This includes removing any unwanted sections of the signal. In our case, we want to eliminate the transition periods and appearance fault time. We can achieve this by identifying the start and end times of these periods and excluding them from the dataset. or retain only the last second of data, by specifying the time range accordingly.

Data Normalization: To ensure consistency in the dataset, this involves rescaling the current signal to meet specific criteria:

Sampling Time: Ensure that all data points have the same time interval between them. If there are variations in the time interval due to irregular sampling, we can resample the data to a uniform time grid.

Data Array: Verify that the data arrays have consistent dimensions. If necessary, interpolate or resample the data to ensure uniform array sizes.

Time Alignment: Make sure that the timestamps or time indices in our dataset are synchronized. Adjust the timestamps, if needed, to ensure that all data points align properly.

By performing these data preprocessing steps, we will have a clean and normalized dataset that is ready for further analysis, such as feature extraction using DWT-ANN or other fault detection techniques. This ensures that this analysis is based on consistent and relevant data.

V.2.2. Feature Extraction Using DWT

In this section, we will delve into the process of applying the Discrete Wavelet Transform (DWT) to the phase A current data in a PV pumping system to extract relevant features for fault detection. We will explore the choice of wavelet functions, decomposition levels, and feature selection criteria, emphasizing their significance in the DWT-based feature extraction process .

V.2.2.1 Applying the Discrete Wavelet Transform (DWT):

The Discrete Wavelet Transform is a powerful mathematical tool that decomposes a signal into different frequency scales, enabling us to capture both high and low-frequency components [88]. In the context of feature extraction for fault detection in a PV pumping system, the following steps are typically involved:

V.2.2.2 Signal Decomposition:

The phase A current data is subjected to DWT decomposition. This process involves splitting the signal into multiple frequency scales, typically referred to as "scales" or "levels." The signal is transformed into approximation coefficients (representing the low-frequency components) and detail coefficients (representing the high-frequency components) [88][89].

The wavelets are mathematically defined by:

$$\Psi_{ab}(t) = \frac{1}{\sqrt{a}} \Psi\left(\frac{t-b}{a}\right) \quad (\text{V.1})$$

Where **a** and **b** denote the scale factor and position factor respectively.

The wavelet transform encompasses two main categories: continuous wavelet transform (CWT) and discrete wavelet transform (DWT) [90]. In DWT, the wavelet is translated and dilated according to discrete values, which requires the discretization of 'a' and 'b' as follows:

$$\begin{cases} a = a_0^m \\ b = n \cdot b_0 \cdot a_0^m \end{cases} \quad (V.2)$$

Where $a_0 > 1$; $b_0 > 0$; a_0 and $b_0 \in \mathbb{Z}$, m and n are integers permitting the control of the dilation and the translation of the original wavelet.

When the current signal of the phase A undergoes processing, it passes through two complementary filters: a high-pass filter (HPF) and a low-pass filter (LPF), producing two distinct signals known as the approximation signal (A) and the detail signal (D). The approximation signal represents the large-scale and low-frequency components of the input, while the detail signal captures the small-scale and high-frequency components[88][89][90].

V.2.2.3 Choice of Wavelet Function

The selection of an appropriate wavelet function is crucial. Wavelet functions come in various shapes and characteristics, and their choice depends on the specific characteristics of the phase A current data. Common wavelet families include Daubechies, Haar, Symlet, and more.

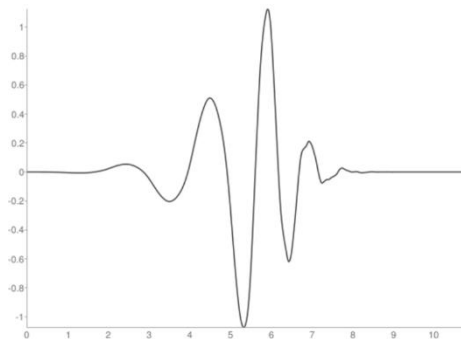


Figure V.2 : wavelet functions (db 6)

The wavelet function should align with the expected frequency content and transient behavior of the data [91].

Through the DWT process, input signals consisting of both low-frequency (LF) and high-frequency (HF) components are decomposed into different frequency bands. Subsequently, down-sampling is applied to obtain the first level of wavelet transformation, and this process continues into N levels.

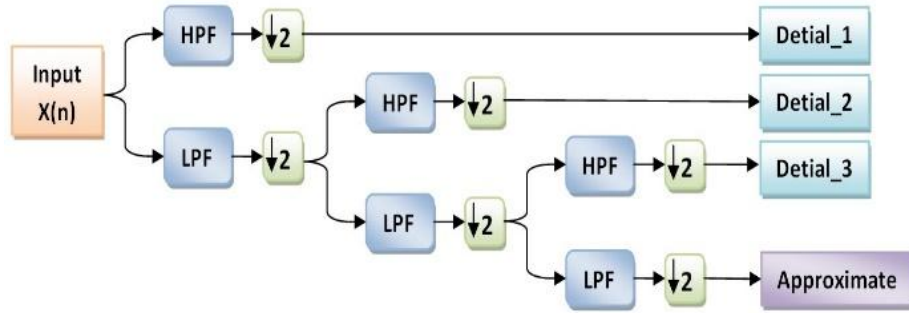


Figure V.3 : DWT implementation procedure [88].

V.2.2.4 Decomposition Levels

Increasing the number of levels provides finer frequency resolution but may also introduce noise. Conversely, too few levels may miss important frequency components. The choice of decomposition levels should strike a balance between capturing relevant details and managing computational complexity [88][90].

To facilitate a reliable and efficient analysis, prior knowledge of the signal levels (N) that need to be processed is essential. The required parameter 'N' can be calculated using the equation:

$$N_{levels} = int \left(\frac{\log (f_e / f_s)}{\log 2} \right) + 2 \tag{V.3}$$

where ' f_s ' denotes the supply frequency, and ' f_e ' represents the sampling frequency. It's worth noting that ' N ' should be an integer, and the appropriate number of decomposition levels can be determined based on knowledge of ' f_s ' and ' f_e '. In our specific case, considering a supply frequency of 50Hz and a sampling frequency of 1kHz, the calculated number of decomposition levels needed is:

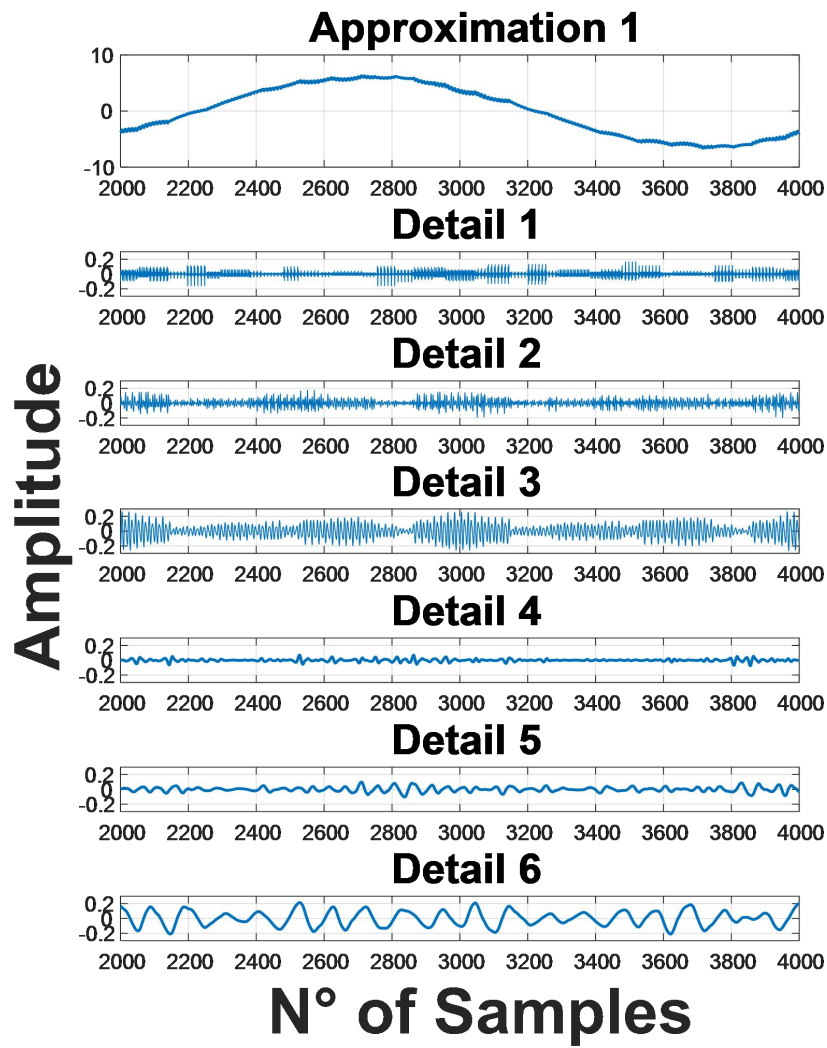
$$N_{levels} = n_{ls} + 2 = int \left(\frac{\log \left(\frac{10^3}{50} \right)}{\log 2} \right) + 2 = 6 \text{ levels} \tag{V.4}$$

Table (V.2) presents the different frequency bands acquired by the discrete wavelet decomposition.

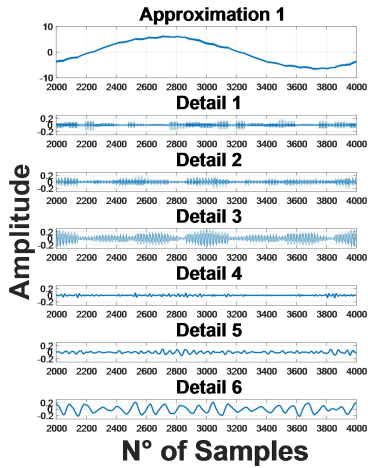
Table V.2 : Frequency bands obtained by multi-level decomposition.

Levels	Approximations		Details	
J=1	A1	0-500	D1	500-1000
J=2	A2	0-250	D2	250-500

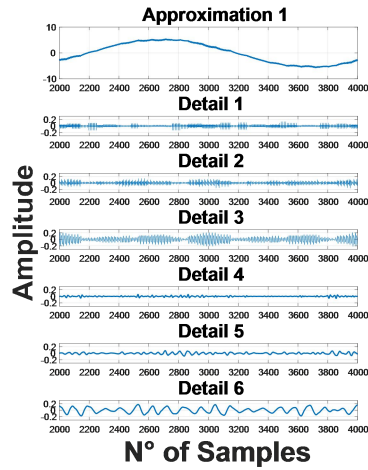
J=3	A3	0-125	D3	125-250
J=4	A4	0-62.5	D4	62.5-125
J=5	A5	0-31.25	D5	31.25-62.5
J=6	A6	0-15.625	D6	15.625-31.25



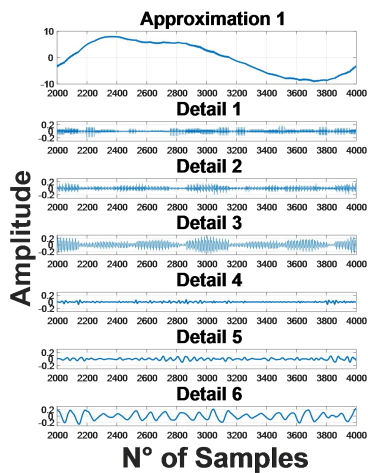
Healthy



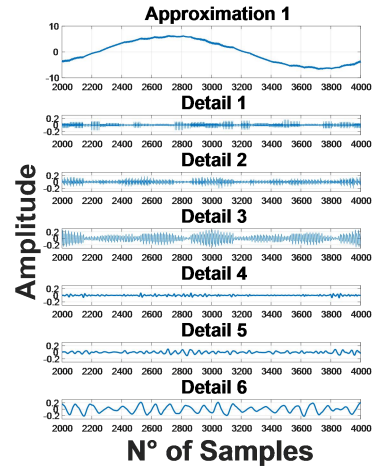
Fault 1 : Boost (OC)



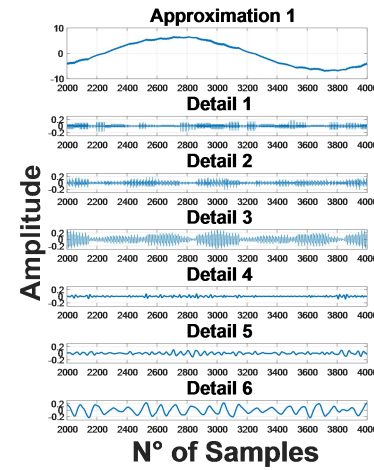
Fault 3 : Buck-Boost (OC)



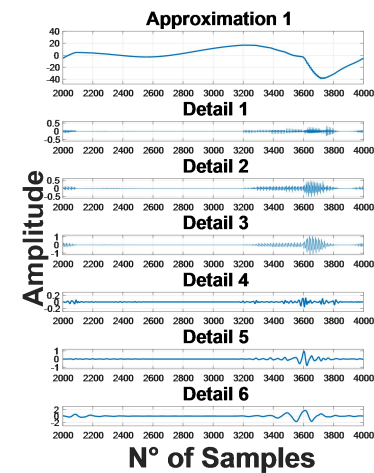
Fault 5 : 3~Inverter (OC)



Fault 2 : Boost (SC)



Fault 4 : Buck-Boost (SC)



Fault 6 : 3~Inverter (SC)

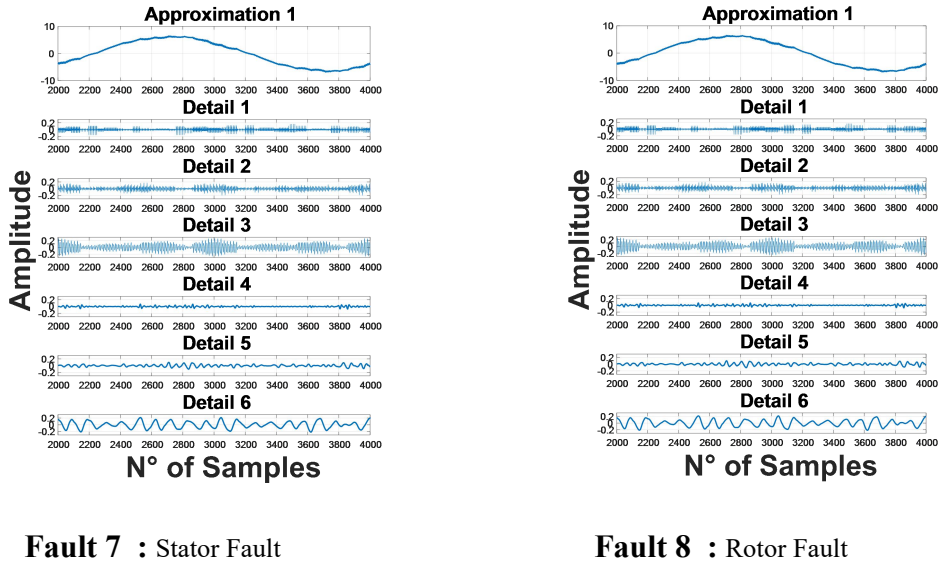


Figure V.4 : Extracted Features.

V.2.2.5 Feature Selection Criteria

Once the signal has been decomposed into approximation and detail coefficients at the selected levels, the next step is to extract relevant features that encapsulate information about the signal's behavior.

We have made certain considerations to optimize the analysis given the complexity of the dataset and the computational resources available. Specifically, we have chosen to focus on Statistical Features, specifically Root Mean Square (RMS), for feature extraction. This choice is motivated by the effectiveness of RMS calculation and its relevance in capturing essential information about the signal's behavior. RMS provides valuable insights into the signal's amplitude and overall energy, making it a dynamic choice for fault detection.

$$RMS = \sqrt{\frac{1}{n} \sum_i x_i^2} \quad (V.5)$$

Where x_i denote the measurements and n is number of measurements.

While Wavelet Transform-Based Features offer detailed frequency information, we understand that they may require significant computational resources. Given this constraint, we have opted for the more computationally efficient RMS approach, which still yields valuable insights into the signal [92].

Furthermore, considering that we have a substantial number of signals to deal with, Feature Ranking and Selection techniques become indispensable. These techniques help mitigate dimensionality issues by identifying and retaining the most informative features for fault detection. This strategy ensures that our analysis focuses

on the most relevant aspects of the data while managing the computational load effectively.

By making these choices, we aim to strike a balance between feature richness and computational feasibility, ultimately enhancing the efficiency and effectiveness of our fault detection system.

V.2.3. ANN Model Development

In this section, we will explore the architecture and implementation of the Artificial Neural Network (ANN) tailored for fault detection in the PV pumping system. We'll delve into the selection of the neural network type, layer and neuron configuration, as well as the training process, which includes the utilization of labeled data, optimization techniques using MATLAB's nntool framework.

V.2.3.1 Neural network type

A Multilayer Perceptron (MLP) is a type of artificial neural network (ANN) architecture that consists of multiple layers of interconnected nodes or neurons. It is one of the most common and fundamental neural network architectures used in machine learning and deep learning. The MLP is often used for a wide range of tasks, including regression, classification, pattern recognition, and function approximation. Therefore, our MLP is designed to use extracted features RMSs of the Discrete Wavelet Transform (DWT) for pattern recognition, ultimately aiding in the classification of faults in PV pumping systems [39][92].

V.2.3.2 Layer and Neurons configuration

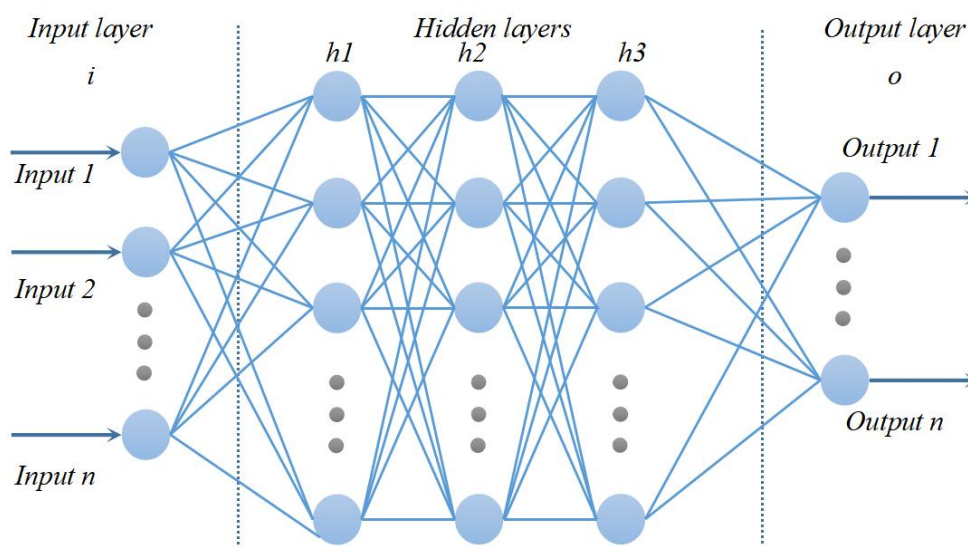


Figure V.5 : Standard Multilayer Perceptron Architecture.

In our specific case, the MLP comprises Five distinct layers:

V.2.3.2.a. Input Layer :

This input layer is comprised of 7 neurons, each signifying one of the features derived through the Discrete Wavelet Transform (DWT).

V.2.3.2.b. Hidden Layers:

Situated between the input and output layers. Neurons within these hidden layers apply weighted sums and activation functions to their received inputs.

- ◆ Hidden Layer 1: The first hidden layer houses 14 neurons.
- ◆ Hidden Layer 2 : The second hidden layer is equipped with 28 neurons.
- ◆ Hidden Layer 3 : The second hidden layer is contains 7 neurons.

V.2.3.2.c. Output Layer:

The output layer's neuron count corresponds to the number of fault classes intended for detection. where it is 4 Neurons, each aligning with one of the 4 output variables as labeled in Table (V.3) used for fault detection in the PV pumping system.

V.2.3.2.d. Connections and Weights:

Neurons in adjacent layers are fully connected, meaning that each neuron in one layer is connected to every neuron in the next layer. Each connection has an associated weight, which the network learns during training to adjust the strength of the connection.

V.2.3.2.e. Activation Functions:

Each neuron, whether in a hidden layer or the output layer, typically applies an activation function to its weighted sum of inputs. Common activation functions include sigmoid, hyperbolic tangent (tanh), and rectified linear unit (ReLU).

In our work Sigmoid activation functions are employed in all layers of the MLP. The sigmoid activation function is chosen for its ability to introduce non-linearity into the network, allowing it to model complex relationships within the data. It also ensures that the outputs of the neurons are within a bounded range, making it suitable for regression tasks as well as classification [93].

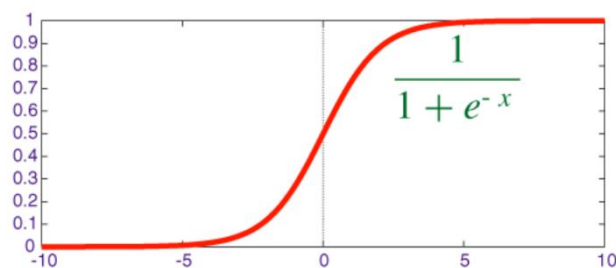


Figure V.6 : Sigmoid activation function.

V.2.3.2.f. Training Algorithm :

The MLP is trained using a supervised learning approach. During training, the network is presented with input data along with corresponding target outputs. It adjusts its weights and biases iteratively using optimization algorithms

The training process typically involves backpropagation, where the error or loss is propagated backward through the network to update the weights. The specific optimization algorithm used determines how these weight updates are performed [94].

In our work The MLP is trained using the Levenberg-Marquardt backpropagation algorithm. This algorithm is known for its fast convergence and ability to find optimal weights and biases for the network. During training, the network iteratively adjusts its parameters to minimize the mean squared error (MSE), which present the measured difference between the predicted output and the actual labels. This latter known as the loss function where was the chosen for this task [94].

V.2.4. Training Process

V.2.4.1 Labeled Data:

The training process requires a labeled dataset, where each data point (extracted features from DWT) is associated with a label indicating whether it corresponds to a normal state or a specific fault condition. It's essential to have a sufficiently large and diverse dataset to train a effective fault detection model.

Table (V.3) represents the corresponding label to each fault; the label consist of 4 variables in binary numerical system which indicates to fault number ("F"n) in decimal numerical system. The objective of using the binary numerical system as target output is to use it as machine code.

Table V.3 : Dataset Label Table

	Output 1	Output 2	Output 3	Output 4	Decimal N°
Healthy	0	0	0	0	0
F1	1	0	0	0	1
F2	0	1	0	0	2
F3	1	1	0	0	3
F4	0	0	1	0	4
F5	1	0	1	0	5
F6	0	1	1	0	6
F7	0	1	1	1	7
F8	1	0	0	0	8

V.2.4.2 Training Conditions and Termination Criteria:

The ANN training process is governed by a set of conditions and termination criteria, which ensure effective convergence. These criteria include:

- **Maximum Number of Epochs:** Training will stop when the maximum number of epochs (repetitions), set at 1000, is reached.
- **Achieving Performance Goal:** The training aims to minimize performance to reach a predefined goal of 0. When this goal is met, training concludes.
- **Minimum Gradient:** Training halts when the performance gradient falls below the specified threshold (`min_grad`) of $1e-7$.
- **Maximum Learning Rate:** If the learning rate (`mu`) exceeds the defined maximum value (`mu_max`) during training, it triggers termination.
- **Validation Performance:** Early stopping is employed using validation vectors. Training stops if validation performance increases more than `max_fail` times in a row without decreasing.

Upon completing the training operation, the resultant ANN model will encompass optimal weight and bias vectors, defining the network's architecture and its capacity for precise predictions based on input data. Validation vectors play a pivotal role in early stopping, with training halting if the model's performance on the validation dataset fails to improve or remains static for `max_fail` consecutive epochs, thus guarding against overfitting and fostering generalization. Test vectors, though not influencing training directly, serve as an additional gauge of the model's proficiency in generalizing to unseen data. The learning rate (`mu`) is a critical hyperparameter, initially set at 0.001 but subject to adaptive refinements during training. `Mu` increases incrementally with `mu_inc` until a performance decrease prompts an adjustment to the network's parameters, followed by a decrease in `mu` using `mu_dec`. This adaptive strategy fine-tunes the model's convergence, enhancing the efficiency of the learning process.

V.2.5. Training Results

The best validation performance achieved was 0.029915 at epoch 509, indicating that the model's predictions on the validation dataset were highly accurate at this stage of training.

The gradient at epoch 509 was $5.3557e-08$, suggesting that the model's convergence was smooth and approaching an optimal state.

The learning rate (`Mu`) underwent adaptive changes throughout training, starting at 0.001 and decreasing to $1e-11$ by epoch 509. This controlled adjustment contributed to effective model convergence.

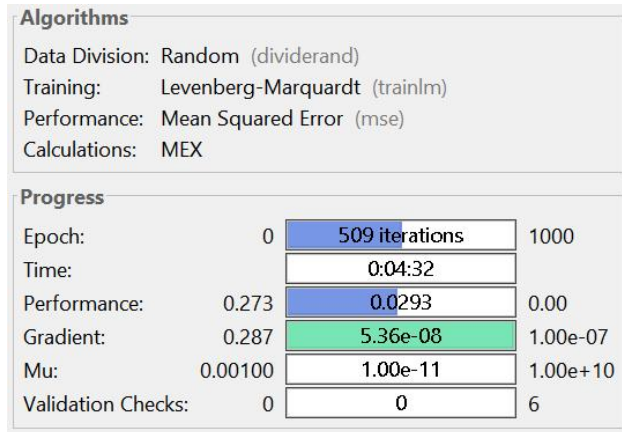


Figure V.7 : ANN training progress.

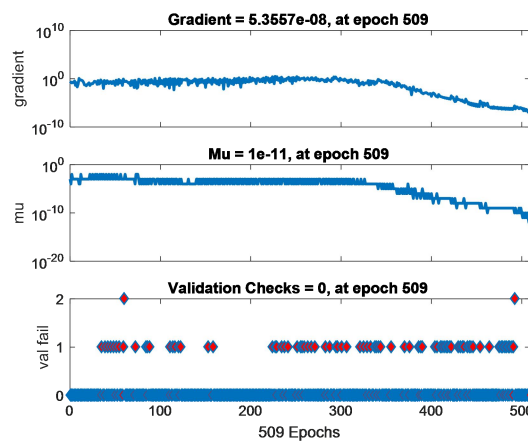


Figure V.8 : ANN training state.

The Multilayer Perceptron Artificial Neural Network (MLP-ANN) has demonstrated impressive performance in our evaluation. At epoch 509, it achieved a Mean Squared Error (MSE) of 0.029915 on the validation dataset. This low MSE value indicates that the model's predictions are remarkably close to the actual target values, showcasing its ability to perform well.

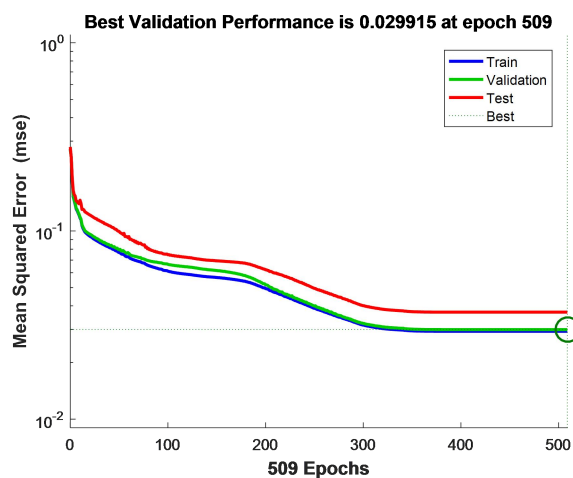


Figure V.9 : Best Validation Performance.

A noteworthy aspect of our results is the similarity observed in the training, validation, and test curves. This suggests that the model has learned effectively, and it does not appear to be overfitting the training data. The consistency in performance across different datasets is a positive sign, reinforcing the model's reliability.

Furthermore, the stability of the curves indicates that the training process was smooth and did not suffer from significant fluctuations or instability issues. This stability is often indicative of well-chosen hyperparameters and a robust training process.

Additionally, while the similarity in test curve behavior is encouraging, it is imperative to thoroughly assess the model's performance on an independent test dataset. This evaluation ensures that the model's success is not limited to the validation data but extends to another unseen scenarios.

R-Correlation coefficient, often denoted as R^2 , is a statistical measure used to evaluate the goodness of fit of a regression model. It provides information about how well the independent variable(s) (predictors) in the model explain the variation in the dependent variable (target). In other words, R^2 quantifies the proportion of the variance in the target variable that is explained by the regression model[95][96][97].

Range: R^2 values range from 0 to 1.

An R^2 of 0 indicates that the model does not explain any of the variance in the dependent variable, meaning it's a poor fit.

An R^2 of 1 indicates that the model explains all of the variance in the dependent variable, meaning it's a perfect fit.

The higher R^2 , the better the model is at explaining the variance.

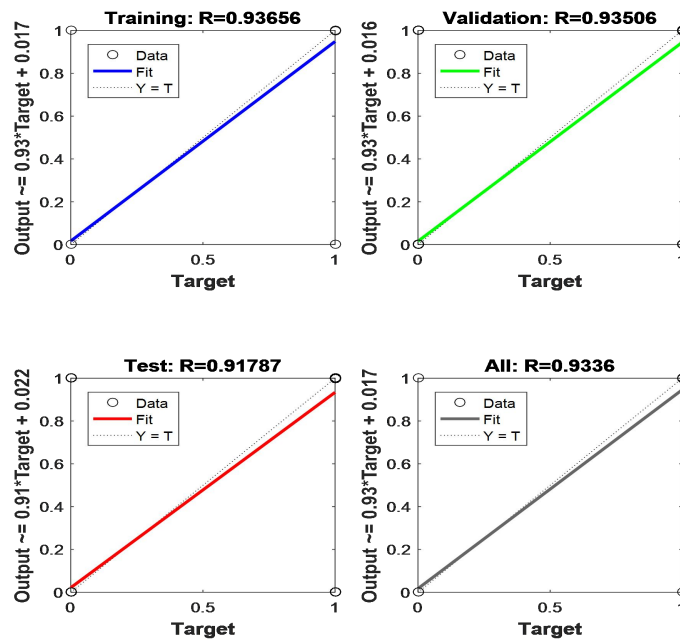


Figure V.10 : Regression plots.

Regression plots of the neural network model on the training, validation, and testing sets.

Our evaluation reveals promising results across different datasets:

Firstly, in the training dataset, the model demonstrates a robust linear relationship with an R^2 value of 0.93656, explaining roughly 93.66% of the variance in the target variable. The linear equation "Output \approx 0.93 * Target + 0.017" summarizes the model's performance in the training phase.

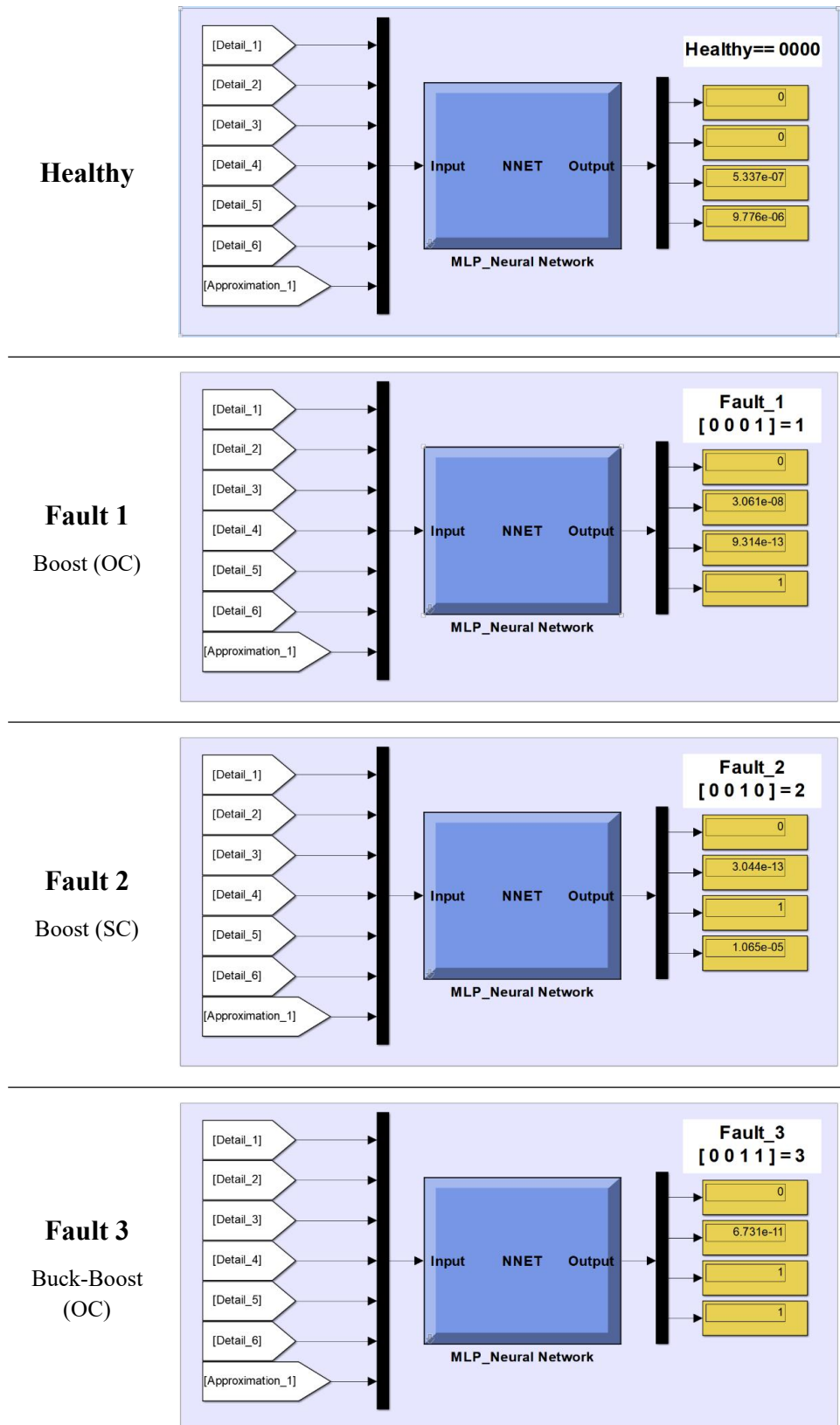
Similarly, on the validation dataset, the model maintains a strong linear fit with an R^2 value of 0.93506, explaining approximately 93.51% of the variance. The linear equation "Output \approx 0.93 * Target + 0.016" corroborates the model's consistency.

The test dataset, while still exhibiting a linear relationship, shows a slightly lower R^2 value of 0.91787. This may be due to variations in the test data, but the model's performance remains respectable. The corresponding linear equation is "Output \approx 0.91 * Target + 0.022."

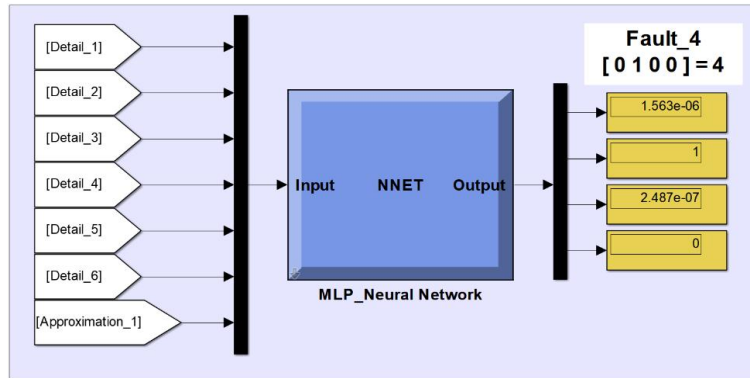
When considering all datasets together, the combined R^2 value of 0.9336 reflects the model's overall ability to capture linear relationships in the entire dataset. The linear equation "Output \approx 0.93 * Target + 0.017" remains consistent across these datasets.

V.3. ANN Results

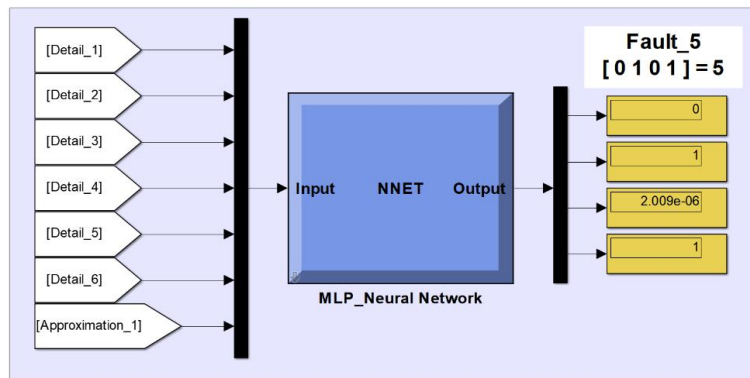
Table V.4 : ANN Results.



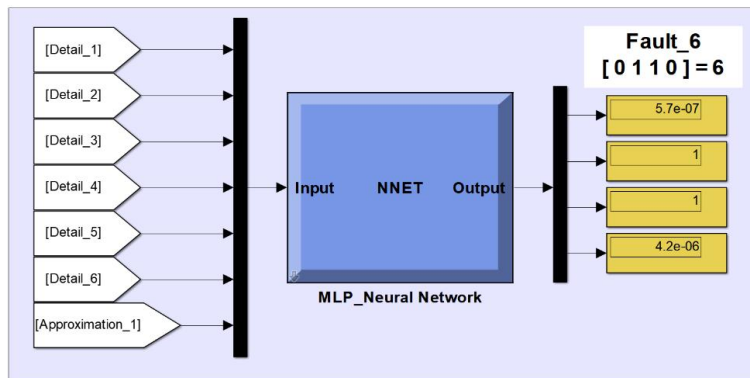
Fault 4
Buck-Boost
(SC)



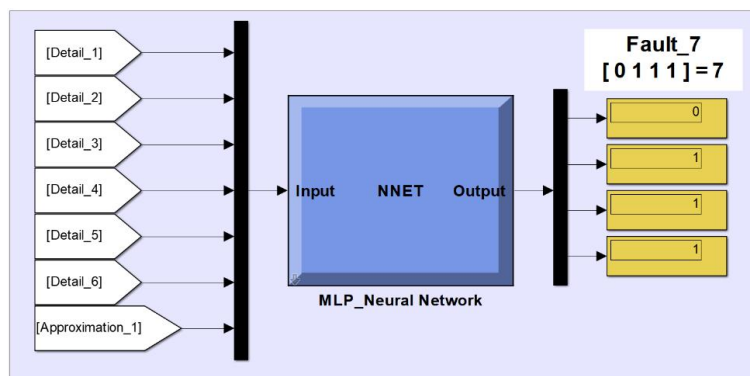
Fault 5
3~Inverter
(OC)

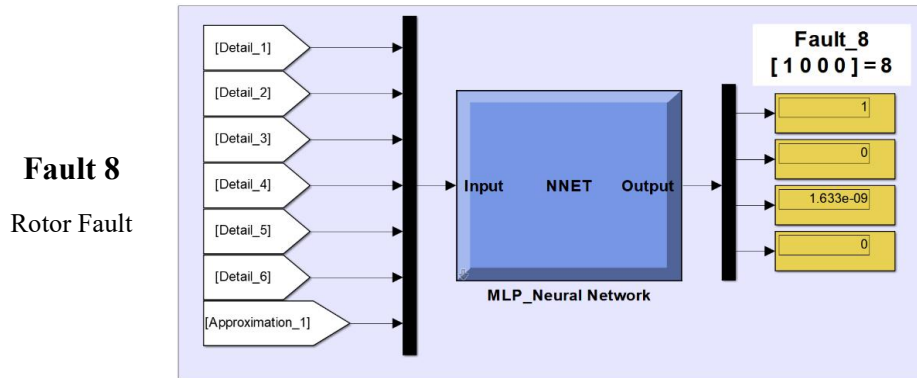


Fault 6
3~Inverter
(SC)



Fault 7
Stator Fault





V.4. Limitations and Challenges

DWT-ANN-based fault detection is a powerful approach, but it does come with certain limitations and challenges that should be considered:

- ❖ **Data Quality Issues:** The effectiveness of DWT-ANN-based fault detection heavily relies on the quality of the input data. Noisy or inconsistent data can lead to inaccurate fault detection results. Therefore, data preprocessing, filtering, and noise reduction techniques are essential to ensure the reliability of the analysis.
- ❖ **Data Volume and Sampling Rate:** Handling large volumes of data, especially in real-time applications, can be challenging. Moreover, high-frequency sampling may result in excessive data, making storage and processing resource-intensive. Efficient data management and storage solutions are required to address these challenges.
- ❖ **Model Complexity:** ANN models can become complex as the number of features and layers increases. Managing model complexity is crucial to prevent overfitting, where the model performs well on the training data but fails to generalize to new data. Techniques like regularization and cross-validation are necessary to strike a balance.
- ❖ **Training Data Availability:** The success of ANN-based models heavily relies on having an adequate amount of labeled training data. In some cases, collecting labeled data for rare fault occurrences can be challenging, leading to imbalanced datasets and reduced model performance for these faults.
- ❖ **Feature Engineering:** Extracting relevant features from raw data is essential. However, determining which features to extract and how to represent them can be a time-consuming process. Moreover, choosing inappropriate features may lead to suboptimal performance.
- ❖ **Computational Resources:** Training deep ANN models can be computationally intensive, requiring significant processing power and memory. This can be a

limitation for resource-constrained environments or when analyzing large datasets.

- ❖ **Generalization:** Ensuring that the trained model can generalize well to unseen data is a persistent challenge. Techniques like cross-validation and regularization help, but achieving robust generalization remains a complex task.
- ❖ **Model Interpretability:** ANNs are often considered "black-box" models, making it challenging to interpret the reasoning behind their predictions. This can be a limitation in scenarios where interpretability is crucial, such as critical systems.
- ❖ **False Positives and Negatives:** Achieving a balance between minimizing false positives and false negatives is a common challenge in fault detection. Overly sensitive models may generate numerous false alarms, while conservative models may miss actual faults.
- ❖ **Adaptation to Changing Conditions:** The fault detection model may need to adapt to changing system conditions or evolving fault patterns. Continuous monitoring and periodic model retraining are necessary to maintain performance.

In summary, while DWT-ANN-based fault detection offers powerful capabilities, it is essential to be aware of and address these limitations and challenges to ensure the reliability and effectiveness of the fault detection system in real-world applications.

V.5. Conclusion

In Chapter 4, titled "Fault Detection of PV Pumping System Using DWT-ANN," we embarked on a crucial journey aimed at enhancing the reliability and performance of photovoltaic (PV) pumping systems by developing a robust fault detection framework. This chapter commenced with an insightful introduction, setting the stage for our exploration of fault detection techniques, specifically leveraging the power of Discrete Wavelet Transform (DWT) and Artificial Neural Networks (ANN).

Throughout this chapter, we meticulously detailed the fault detection framework's key components, from data acquisition and preprocessing to feature extraction using DWT and the development of the ANN model. The process involved acquiring and preparing simulation data from PV pumping systems, applying DWT to extract meaningful features, and constructing a neural network model capable of discerning faults within the system.

One of the most significant highlights of this chapter was the presentation of results. We showcased the framework's effectiveness in detecting faults, providing evidence of its potential to enhance the reliability of PV pumping systems. Additionally, we acknowledged the limitations and challenges faced during the development and implementation of the framework, emphasizing the importance of continuous improvement and research in this domain.

In conclusion, Chapter 4 has ushered us into the realm of fault detection in PV pumping systems, equipping us with a robust framework that has the potential to significantly improve the reliability and performance of these systems. As we move forward in our exploration of fault-tolerant control and other advanced techniques in subsequent chapter, the foundation established in this chapter will continue to play a pivotal role in addressing the unique challenges posed by faults in PV pumping systems. The insights gained here set the stage for future advancements and innovations in this critical field.

VI Chapter 06 : Tolerant Control For PV Pumping System

VI.1. Introduction

In an era where sustainability and resource management are at the forefront of global concerns, the reliability of PV pumping systems is not merely an engineering endeavor—it is a commitment to the well-being of communities and ecosystems alike. The sixth chapter stands as a testament to this commitment, offering a glimpse into the potential of fault-tolerant control to transform the landscape of solar PV pumping.

The sixth chapter of this thesis embarks on a profound exploration, one that holds the promise of enhancing the resilience and reliability of PV pumping systems. It is within this chapter that we delve into the intricacies of designing a Fault Tolerant Control (FOC) system, empowered by the adaptive Fuzzy-PID (Proportional-Integral-Derivative) controller. Our primary mission: to fortify the induction motor, the heart of the PV pumping system, against the perils of stator and rotor faults.

VI.2. Classic vector control

Scalar control is the oldest method used for controlling the asynchronous machine. The simplicity of implementation of this method makes it preferred for systems that do not require operations at very low speed and high torque or high performance. In other cases, the vector method must be used [98][99].

The main objective of vector control of asynchronous machines is to improve their dynamic behavior. A lot of work has been done in this area, the main goal is to be able to control the motor and obtain a behavior similar to that of the direct current machine [60].

VI.2.1. Principle of vector control by flux orientation

The oriented flux method consists of choosing a system of axes (d, q), a two-phase rotating reference frame oriented on φ_r (rotor flux), φ_s (stator flux) or φ_m (air gap flux) and a type of control allowing the torque and flux to be decoupled as in the case of a direct current machine.

As part of this work we study the oriented rotor flux vector control, which is the most used and whose principle consists of eliminating the coupling problem between the armature and the inductor. The stator current is then decomposed into two quadrature components in a reference frame linked to the rotating field such that one of the components controls the flux and the other the torque.). The main objective of vector control of asynchronous machines is to improve their operation in dynamic mode [60][100].

VI.2.2. Asynchronous machine Model for control purpose

As part of this work, we were interested in models of the asynchronous machine which make it possible to simulate its operation in transient regimes as well as those which lead to a control following a vector control scheme by orientation of rotor or

stator flux . We will subsequently see the model which allows us to take into account failures at the stator, the rotor or combined failures (stator and rotor).

For the equation, we retain the same hypotheses and the same transformations (Clark and Park) used in the 3rd chapter.

The equations which link the flux, the torque and the stator current arise from the Park model with four parameters presented in equation (III.61). Indeed, the choice of the reference d-q rotating at ω_s (reference linked to the rotating field) and fixed on the rotor flux amounts to positing that:

$$\varphi_{dr} = \varphi_r ; \varphi_{qr} = 0 \quad (VI.1)$$

The arrangement of equations (III-61) and (VI.1) allows us to obtain the equations corresponding to the control model of the machine supplied with voltage by orientation of the rotor flux:

$$\left\{ \begin{array}{l} \varphi_{dr} = \varphi_r \\ V_{ds} = R_s \cdot I_{ds} + \sigma L_{sc} \frac{dI_{ds}}{dt} + \frac{n_b \cdot M_{sr}}{2L_{rc}} \cdot \frac{d\varphi_r}{dt} - \omega_s \cdot \sigma \cdot L_{sc} \cdot I_{qs} \\ V_{qs} = R_s \cdot I_{qs} + \sigma L_{sc} \frac{dI_{qs}}{dt} + \omega_s \cdot \frac{n_b \cdot M_{sr}}{2L_{rc}} \varphi_r + \omega_s \sigma \cdot L_{sc} \cdot I_{ds} \\ T_r \cdot \frac{d\varphi_r}{dt} + \varphi_r = \frac{3}{2} M_{sr} \cdot I_{ds} \\ \omega_r = \frac{3}{T_r \cdot \varphi_r} M_{sr} \cdot I_{qs} \\ C_e = \frac{3}{4} p \cdot \frac{n_b \cdot M_{sr}}{L_{rc}} \cdot \varphi_r \cdot I_{qs} \end{array} \right. \quad (VI.2)$$

Where:

$$T_s = \frac{L_{sc}}{R_s} \quad et \quad T_r = \frac{L_{rc}}{R_{rdq}}$$

Applying the Laplace transformation, the previous equations can be written in the following form:

$$\left\{ \begin{array}{l}
 \varphi_r = \varphi_{dr} \\
 V_{ds} = (R_s + s \cdot \sigma \cdot L_{sc}) I_{ds} + s \cdot \frac{n_b \cdot M_{sr}}{2 \cdot L_{rc}} \cdot \varphi_r - \omega_s \cdot \sigma \cdot L_{sc} \cdot I_{qs} \\
 V_{qs} = (R_s + s \cdot \sigma \cdot L_{sc}) I_{qs} + \omega_s \cdot \sigma \cdot L_{sc} \cdot I_{ds} + \omega_s \cdot \frac{n_b \cdot M_{sr}}{2 \cdot L_{rc}} \varphi_r \\
 \varphi_r = \frac{\frac{3}{2} M_{sr}}{1 + s \cdot T_r} \cdot I_{ds} \\
 \omega_r = \frac{\frac{3}{2} M_{sr}}{T_r \varphi_r} \cdot I_{qs} \\
 C_e = \frac{3}{4} p \cdot \frac{n_b \cdot M_{sr}}{L_{rc}} \cdot \varphi_r \cdot I_{qs}
 \end{array} \right. \quad (VI.3)$$

There are direct and indirect vector control methods:

In indirect control, the Park angle θ_s is calculated from the stator pulsation, itself reconstituted using the speed of the machine and the rotor pulsation ω_r . Regarding direct control, the Park angle is calculated directly using the measured or estimated quantities. In our study we will adopt indirect vector control.

The vector control is called flux open loop if there is no flux regulation. The flux is imposed in this case by I_{ds} , moreover the stator pulsation can only be estimated by the relation VI.3. In the flux closed loop version, this pulsation is estimated from the value of the rotor flux or the magnetizing current. In this case, we take into account the rotor time constant T_r .

VI.2.3. Indirect vector control

Indirect vector control is the most used in general. This is explained by the fact that in the indirect method, knowledge of the position of the rotor flux is not necessary. However, it requires a good knowledge of the machine parameters, more particularly the rotor time constant, which varies considerably with temperature and saturation level. A bad estimation of the rotor time constant therefore implies an error in the calculation of the sliding speed and consequently brings a degradation of the performance of the control which results in oscillations in the torque of the machine [60][101][102].

Figure (VI.1) represents the block diagram of the indirect rotor field orientation vector control of the asynchronous machine, with speed regulation.

The calculation of θ_s is done by summing the "rotor pulsation" with the electrical speed ($\omega_s = \omega_r + p.\Omega$), which gives the "stator pulsation" then by integrating the latter, we obtain θ_s :

$$\theta_s = \int \omega_s .dt = \int (p.\Omega + \frac{2}{T_r} \frac{M_{sr}}{\phi_r^*} .I_{qs}^*) .dt \tag{VI.4}$$

The complete schematic of the oriented rotor flux indirect vector control is as follows:

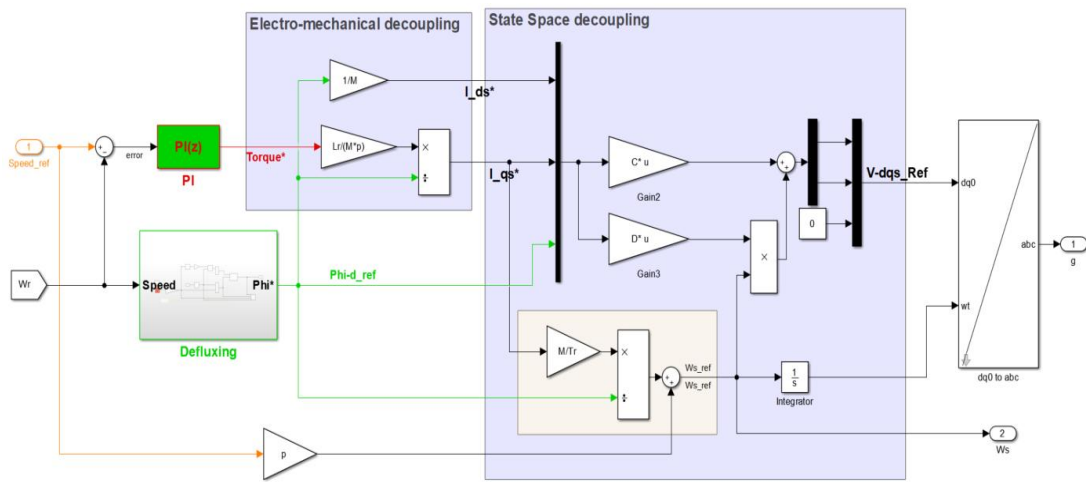


Figure VI.1 : Speed regulation by indirect vector control.

The voltage supply is obtained by imposing reference voltages at the input of the inverter control. These voltages make it possible to define the cyclical ratios on the arms of the inverter so that the voltages delivered by this inverter to the terminals of the machine stator are as close as possible to the reference voltages.

Estimation

This function is responsible for developing the flux vector and the current components I_{ds} and I_{qs} from the digital resolution of the system (asynchronous machine).

Decoupling

The voltages V_{ds} and V_{qs} are coupled, the equations are written:

$$\begin{cases} V_{ds} = \sigma L_{sc} \frac{dI_{ds}}{dt} + \left(R_s + R_{dqr} \frac{3 \cdot n_b \cdot M_{sr}^2}{4L_{rc}^2} \right) I_{ds} - \omega_s \cdot \sigma \cdot L_{sc} \cdot I_{qs} - R_{dqr} \frac{3 \cdot n_b \cdot M_{sr}^2}{4L_{rc}^2} \varphi_r \\ V_{qs} = \sigma L_{sc} \frac{dI_{qs}}{dt} + \left(R_s + R_{dqr} \frac{3 \cdot n_b \cdot M_{sr}^2}{4L_{rc}^2} \right) I_{qs} + \omega_s \cdot \sigma \cdot L_{sc} \cdot I_{ds} + \omega \frac{n_b \cdot M_{sr}}{2L_{rc}} \varphi_r \end{cases} \quad (VI.5)$$

Where :

$$\begin{aligned} \varphi_r &= \frac{\frac{3}{2} M_{sr}}{1 + s \cdot T_r} \cdot I_{ds} \\ \omega_r &= \frac{\frac{3}{2} M_{sr}}{T_r \varphi_r} \cdot I_{qs} \end{aligned} \quad (VI.6)$$

These expressions can be used as they are to carry out vector control; but they have a big disadvantage: the voltages V_{ds} and V_{qs} influence both I_{ds} and I_{qs} and therefore the flux and the torque (coupling between the actions on the d and q axes).

It is therefore necessary to achieve a decoupling between V_{ds} and V_{qs} which makes it possible to control independently (the torque by the I_{qs} component and the rotor flux by the I_{ds} component).

There are different decoupling techniques:

- ✓ Decoupling uses a regulator;
- ✓ Decoupling by state feedback;
- ✓ Decoupling by compensation.

In our study we will adopt the state feedback decoupling method; where we use [C] and [D] matrixs to Idq currents to get V_{dq} voltages references to feed the inverter.

$$[C] = \begin{bmatrix} R_s & 0 & 0 \\ 0 & R_s & 0 \end{bmatrix} \quad ; \quad [D] = \begin{bmatrix} 0 & -\sigma L_s & 0 \\ \sigma L_s & 0 & \frac{M}{L_r} \end{bmatrix} \quad (VI.7)$$

In this case the flow cannot be adjusted, it is deduced from the speed from the defluxing block. This block is defined by the following nonlinear relation

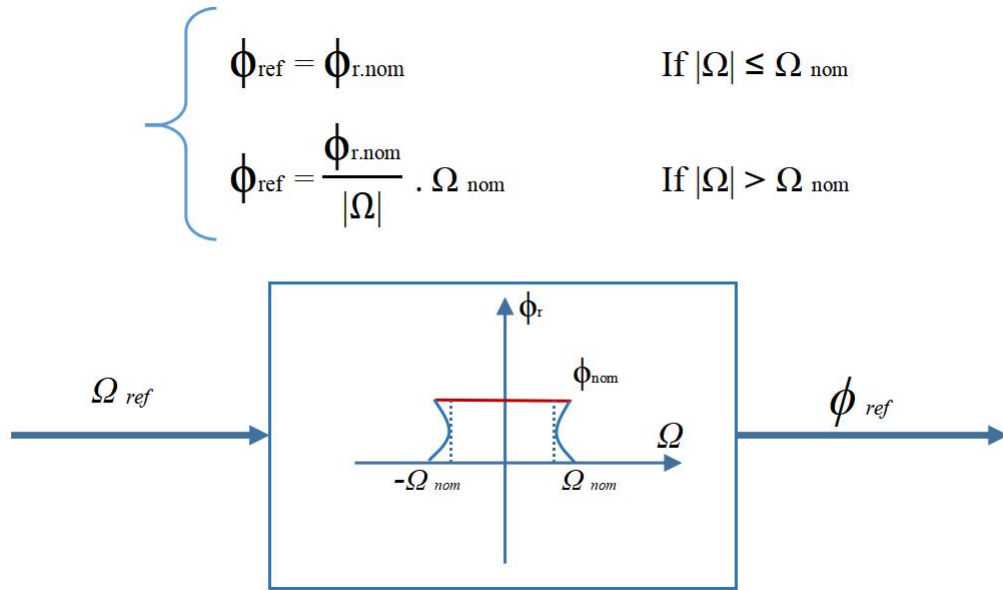


Figure VI.2 : Field weakening.

VI.3. Adaptive-Fuzzy-PID based Field-Oriented Control

while Field-Oriented Control (FOC) is a sophisticated technique widely employed in motor control systems to achieve precise speed and torque control. To enhance the performance and adaptability of FOC-based systems, the integration of advanced control strategies has become increasingly vital. Furthermore, ensuring robustness and reliability is of paramount importance, especially in applications where system failures or disturbances can have significant consequences.

This section delves into the concept of using an Adaptive-Fuzzy-PID controller which is a hybrid control approach that combines the advantages of traditional PID control with the adaptability of fuzzy logic as a part of Field-Oriented Control (FOC) based speed control with a focus on its role as a tolerant control strategy. as the Tolerant control is the capacity of a system to maintain acceptable performance even in the presence of faults, uncertainties, or disturbances. Thus, Adaptive-Fuzzy-PID controller, with its ability to adapt to varying conditions, lends itself naturally to this purpose.

The structure of the fuzzy-PID controller can be broken down into several key components, each serving a distinct role in the control system. Here's a structured breakdown of the fuzzy-PID controller's components and their functions:

VI.3.1. PID Controller:

The PID controller is a classic control component that consists of three main elements: Proportional (P), Integral (I), and Derivative (D) actions. These components collectively regulate the control output based on the error signal (the difference

between the desired setpoint and the current process variable). The PID controller provides basic control functionality by adjusting the control output to minimize the error signal. The proportional component responds to the current error, the integral component handles accumulated errors over time, and the derivative component accounts for the rate of change of the error [103].

The transfer function of a PID controller can be represented in various forms, providing flexibility in adjusting its parameters for different control applications. The standard continuous-time PID transfer function is expressed as:

$$G(s) = K_p + \frac{K_i}{s} + K_d \cdot s \quad (\text{VI.8})$$

Here, K_p , K_i , and K_d represent the proportional, integral, and derivative gains, respectively. Another equivalent form is given as:

$$G(s) = K_p \left(1 + \frac{1}{T_i \cdot s} + T_d \cdot s \right) \quad (\text{VI.9})$$

In this form, T_i represents the integral time constant ($T_i = K_p/K_i$), and T_d represents the derivative time constant ($T_d = K_d/K_p$). These constants help in fine-tuning the controller's response.

Tuning the parameters of a PID controller, whether using K_p , K_i , and K_d or K_p , T_i , and T_d , is a critical task to achieve desired control system performance. Finding the optimal adjustments for a given process can be challenging, as it depends on the specific characteristics and requirements of the system.

In the upcoming section, an online gain scheduling scheme for the PID controller, based on fuzzy rules, will be introduced. This approach aims to adaptively adjust the PID controller's parameters in real-time to optimize control performance based on changing operating conditions.

VI.3.2. Adaptive Fuzzy Logic Controller (FLC)

Description: The adaptive Fuzzy Logic Controller is a component that uses fuzzy logic to make decisions and adjust control parameters.

Function: In the adaptive fuzzy-PID controller, the FLC's primary role is to regulate the parameters of the PID controller (k_p , k_i , and k_d) in real-time based on fuzzy logic control rules. These rules take into account the system's current state and operating conditions to dynamically adapt the PID gains. The method assumes that the proportional gain (K_p) and derivative gain (K_d) fall within predefined ranges, denoted as $[K_p_min, K_p_max]$ and $[K_d_min, K_d_max]$, respectively. These ranges are established based on the specific control system requirements and constraints. To simplify the fuzzy logic-based control, the K_p and K_d values are normalized into the range between zero and one using the following linear transformation:

$$Kp_normalized = (Kp - Kp_min) / (Kp_max - Kp_min) \tag{VI.10}$$

$$Kd_normalized = (Kd - Kd_min) / (Kd_max - Kd_min)$$

Where:

Kp and Kd are the original, non-normalized proportional and derivative gains, respectively.

Kp_min and Kp_max represent the minimum and maximum allowable values for Kp , defining the range within which it can vary.

Kd_min and Kd_max similarly specify the minimum and maximum bounds for Kd .

The purpose of this normalization is to convert the original gain values into a standardized range between zero and one. This standardized range simplifies the fuzzy logic control process since fuzzy rules and reasoning are typically designed to work with normalized input values. By performing this transformation, the fuzzy gain scheduler can work with the normalized gains, making it easier to generate appropriate control parameters in response to the system's operating conditions.

Once the normalized gains ($Kp_normalized$ and $Kd_normalized$) are available, fuzzy rules and reasoning can be applied to determine the appropriate control parameters (Kp , Ki , and Kd) in real-time based on the current state of the system. This dynamic adaptation allows the PID controller to respond effectively to varying conditions, resulting in improved control system performance.

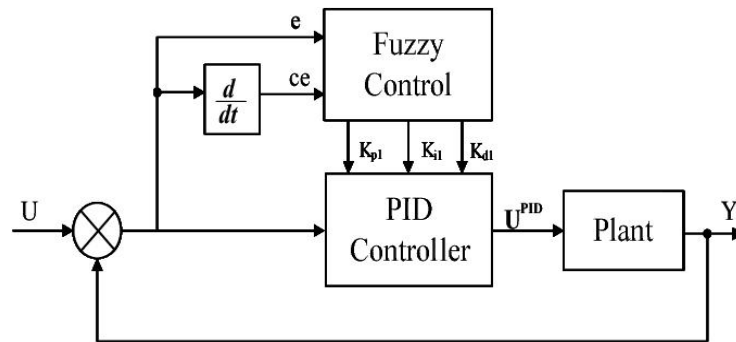


Figure VI.3 : Structure of Adaptive Fuzzy PID controller.

In the proposed scheme, the determination of PID parameters relies on the current error ($e(k)$) and its first difference ($\Delta e(k)$). Specifically, the integral time constant (T_i) is determined with reference to the derivative time constant (T_d):

$$T_i = a \cdot T_d \tag{VI.11}$$

And the integral gain (K_i) is then calculated as:

$$K_i = Kp / (a \cdot Td) = Kp^2 / (a \cdot Kd) \tag{VI.12}$$

K_p _normalized, K_d _normalized, and a are determined using a set of fuzzy rules of the form:

- ◆ "if $e(k)$ is A_i and $\Delta e(k)$ is B_i , then K_p _normalized is C_i , K_i is D_i , and $a = a_i$."
- ◆ A_i and B_i are fuzzy sets defined on corresponding supporting sets.
- ◆ C_i and D_i represent fuzzy sets associated with K_p _normalized and K_i .
- ◆ a_i is a constant.

Membership functions (MF) for the fuzzy sets related to $e(k)$ and $\Delta e(k)$ are illustrated in Figure (VI.4). These sets include descriptors such as "N" for negative, "P" for positive, "ZO" for approximately zero, "S" for small, "M" for medium, and "B" for big. For instance, "NM" stands for negative-medium, "PB" represents positive big, and so on.

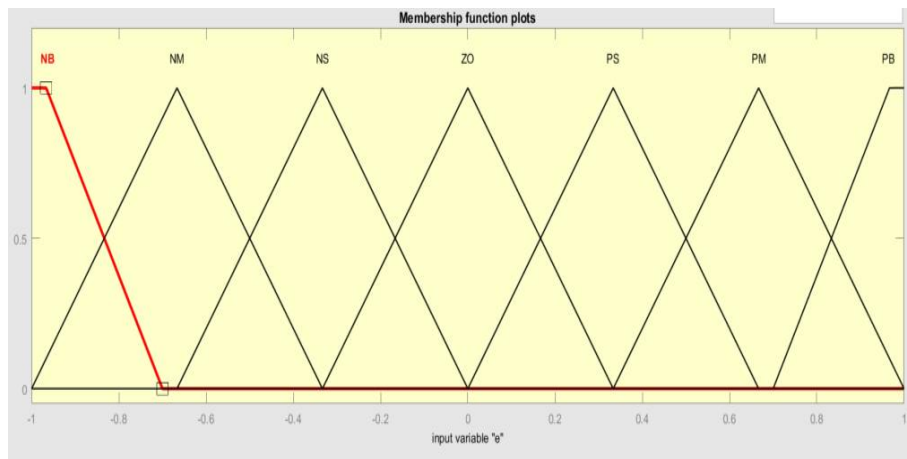


Figure VI.4 : Membership Functions For $e(k)$ and $\Delta e(k)$

The fuzzy sets C_i and D_i can be categorized as either "Big" or "Small" and are defined by the membership functions shown in Figure (VI.5).

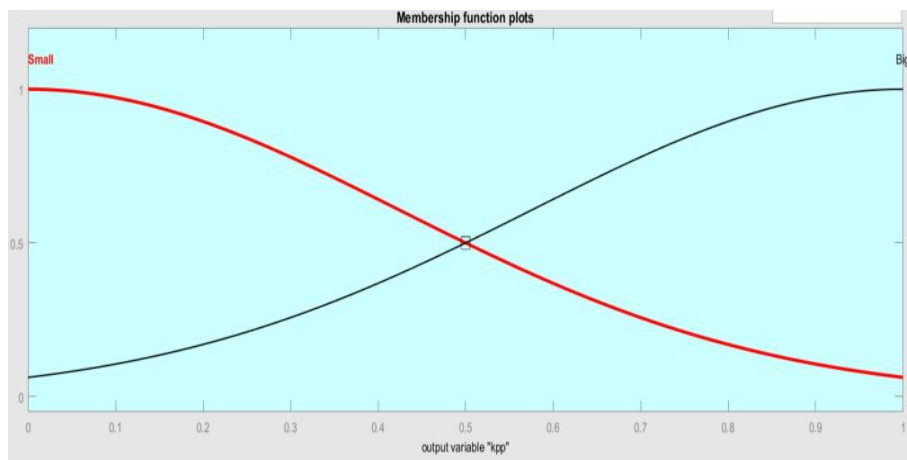


Figure VI.5 : Membership Functions For K_p _normalized and K_d _normalized

These membership functions describe the relationship between the grade of the membership function (denoted as μ) and the variable x (which can be either K_p _normalized or K_d _normalized). The expressions for these membership functions are as follows:

For "Small":

$$\mu_{small}(x) = -1/4 * \ln(x) \quad \text{or} \quad x_{small}(\mu) = \exp(-4\mu) \quad \text{(VI.13)}$$

For "Big":

$$\mu_{big}(x) = -1/4 * \ln(1-x) \quad \text{or} \quad x_{big}(\mu) = 1 - \exp(-4\mu) \quad \text{(VI.14)}$$

These fuzzy rules and membership functions form the basis of the fuzzy logic-based gain scheduling scheme. By evaluating the current error and its first difference against these rules and membership functions, the controller can adaptively determine suitable values for K_p _normalized, K_d _normalized, and a , thereby optimizing the PID control parameters based on the system's real-time operating conditions.

Indeed, the fuzzy rule around a_i specifies:

"If $e(k)$ is "PB" (positive big) and $\Delta e(k)$ is "ZO" (approximately zero), then K_p _normalized is "Big," K_d _normalized is "Small," and $a = 2$."

It's worth noting that a can also be treated as a fuzzy number, which has a singleton membership function, as illustrated in Figure (VI.6). In this case, when a is "Small," it becomes precisely equal to 2.

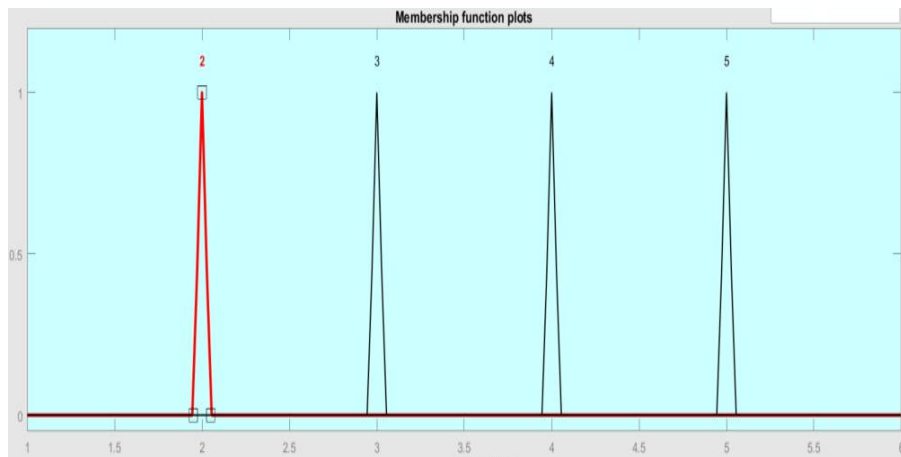


Figure VI.6 : Membership Functions For ‘a’

The choice of a plays a significant role in controlling the system's response. In the context of fuzzy logic control, it can be understood that a smaller value of a implies a preference for a small control signal to avoid large overshoot. Consequently, this suggests that the PID controller should have a small proportional gain, a large

derivative gain, and a small integral gain to achieve the desired control objectives [103].

For example, the following fuzzy rule is established based on this reasoning:

"If $e(k)$ is "ZO" (approximately zero) and $\Delta e(k)$ is "NB" (negative big), then $K_p_normalized$ is "Small," $K_d_normalized$ is "Big," and $a = 5$."

These fuzzy rules and the fuzzy number for a guide the adaptive adjustment of the PID controller's parameters, ensuring that the control system responds appropriately to the current error and its first difference while striving to achieve the desired control objectives, such as minimizing overshoot.

The process of adapting the proportional gain ($K_p_normalized$), derivative gain ($K_d_normalized$), and a is guided by a set of fuzzy rules, as presented in Table (VI.1). The tuning rules for each of these parameters are outlined in Tables (VI.2) and (VI.3), respectively. In these tables, "B" represents "Big," and "S" represents "Small," indicating the direction of adjustment for each parameter.

Table VI.1 : Fuzzy Tuning Rules For ' $K_p_normalized$ '

		$\Delta e(k)$						
		NB	NM	NS	ZO	PS	PM	PB
$e(k)$	NB	B	B	B	B	B	B	B
	NM	S	B	B	B	B	B	S
	NS	S	S	B	B	B	S	S
	ZO	S	S	S	B	S	S	S
	PS	S	S	B	B	B	S	S
	PM	S	B	B	B	B	B	S
	PB	B	B	B	B	B	B	B

Table VI.2 : Fuzzy Tuning Rules For ' $K_d_normalized$ '

		$\Delta e(k)$						
		NB	NM	NS	ZO	PS	PM	PB
$e(k)$								
	NB	S	S	S	S	S	S	S

	NM	B	B	S	S	S	B	B
	NS	B	B	B	S	B	B	B
	ZO	B	B	B	B	B	B	B
	PS	B	B	B	S	B	B	B
	PM	B	B	S	S	S	B	B
	PB	S	S	S	S	S	S	S

Table VI.3 : Fuzzy Tuning Rules For ‘ a ’

		$\Delta e(k)$						
		NB	NM	NS	ZO	PS	PM	PB
e(k)	NB	2	2	2	2	2	2	2
	NM	3	3	2	2	2	3	3
	NS	4	3	3	2	3	3	4
	ZO	5	4	3	3	3	4	5
	PS	4	3	3	2	3	3	4
	PM	3	3	2	2	2	3	3
	PB	2	2	2	2	2	2	2

Once the values of K_p _normalized, K_d _normalized, and a have been determined based on the fuzzy rules and fuzzy number for a , the PID controller's parameters can be calculated using the following equations derived from the earlier expressions:

K_p is determined as:

$$K_p = (K_p_max - K_p_min) * K_p_normalized + K_p_min \quad (VI.15)$$

Here, K_p _min and K_p _max represent the minimum and maximum allowable values for K_p .

K_d is calculated as:

$$K_d = (K_d_max - K_d_min) * K_d_normalized + K_d_min \quad (VI.16)$$

Similarly, Kd_min and Kd_max denote the minimum and maximum bounds for Kd .

Ki is obtained through:

$$Ki = Kp^2 / (a \cdot Kd) \tag{VI.17}$$

This equation relates Ki to the calculated Kp and Kd values, as well as the determined value of a .

These calculations ensure that the PID controller's parameters are adjusted according to the fuzzy rules and the specific operating conditions of the control system, thereby achieving desired control performance while considering constraints on the proportional and derivative gains.

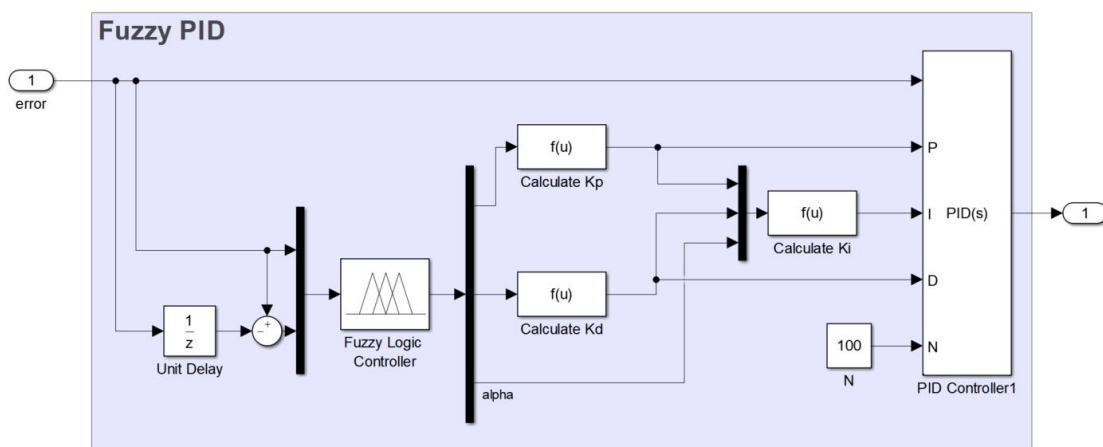


Figure VI.7 : Fuzzy PID controller.

VI.4. Stator Fault Results

(Short Circuits Between Winding Turns)

- Open Loop Control: In the open-loop control system, when a stator fault occurs, we observe a more significant steady-state error. This means that the system's ability to maintain the desired speed is compromised, resulting in a less accurate performance. Furthermore, when the fault manifests, the speed of the system increases by approximately 1.2%. This speed increase is accompanied by a higher power consumption, indicating inefficiencies. Additionally, disequilibria in the system are evident, suggesting an unstable response to the fault.

- FOC Control: In the field-oriented control (FOC) system, we observe an improvement in steady-state error compared to open-loop control. When a stator fault occurs, the speed of the system increases by approximately 0.8%, which is a more moderate deviation compared to open-loop control. However, the system still experiences an increase in power consumption, indicating some inefficiencies.

Interestingly, in this case, there is less speed correction observed when the fault occurs, suggesting that the FOC control system is better at maintaining speed stability despite the fault.

- FOC Based adaptive Fuzzy_PID: The FOC control system augmented with Fuzzy_PID exhibits the most promising results. Notably, there is no steady-state error, indicating that the system can maintain the desired speed even in the presence of a stator fault. When the fault occurs, the speed increases by a mere 0.4%, which is a minimal deviation. Additionally, the system consumes less power, signifying improved efficiency. Furthermore, there is more efficient speed correction observed when the fault occurs, highlighting the system's robustness and ability to adapt to faults.

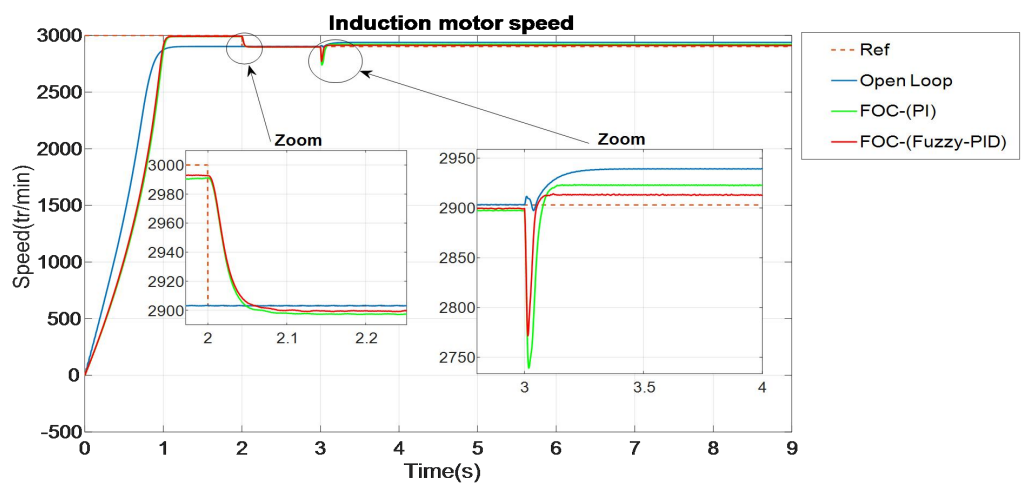


Figure VI.8 : Stator Fault Results (Speed).

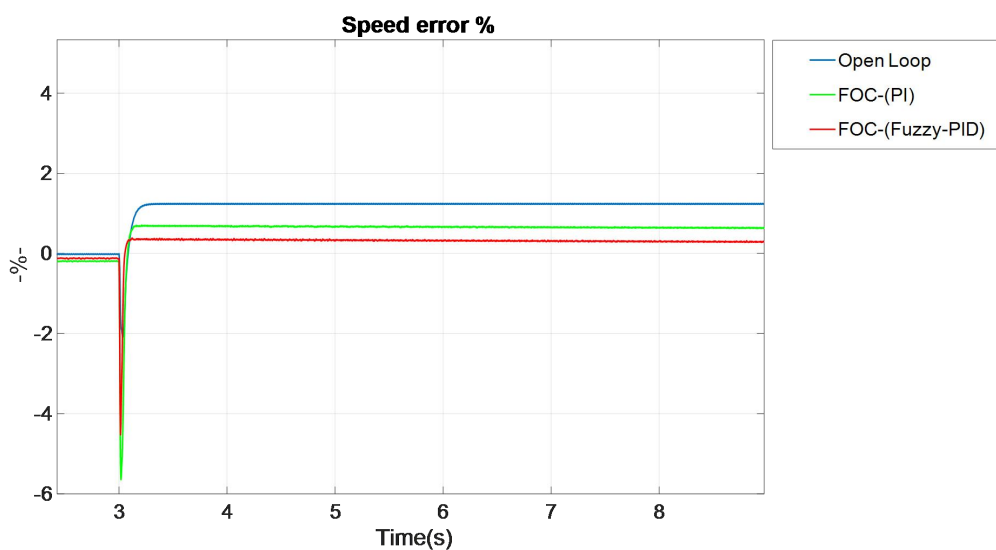


Figure VI.9 : Stator Fault Results (Error).

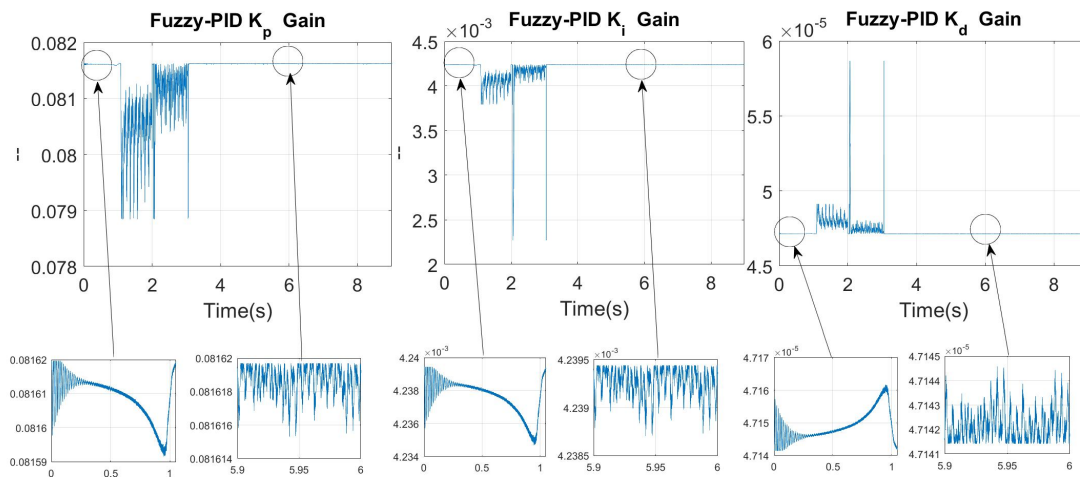


Figure VI.10 : Stator Fault Results (Kp, Ki and Kd).

VI.5. Rotor Fault Results

(Rotor Bar Damage)

- Open Loop Control: In the open-loop control system, when a rotor fault, specifically rotor bar damage, occurs, we observe a significant decrease in speed, amounting to -2%. This decrease is accompanied by oscillations between -1.8% and -2.2%, indicating a highly unstable response to the fault. Additionally, there is an increase in power consumption, suggesting inefficiencies in the system. Notably, there is no observed speed correction when the fault occurs, indicating that the open-loop control system struggles to adapt to rotor faults.

FOC Control: Under FOC control, when a rotor fault occurs, the speed decreases by a lesser margin, approximately -1.25%, with oscillations between -1% and -1.5%. This indicates a more stable response compared to open-loop control. While there is still an increase in power consumption when the fault occurs, it is relatively less pronounced. However, similar to open-loop control, there is limited speed correction observed.

FOC Based adaptive Fuzzy_PID: The FOC control system equipped with Fuzzy_PID showcases the most favorable outcomes when dealing with rotor faults. Here, when the fault occurs, the speed decreases by a mere -0.5%, with less oscillation between -0.4% and -0.6%. This signifies a highly stable response to rotor faults. Furthermore, the system consumes less power, indicating improved efficiency. Notably, there is more efficient speed correction observed over time, underlining the adaptive and robust nature of the FOC-based Fuzzy_PID control system.

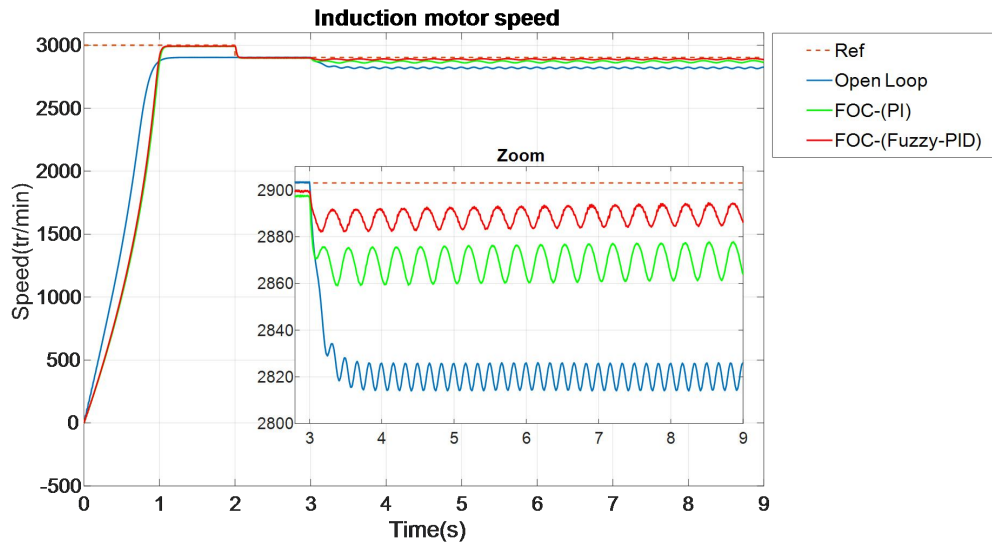


Figure VI.11 : Rotor Fault Results (Speed).

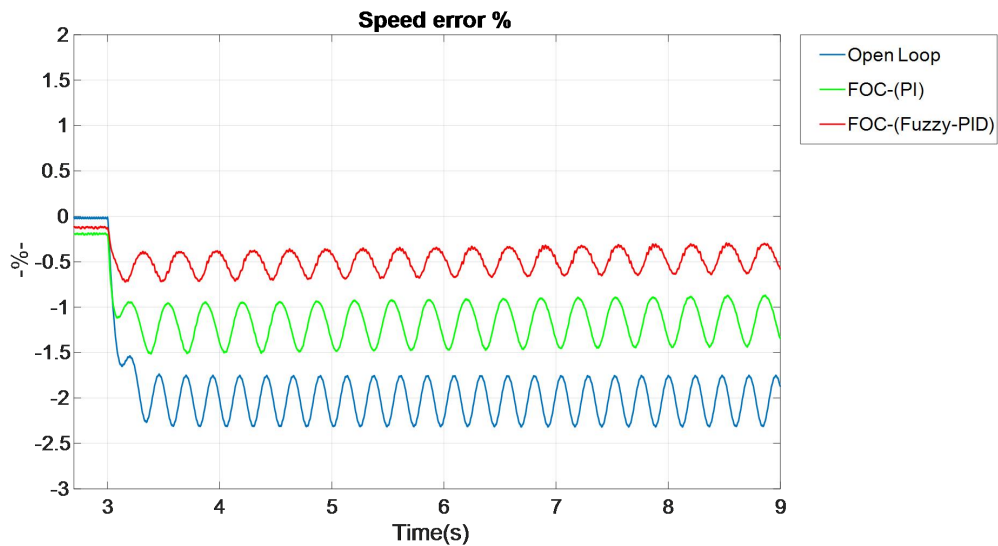


Figure VI.12 : Rotor Fault Results (Error).

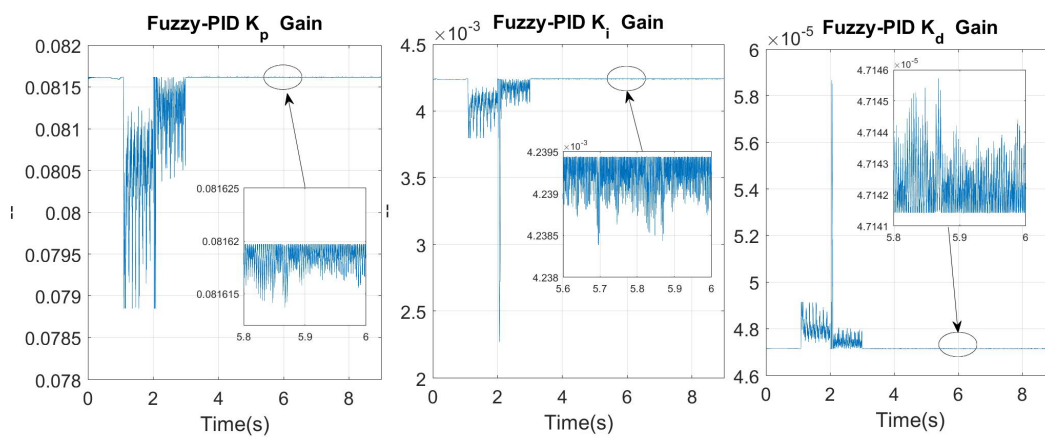


Figure VI.13 : Rotor Fault Results (K_p , K_i and K_d).

VI.6. Conclusion

In the ever-evolving landscape of electrical machinery and control engineering, the sixth chapter of this thesis has delved into a critical realm: the design and implementation of Fault Tolerant Control (FOC) using adaptive Fuzzy-PID (Proportional-Integral-Derivative) controller for induction motors, specifically targeting stator and rotor faults. This chapter has been an exploration of resilience, adaptability, and precision in the context of fault tolerance.

Throughout our journey in this chapter, we have examined the theoretical foundations of FOC- adaptive Fuzzy-PID, unraveling the intricacies of how this innovative control strategy operates in the presence of stator and rotor faults. Its ability to adapt the control strategy in criculer-time, and mitigate their effects has been showcased through rigorous testing and validation.

The results presented herein bear testament to the effectiveness of FOC- adaptive Fuzzy-PID. Under various fault scenarios, the control strategy has consistently demonstrated its capacity to maintain optimal motor performance, even when subjected to external disturbances. This robustness is a testament to the potential of this approach in safeguarding induction motors against the detrimental effects of faults.

General Conclusion

In summary, this thesis has delved into the intricate world of fault diagnosis and fault-tolerant control within the realm of photovoltaic solar pumping systems. These systems offer a plethora of benefits, including cost reduction, environmental friendliness, and heightened reliability. However, they are not impervious to technical challenges, especially when it comes to the occurrence of faults and failures. Through systematic categorization of these faults, the development of advanced diagnostic techniques, and the crafting of robust fault-tolerant control strategies, this research endeavors to tackle these challenges head-on, ultimately aiming to amplify the performance, efficiency, and longevity of solar PV pumping systems.

This journey embarked with the construction of a comprehensive mathematical model for the solar PV pumping system, meticulously capturing its components, behavior, and interactions. The subsequent introduction of simulated faults replicated real-world scenarios and unveiled their effects on system performance and parameters. This foundational work laid the groundwork for the innovative fault detection and tolerant control techniques that followed.

The fault detection technique, harnessing the combined power of the Discrete Wavelet Transform (DWT) and Artificial Neural Networks (ANN), stood as a testament to the capabilities of data analysis and machine learning. By recognizing deviations from normal system behavior, this technique provides system operators with a proactive tool for swift fault identification and resolution. Its impact is far-reaching, from reducing downtime to minimizing maintenance expenditures.

Concurrently, the fault-tolerant control strategy, built upon Field-Oriented Control (FOC) and fortified with an adaptive Fuzzy-PID controller, demonstrated the system's capacity to adapt and uphold peak performance in the face of faults. This resilient control approach elevates system reliability, mitigates the risk of catastrophic failures, and ensures the seamless continuity of operations.

The implications of this research extend beyond the confines of academia. By enhancing fault diagnosis and tolerant control techniques, this work stands to guarantee uninterrupted water supply services, trim operational costs, and stretch the system's lifecycle. Whether in remote, resource-constrained regions or more conventional settings, the benefits are tangible and far-reaching.

Looking ahead, the integration of artificial intelligence (AI) into fault detection and tolerant control holds immense promise. AI algorithms are adept at sifting through colossal datasets, spotting intricate patterns, and identifying anomalies that may elude human observation. The future beckons us to explore the synergy between AI and fault-tolerant strategies, potentially catapulting the performance and reliability of photovoltaic solar pumping systems to unprecedented heights.

In conclusion, this thesis underscores the pivotal role played by fault diagnosis and tolerant control in safeguarding the efficiency, safety, and sustainability of solar PV pumping systems. These techniques are not mere theoretical constructs but pragmatic tools that wield a profound impact on the real-world operation and maintenance of these systems. As we navigate the ever-evolving landscape of solar energy technologies, the lessons learned and innovations unearthed in this research will remain in the service of the continued success of solar PV pumping systems across the globe.

Perspectives and Future Directions

The research conducted in the realm of fault diagnosis and tolerant control for solar PV pumping systems not only advances the state of these systems but also sets the stage for broader applications and future research endeavors. Several pivotal perspectives and future directions emerge:

Cross-Domain Application: Techniques developed can be applied beyond solar PV pumping, enhancing fault management in various industrial systems. Their transferability improves system reliability and performance across sectors.

Field Testing and Validation: Rigorous testing under diverse conditions validates the effectiveness of fault diagnosis and tolerant control techniques, ensuring their utility in practical scenarios.

Hybrid Renewable Energy Systems: Solar PV pumping can integrate with other renewable sources in hybrid systems. Tailored fault diagnosis and tolerant control strategies ensure reliable operation, contributing to complex energy systems' efficiency.

Energy Efficiency Optimization: Optimizing energy consumption during fault-tolerant operations is crucial. Dynamic control strategies can enhance the overall efficiency of renewable energy systems, benefiting diverse applications and contributing to a sustainable energy future.

In summary, the perspectives and future directions in the field of fault diagnosis and tolerant control extend far beyond solar PV pumping systems. The versatility and adaptability of these techniques enable their application in diverse domains, while rigorous field testing and validation ensure their practical effectiveness. Embracing the era of hybrid renewable energy systems and prioritizing energy efficiency optimization will be pivotal in shaping the future of fault management in the context of renewable energy. By addressing these aspects, we can foster innovation, bolster system resilience, and drive sustainable practices across various sectors of industry and engineering.

Referances

- [1]. Brihmat, F. (2012). "Etude conceptuelle d'un système de conditionnement de puissance pour une centrale hybride PV/Eolien," Mémoire de Magister, Université de Tizi-Ouzou.
- [2]. Abouda, S. (2015). "Contribution à la commande des systèmes photovoltaïques: Application aux systèmes de pompage," Thèse, Université de Reims Champagne-Ardenne & École Nationale d'Ingénieurs de Sfax.
- [3]. Boukhers, D. (2007). "Optimisation d'un système d'énergie photovoltaïque application au pompage," Mémoire de Magister, Université de Constantine.
- [4]. Abdelhak, A. H. (2018). "Contribution à l'étude des systèmes photovoltaïques avec stockage connectés au réseau," Thèse, University Mustapha Stambouli of Mascara.
- [5]. Soualmia, A. (2014). "Intégration de la Production Décentralisée dans un Système de Pompage Photovoltaïque," Magister en Electronique, Université Constantine 1.
- [6]. Meunier, S. (2019). "Optimal design of photovoltaic water pumping systems for rural communities – a technical, economic and social approach," Thèse de doctorat, Université Paris-Saclay.
- [7]. Bounechba, H. (2017). "Contribution à l'étude d'un système de pompage photovoltaïque," Thèse, Université des Frères Mentouri Constantine.
- [8]. Zhao, Y. (2015). "Fault Detection, Classification and Protection in Solar Photovoltaic Arrays," Doctor of Philosophy, Northeastern University, Boston, Massachusetts.
- [9]. Bouhafis, A. (2022). "Photovoltaic system, control, analysis and fault diagnosis," Degree of Doctorate, Kasdi Merbah University, Ouargla.
- [10]. Tourqui, D. (2016). "Amélioration de la stabilité d'un réseau électrique par l'intégration des sources d'énergies renouvelables," Thèse, Université Ibn Khaldoun de Tiaret.
- [11]. Lazizi, A. (2019). "Modélisation, contrôle et gestion énergétique d'une installation de pompage solaire," Thèse, Université M'Hamed Bougara-Boumerdes.
- [12]. Aoufi, S. (2014). "Modélisation et commande d'un système de pompage photovoltaïque," Mémoire de Magister, Université Ferhat Abbas — Setif-1.
- [13]. Cabal, C. (2008). "Optimisation énergétique de l'étage d'adaptation électronique dédié à la conversion photovoltaïque," Thèse de Doctorat, Université de Paul Sabatier III, Toulouse, France.
- [14]. Cid-Pastor, A. (2006). "Conception et réalisation de modules photovoltaïque électronique," Thèse de doctorat, Université Paul Sabatier, Toulouse.
- [15]. Louazene, M. L. (2015). "Contribution à l'optimisation des systèmes photovoltaïques utilisés pour l'irrigation dans les zones sahariennes – Application zone de Ouargla," Doctorat, Université El Hadj Lakhdar - Batna.

- [16]. Wurfel, P. (2009). "Physics of Solar Cells: From Basic Principles to Advanced Concepts," Edition Wiley & Sons.
- [17]. Makhloufi, S. (2013). "Contribution à l'optimisation des installations photovoltaïques par des commandes intelligentes," Thèse de doctorat en sciences, Université de Batna.
- [18]. Bouchakour, A. (2018). "Modélisation et Simulation d'un Système de Pompage Photovoltaïque," Docteur, Université Djillali Liabes de Sidi-Bel-Abbès.
- [19]. Aissa, M. (2011). "Modélisation et commande d'une chaîne de pompage photovoltaïque," Magister, Université Abou Bekr Belkaid - Tlemcen.
- [20]. Mahammedi, A. (2020). "Contribution to the control of a Power Converter with Improved Topologies Associated with a Photovoltaic Generator Based on Advanced Techniques," Ph.D., Djelfa University, FST.
- [21]. Saeed, M. A. E. (2015). "Study, Design and Performance Analysis of Grid-Connected Photovoltaic Power System," Ph.D., Minia University.
- [22]. Zhang, L. (2019). "A study of solar photovoltaic systems and its applications in modern power systems," Doctor of Philosophy, The University of Western Australia.
- [23]. Bouacha, S. (2021). "A Study on Photovoltaic Power Plant Connected to the Distribution Network," Doctoral Thesis, École Nationale Polytechnique.
- [24]. Tamizhmani, G. et al. (2011). "Photovoltaic Module Power Rating per IEC 61853-1 Standard," Report of Arizona State University, Photovoltaic Reliability Laboratory (PRL).
- [25]. Chenni, R. (2007). "Etude technico-économique d'un système de pompage photovoltaïque dans un village solaire," Thèse de doctorat en sciences en physique énergétique, Université de Constantine.
- [26]. Bouden, A. (2008). "Analyse optimisée de systèmes de pompage photovoltaïque," Mémoire de Magister, Université de Mentouri Constantine.
- [27]. Serir, C. (2012). "Optimisation des systèmes de pompage photovoltaïque," Mémoire de Magister, Université Abderrahmane Mira de Béjaia.
- [28]. Maurice, K. T. S. (2007). "Système Photovoltaïque: Dimensionnement pour pompage d'eau, pour une irrigation goutte-à-goutte," DEA en Physique, Université de Ouagadougou, Burkina-Faso.
- [29]. Benlarbi, K. (2001). "Optimisation floue, Neuronale et neuro-floue d'un système de pompage photovoltaïque entraîné par différentes machines électriques: Machines à induction, machines synchrone à aimants permanents et machine à courant continu," Mémoire de Magister, Université Mustapha Ben Boulaid Batna 2.
- [30]. Diaf, S. (2002). "Etude et optimisation des systèmes de pompage photovoltaïque," Mémoire de Magister, Université de Boumerdes.
- [31]. Hadj Arab, A., Benghanem, M., & Gharbi, A. (2005). "Dimensionnement de Systèmes de Pompage Photovoltaïque," Revue Energies Renouvelables, Vol. 8, 19 - 26.

- [32]. Kilic, E. (2005). Fault Detection and Diagnosis in Nonlinear Dynamical Systems (Ph.D. thesis). Middle East Technical University.
- [33]. Dhimish, M. (2018). Fault Detection and Performance Analysis of Photovoltaic Installations (Ph.D. thesis). The University of Huddersfield.
- [34]. Li, B. (2021). Health monitoring of photovoltaic modules using electrical measurements (Ph.D. thesis). Université Paris-Saclay.
- [35]. García-Gutiérrez, L. A. (2019). Development of an Active-Fault Tolerant Control Applied to PV systems (Ph.D. thesis). Université Paul Sabatier - Toulouse III; Universidad de los Andes (Bogotá).
- [36]. Sapountzoglou, N. (2019, November). Fault detection and isolation for low voltage distribution grids with distributed generation (Ph.D. thesis). Université Grenoble Alpes.
- [37]. Venkatakrishnan, G.R., et al. (2023). Detection, location, and diagnosis of different faults in large solar PV system - A review.
- [38]. Mustafa, M. O. (2015, March). On Fault Detection, Diagnosis, and Monitoring for Induction Motors (Ph.D. thesis). Luleå University of Technology.
- [39]. Zare, S. (2018). Fault Detection and Diagnosis of Electric Drives Using Intelligent Machine Learning Approaches (Master's thesis). Electronic Theses and Dissertations.
- [40]. Han, X. (2021). Observer based fault diagnosis and fault tolerant control of nonlinear systems (Ph.D. thesis). INSA de Toulouse.
- [41]. Raza, M. T. (2016). Fault Diagnosis and Fault Tolerant Control of Switched Dynamical Systems. Nilore, Islamabad, Pakistan.
- [42]. Arwin, M. A. (2022, May 10-13). Overview on Fault Detection and Isolation. Paper presented at ICEANS 2022, Konya, Turkey.
- [43]. Kaijuka, P. (2020). Fault-tolerant Control (FTC) Applied to an Inherently Redundant Electromechanical Railway Track Switch (Ph.D. thesis). Loughborough University.
- [44]. Nyberg, M. (1999). Model-Based Fault Diagnosis Methods, Theory, and Automotive Engine Applications (Ph.D. thesis). Linköping University.
- [45]. Nguyen, T. N. (2020). Model-Based Diagnostic Frameworks for Fault Detection and System Monitoring in Nuclear Engineering Systems (Ph.D. thesis). University of Michigan.
- [46]. Zhao, X. (2012). Data-Driven Fault Detection, Isolation, and Identification of Rotating Machinery: with Applications to Pumps and Gearboxes (Ph.D. thesis). University of Alberta.
- [47]. Doherty, N. F. (2010). Knowledge-based approaches to fault diagnosis. The development, implementation, evaluation, and comparison of knowledge-based systems, incorporating deep and shallow knowledge, to aid in the diagnosis of faults in complex hydro-mechanical devices (Doctoral dissertation). University of Bradford.

- [48]. Kodavade, D. V. (2016). Knowledge Based Approach For Fault Diagnosis In Electronic Circuit Boards. *International Journal of Control and Automation*, 9(1), 293-308. <http://dx.doi.org/10.14257/ijca.2016.9.1.27>
- [49]. Khan, S. S. (2021, May). A Comprehensive Review of Fault Diagnosis and Tolerant Control in DC-DC Converters for DC Microgrids. *IEEE Access*, PP(99), 1-1. 10.1109/ACCESS.2021.3083721
- [50]. Alibek, K. (2022, February). FAULT DETECTION AND DIAGNOSIS USING HYBRID ARTIFICIAL NEURAL NETWORK BASED METHOD (Doctoral dissertation). Memorial University of Newfoundland.
- [51]. Stoican, F. (2011). Fault tolerant control based on set-theoretic methods (Ph.D. thesis). École Supérieure d'Electricité.
- [52]. Maamouri, R. (2017, December). Diagnostic et Commande Tolérante aux Défauts Appliqués à un Système de Conversion Électromécanique à Base d'une Machine Asynchrone Triphasée (Doctoral dissertation, École Doctorale ED184 – Université de Sousse).
- [53]. Jiang, L. L. (2014). Modeling and optimization of photovoltaic systems under partially shaded and rapidly changing conditions (Doctoral thesis). Nanyang Technological University, Singapore.
- [54]. Aly, A. E. M. M. (2005). Modelling and Simulation of a Photovoltaic Fuel Cell Hybrid System (Ph.D. thesis). University of Kassel.
- [55]. Kaced, K. (2018). Étude des techniques MPPT pour systèmes photovoltaïques dans des conditions partiellement ombragées (Ph.D. thesis). École Nationale Polytechnique ENP.
- [56]. Sabzehgar, R. (2011). Control strategies of DC-bus voltage in islanded operation of microgrid. In 4th International Conference on Electric Utility Deregulation and Restructuring and Power Technologies (DRPT).
- [57]. Johansson, B. (2005). DC-DC Converters - Dynamic Model Design and Experimental Verification (Doctoral thesis, Lund Institute of Technology).
- [58]. Lorentz, V. (2009). Bidirectional DC Voltage Conversion for Low Power Applications (Doctoral thesis, University Louis Pasteur of Strasbourg).
- [59]. Mutasem, A. (2017, February). Modeling of Three-phase SPWM Inverter. Jordan University of Science and Technology.
- [60]. Laribi, S. S. (2016). Contribution à la Commande et Diagnostic des Défauts Statoriques et Rotoriques de la Machine Asynchrone à d'Écureuil (Doctoral dissertation, Université des Sciences et de Technologie D'Oran Mohamed BOUDIAF).
- [61]. Abdelghani, B. (2018). Simulation et Modélisation de Pompage Photovoltaïque (Master's thesis, Université BADJI MOKHTAR Annaba).
- [62]. Gergaud, O. (2002). Modélisation Énergétique et Optimisation Économique d'un Système de Production Éolien et Photovoltaïque Couplé au Réseau et Associé à un Accumulateur (Doctoral dissertation, Thèse de doctorat de l'école normale supérieure de CACHAN).

- [63]. Darikas, G. (2018, May). Design and Implementation of a Battery Management System for Lithium-Ion Batteries Suitable for Automotive Applications (Diploma Thesis). Thessaloniki.
- [64]. Al-Majidi, S. D. A. (2020, September). Efficient Maximum Power Point Tracking Techniques for a Grid-connected Photovoltaic System using Artificial Intelligence (Doctoral dissertation, Brunel University London).
- [65]. Bi, Z. (2021, September). Intelligent Global Maximum Power Point Tracking Strategies Based on Shading Perception for Photovoltaic Systems (Doctoral dissertation, University of Liverpool).
- [66]. Dong, B., Li, Y., & Zheng, Z. (2011). Control Strategies of DC-bus Voltage in Islanded Operation of Microgrid. In 2011 4th International Conference on Electric Utility Deregulation and Restructuring and Power Technologies (DRPT) (pp. 1671-1674).
- [67]. Zhou, X., et al. (2020, September). DC Bus Voltage Control of Grid-Side Converter in Permanent Magnet Synchronous Generator Based on Improved Second-Order Linear Active Disturbance Rejection Control. *Energies*.
- [68]. Nejad, S. (2017, May). Adaptive Techniques for Estimation and Online Monitoring of Battery Energy Storage Devices (Ph.D. thesis). The University of Sheffield.
- [69]. Berliner, M. D. (2023, February). Simulating, Controlling, and Understanding Lithium-ion Battery Models (Ph.D. thesis). Massachusetts Institute of Technology.
- [70]. Althobaiti, A. O. (2017, November). Proportional Resonant Control of Three-Phase Grid-Connected Inverter During Abnormal Grid Conditions (Ph.D. thesis). Newcastle University.
- [71]. Zhang, W. (2013, September). Advanced Control of Induction Motors (Ph.D. thesis). University of Liverpool.
- [72]. Otkun, Ö. (2020). Scalar speed control of induction motors with difference frequency. *Journal of Polytechnic*, 23(2), 267-276.
- [73]. Sae-Kok, W. (2008). Converter fault diagnosis and post-fault operation of a doubly-fed induction generator for a wind turbine (Ph.D. thesis). University of Strathclyde.
- [74]. Khelouat, S. (2021, July 10). Contribution on Observation and Fault Diagnosis of A Multicellular Converter (Ph.D. thesis). Ecole Nationale Polytechnique.
- [75]. Tsinetakes, J. (2022). Incipient Soft-Fault Detection in DC-DC Converters through Switching Observers (Ph.D. thesis). Drexel University.
- [76]. Shao, S. (2015, July). The application of Sliding Mode Observers to Fault Detection and Isolation for Multilevel Converters (Ph.D. thesis). University of Nottingham.
- [77]. Hu, R. (2019). Stator Winding Fault Detection Techniques for Permanent Magnet Machine Drives (Ph.D. thesis). University of Sheffield.
- [78]. Trachi, Y. (2017). On induction machine faults detection using advanced parametric signal processing techniques (Doctoral dissertation, Université de Bretagne occidentale - Brest).

- [79]. Singh, M. (2020). Fault Diagnosis of a Three-phase induction motor using Stockwell transform and machine learning techniques (Doctoral dissertation, Indian Institute of Technology Jodhpur).
- [80]. Vana, Z. (2014). Discrete Wavelet Transform in Linear System Identification (Doctoral Thesis, Czech Technical University in Prague).
- [81]. Mayeli, A. (2005). Discrete and Continuous Wavelet Transformations on the Heisenberg Group (Doctoral dissertation, Technische Universitat Munchen).
- [82]. Olkkonen, J. T. (Ed.). (2011). Discrete Wavelet Transforms - Theory and Applications. InTech. <https://doi.org/10.5772/649>
- [83]. Mimouni, A., Laribi, S., Sebaa, M., Allaoui, T., & Bengharbi, A. A. (2023). Fault diagnosis of power converters in a grid-connected photovoltaic system using artificial neural networks. *Electrical Engineering & Electromechanics*, (1), 25–30. <https://doi.org/10.20998/2074-272X.2023.1.04>
- [84]. Nonyane, P. (2016, January). The Application of Artificial Neural Networks to Transmission Line Fault Detection and Diagnosis. *Magister Technologiae*, the University of South Africa.
- [85]. Arunthavanathan, R. (2022, May). Machine Learning Methods for Fault Detection and Diagnosis of Digitalized Processing System (Doctoral dissertation, Faculty of Engineering and Applied Science, Memorial University of Newfoundland).
- [86]. Jayamaha, D. K. J., Lidula, N. W., & Rajapakse, A. (n.d.). Wavelet-Multi Resolution Analysis Based ANN Architecture for Fault Detection and Localization in DC Microgrids. *IEEE Access*, 1–1. doi: 10.1109/access
- [87]. Ankar, S., Sahu, U., & Yadav, A. (2020). Wavelet-ANN Based Fault Location Scheme for Bipolar CSC-Based HVDC Transmission System. 2020 First International Conference on Power, Control, and Computing Technologies (ICPC2T). doi: 10.1109/icpc2t48082.2020.9071450
- [88]. Bengharbi, A. A., Laribi, S., Allaoui, T., & Mimouni, A. (2022). Photovoltaic system faults diagnosis using discrete wavelet transform based artificial neural networks. *Electrical Engineering & Electromechanics*, (6), 42–47. <https://doi.org/10.20998/2074-272X.2022.6.07>
- [89]. DjamelEddine, C. B., B., A., & Mokhtar, B. (2018). Detection of a two-level inverter open-circuit fault using the discrete wavelet transforms technique. 2018 IEEE International Conference on Industrial Technology (ICIT). doi: 10.1109/icit.2018.8352206
- [90]. Souad, L. Azzedine, B., Eddine, C. B. D., Boualem, B., Samir, M., & Youcef, M. (2018). Induction machine rotor and stator faults detection by applying the DTW and N-F network. 2018 IEEE International Conference on Industrial Technology (ICIT).
- [91]. Defdaf, M., et al. (2021, January 7). A new transform discrete wavelet technique based on artificial neural network for induction motor broken rotor bar faults diagnosis. *Research Article*. DOI: 10.1002/2050-7038.12807

- [92]. Thomas, P., & Suhner, M.-C. (2015). A new multilayer perceptron pruning algorithm for classification and regression applications. *Neural Processing Letters*.
- [93]. Jozanikohan, G., Norouzi, GH., Sahabi, F., et al. (2015). The application of multilayer perceptron neural network in volume of clay estimation: Case study of Shurijeh gas reservoir, Northeastern Iran. *Journal of Natural Gas Science and Engineering*.
- [94]. Bengharbi, A. A., Laribi, S., Allaoui, T., & Mimouni, A. (2023). Open-circuit fault diagnosis for three-phase inverter in photovoltaic solar pumping system using neural network and neuro-fuzzy techniques. *Electrica*, 23(3), 505-515.
- [95]. Armstrong, R. A. (2019). Should Pearson's correlation coefficient be avoided? *Ophthalmic Physiol Opt*. <https://doi.org/10.1111/opo.12636>
- [96]. Odom, L. R., & Morrow, J. R., Jr. (2006). What's this r? A Correlational Approach to Explaining Validity, Reliability and Objectivity Coefficients. *Measurement in Physical Education and Exercise Science*.
- [97]. Asuero, A. G., Sayago, A., & González, A. G. (2006). The Correlation Coefficient: An Overview. *Critical Reviews in Analytical Chemistry*.
- [98]. Yu, J., Zhang, T., & Qian, J. (2011). Modern control methods for the induction motor. *International Energy-Efficiency Standards and Testing Methods*.
- [99]. Yahyaoui, I., & Cantero, A. S. (2018). Scalar and Vector Control of Induction Motor for Online Photovoltaic Pumping. *Advances in Renewable Energies and Power Technologies*.
- [100]. Abu-Rub, H., Iqbal, A., & Guzinski, J. (n.d.). High performance control of AC drives with MATLAB/Simulink models. ISBN 978-0-470-97829-0.
- [101]. Jain, J. K. (2017, December). Stability Analysis and Robust Controller Design of Indirect Vector Controlled Induction Motor (Doctoral dissertation, National Institute of Technology Rourkela).
- [102]. Petri, A.-M. (2023). Theoretical And Experimental Research Of The Propulsion System For An Electric Vehicle (Doctoral dissertation, Cluj-Napoca).
- [103]. Zhao, Z.-Y. (1993, September/October). Fuzzy Gain Scheduling of PID Controllers. *IEEE TRANSACTIONS ON SYSTEMS, MAN, AND CYBERNETICS*.

Appendices

Characteristics of the photovoltaic module «Aavid Solar ASMA-180M»

Open circuit voltage	$V_{co} = 45 \text{ V}$
Short circuit current	$I_{sc} = 5.5 \text{ A}$
Maximum power	$P_m = 180 \text{ W}$
Voltage at the point of maximum power	$V_m = 36 \text{ V}$
Current at maximum power point	$I_m = 5 \text{ A}$

The technical characteristics of the battery (Lithium-Ion)

Nominal voltage (V)	380 V
Rated capacity (Ah)	25 Ah
Nominal discharge current (A)	10.86 A
Internal resistance (Ohms)	0.152 Ohms
Capacity (Ah) at nominal voltage	22.60 Ah

Centrifugal pump

Power absorb	$P_a = 521 \text{ W}$
Nominal rotation speed	$w = 314 \text{ rd/s}$
Maximum flow rate	$Q_{max} = 0.008 \text{ m}^3 / \text{s}$
Maximum Head 'lift'	$H_r = 30 \text{ m}$
Acceleration of gravity	$g = 9.81 \text{ m /s}^2$
The density of water	$\rho = 1000 \text{ Kg/m}^2$

Electrical machine parameters

Rated power	$P_n = 1.5 \text{ kW}$
Voltage	$V = 220/380 \text{ V}$
Current	$I = 5.2/3.5 \text{ A}$
Nominal rotation speed	$N = 3000 \text{ rpm}$
Number of pole pairs	$p = 1$
Stator cyclic inductance	$L_s = 0.274 \text{ H}$
Rotor cyclic inductance	$L_r = 0.274 \text{ H}$
Mutual cyclic inductance	$M = 0.258$
Stator resistance	$R_s = 4.805 \text{ } \Omega$
Rotor resistance $R_r = 4.2 \text{ } \Omega$	$R_r = 3.805 \text{ } \Omega$
Inertia	$J = 0.031 \text{ N.m}$
Coefficient of friction	$F = 0.0012$

Perturb and Observe Maximum Power Point Tracking Algorithm

```
function DutyCycle = POMPPT(F, DD, DLT, V, I)
    % POMPPT - Perturb and Observe Maximum Power Point Tracking
    % F: Flag (0 or 1) indicating (OFF/ON)
    % DD: Initial duty cycle
    % DLT: Step size for duty cycle adjustments
    % V: Current voltage from the solar panel
    % I: Current current from the solar panel
    % Constants and persistent variables
    Dmax = 0.75; % Maximum duty cycle
    Dmin = 0; % Minimum duty cycle
    Dinit = DD; % Initial duty cycle
    deltaD = DLT; % Step size for duty cycle adjustments
    % Initialize persistent variables on the first function call
    persistent Vold Pold Dold;
    if isempty(Vold)
        Vold = 0;
        Pold = 0;
        Dold = Dinit;
    end
    % Calculate current power
    P = V * I;
    % Calculate changes in voltage and power
    dV = V - Vold;
    dP = P - Pold;
    % Check for changes and adjust duty cycle accordingly
    if dP ~= 0 && F ~= 0
        if dP < 0
            if dV < 0
                % If power decreased and voltage decreased, decrease duty cycle
                DutyCycle = Dold - deltaD;
            else
                % If power decreased and voltage increased, increase duty cycle
                DutyCycle = Dold + deltaD;
            end
        else
            if dV < 0
                % If power increased and voltage decreased, increase duty cycle
                DutyCycle = Dold + deltaD;
            else
                % If power increased and voltage increased, decrease duty cycle
                DutyCycle = Dold - deltaD;
            end
        end
    else
        % No change in power or flag, or unanticipated change
        DutyCycle = Dold;
    end
    % Ensure duty cycle is within the specified limits
    if DutyCycle >= Dmax || DutyCycle <= Dmin
        DutyCycle = Dold;
    end
    % Update persistent variables
    Dold = DutyCycle;
    Vold = V;
    Pold = P;
end
```

Incremental Conductance MPPT Algorithm

```
function DutyCycle = INC_MPPT(V, I, Vmax, Vmin, StepSize, DutyCycle)
    % INC_MPPT - Incremental Conductance MPPT Algorithm
    % V: Current voltage from the solar panel
    % I: Current current from the solar panel
    % Vmax: Maximum allowable voltage
    % Vmin: Minimum allowable voltage
    % StepSize: Step size for duty cycle adjustments
    % DutyCycle: Initial duty cycle

    % Calculate the instantaneous power
    P = V * I;

    % Calculate the conductance (dP/dV)
    Conductance = I / V;

    % Check if the conductance matches the negative of the conductance at
MPP
    if Conductance < -P / V
        % Increase the duty cycle
        DutyCycle = DutyCycle + StepSize;
    elseif Conductance > -P / V
        % Decrease the duty cycle
        DutyCycle = DutyCycle - StepSize;
    end

    % Ensure that the duty cycle stays within the allowed bounds
    if DutyCycle > 1
        DutyCycle = 1;
    elseif DutyCycle < 0
        DutyCycle = 0;
    end

    % Calculate the new voltage
    Vnew = DutyCycle * (Vmax - Vmin) + Vmin;

    % Update the duty cycle only if the new voltage is within bounds
    if Vnew <= Vmax && Vnew >= Vmin
        DutyCycle = (Vnew - Vmin) / (Vmax - Vmin);
    end
end
```

Boost Converter Parameters Calculation

```
% Given Parameters
P = 2160;          % Power (in watts)
F = 10000;        % Switching frequency (in Hz)
Vin = 432;        % Input voltage (in volts)
Vout = 600;       % Output voltage (in volts)
r0 = 0.1;         % Ripple factor for input current
r1 = 0.01;        % Ripple factor for input voltage
r2 = 0.02;        % Ripple factor for output voltage

% Calculate input and output currents
Iin = P / Vin;    % Input current (in amperes)
Iout = P / Vout;  % Output current (in amperes)

% Calculate ripple values
deltI = Iin * r0; % Ripple in input current (in amperes)
deltVin = Vin * r1; % Ripple in input voltage (in volts)
deltVout = Vout * r2; % Ripple in output voltage (in volts)

% Calculate duty cycle
d = 1 - (Vin / Vout); % Duty cycle

% Calculate inductor value (L1)
L1 = (Vin * d) / (deltI * F); % Inductor value (in henries)

% Calculate input capacitor value (Cin)
Cin = (Vin * d) / (8 * F^2 * L1 * deltVin); % Input capacitor value (in
farads)

% Calculate output capacitor value (C1)
C1 = (Iout * d) / (deltVout * F); % Output capacitor value (in farads)

% Calculate load parameters
Load1 = P / Iout^2; % Load resistance (in ohms)
Load2 = Vout / Iout; % Load impedance (in ohms)

% Display results
fprintf('Boost Converter Parameters:\n');
fprintf('-----\n');
fprintf('Inductor Value (L1): %.6f H\n', L1);
fprintf('Input Capacitor Value (Cin): %.6f F\n', Cin);
fprintf('Output Capacitor Value (C1): %.6f F\n', C1);
fprintf('Load Resistance (Load1): %.6f ohms\n', Load1);
fprintf('Load Impedance (Load2): %.6f ohms\n', Load2);
```

Bidirectional buck-boost converter Parameters Calculation

```
%% Input (Insert Variable Here)
Vl = 384;           % Low Voltage Source (V)
Vh = 600;           % High Voltage Source (V)
P = 8000;           % Power Transfer (W)
f = 10000;          % Switching Frequency (Hz)
Krl = 0.01;         % Low Voltage Ripple Factor
Krh = 0.01;         % High Voltage Ripple Factor

%% Calculation
Rl = Vl^2 / P;      % Resistance at Low
Voltage Side
Rh = Vh^2 / P;      % Resistance at High
Voltage Side
Dbck = Vl / Vh;     % Buck Mode Duty Cycle
Dbst = 1 - Dbck;    % Boost Mode Duty
Cycle
Lbck = (1 - Dbck) * Rl / (2 * f); % Minimum Inductance
for Buck Mode
Lbst = Dbst * (1 - Dbst)^2 * Rh / (2 * f); % Minimum Inductor for
Boost Mode

% Minimum Inductor for Both Modes
if Lbck > Lbst
    L = Lbck;
else
    L = Lbst;
end

Cl = (1 - Dbck) / (8 * L * Krh * f^2); % Capacitance at Low
Voltage Side
Ch = Dbst / (Rl * Krl * f);           % Capacitance at High
Voltage Side

%% Display
fprintf('In buck mode, D = %.2f%%.\nIn boost mode, D = %.2f%%\n',
Dbck * 100, Dbst * 100);
fprintf('\nL = %.6f H\nCl = %.6f F\nCh = %.6f F\nRl = %.2f
ohm\nRh = %.2f ohm\n', L, Cl, Ch, Rl, Rh);
```